Newsletter of the Climate Variability and Predictability Programme (CLIVAR)

Exchanges

No 53 (Volume 15 No 2) April 2010

CLIVAR VAMOS Ocean-Cloud-Atmosphere-Land Study VOCALS

"The NSF C-130 flies by the NOAA Ronald H Brown underneath the stratocumulus during a research mission far off the Chilean coast on the 11th November 2008. Photo courtesy Cameron McNaughton, University of Hawaii"

"Students from the Universidad de Arturo Prat, launch one of the four-times daily radiosondes from their shoreside campus in Iquique, Chile. Photo courtesy Carlye Calvin, UCAR"

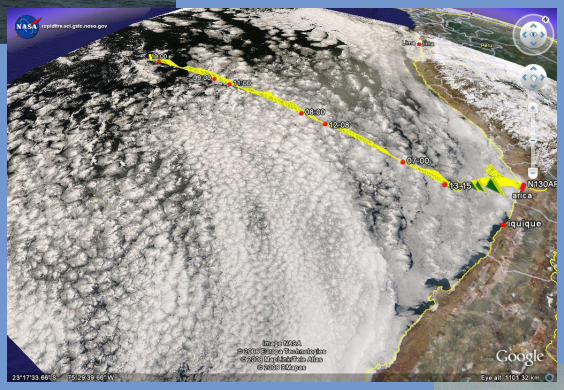

"C-130 Flight track overlaid on a MODIS satellite image."

"The NSF/NCAR C-130 preparing for a night-time take-off. Photo: Robert Wood"

"The Peruvian IMARPE R/V Jose Olaya"

CLIVAR is an international research programme dealing with climate variability and predictability on time-scales from months to centuries. CLIVAR is a component of the World Climate Research Programme (WCRP). WCRP is sponsored by the World Meteorological Organization, the International Council for Science and the Intergovernmental Oceanographic Commission of UNESCO.

WCRP World Climate Research Programme

Editorial

I'm pleased indeed to be able to introduce this edition of Exchanges featuring papers describing current results from VOCALS, the VAMOS Ocean-Cloud-Atmosphere-Land Study, a major field and modelling programme in the southeastern Pacific focused on diurnal to interannual timescales. I'm grateful indeed to Nico Caltabiano and Roberto Mechoso for bearing the brunt of the task of editors for this edition and, as always, to Sandy Grapes for her work on the layout. In addition to the VOCALS papers this edition of Exchanges also includes a short account of the recent WCRP co-sponsored Workshop on "Predicting the Climate of the Coming Decades" (Miami, USA, 11-14 January 2010) and early notification of the WCRP Open Science Conference "Climate Research in Service to Society". I had hoped to have space for a report back from the last meeting of the JSC for WCRP (Antalya, Turkey, 15-19 February 2010) but will hold that back until the next edition.

Howard Cattle

Climate Research in Service to Society

The World Climate Research Programme (http://wcrp.wmo.int) will host a major international Open Science Conference (OSC) on 24-28 October 2011 in Denver, Colorado, USA.

A better understanding of the behaviour of the climate system and its interactions with other Earth system components is critical to predict its future evolution, reduce vulnerability to high impact weather and climate events, and sustain life. To prepare for meeting these challenges, the WCRP Open Science Conference provides a unique opportunity to bring together major disciplines and leaders of the Earth system research community to help identify opportunities to advance further understanding and prediction of variability and change in the Earth's climate system from seasons to centuries, and from regions to the entire globe.

Through active dialogue among the international environmental change research experts, the OSC will:

- Appraise the current state of climate science, thereby making a measurable scientific contribution to the Fifth Assessment Report (AR5) of the Intergovernmental Panel on Climate Change (IPCC);
- Identify key opportunities and challenges in observations, modelling and analysis towards understanding and predicting the Earth's climate system;
- Facilitate discussion on interdisciplinary research required to understand and predict responses of the Earth as a system to climate variability and change, thus helping chart the path forward over the ensuing decades
- Highlight priority research in support of the Global Framework for Climate Services initiated at the World Climate Conference -3.

By entraining early career scientists and students from across the world, especially less-developed and developing nations and regions, the OSC will facilitate growth of the diverse future workforce needed to meet the increasingly complex scientific challenges of the future.

The conference aims to attract the world's experts to provide a unique synthesis of current research findings on climate variability and change, to identify the most urgent scientific issues and research challenges, and to ascertain how the WCRP can best facilitate research and develop partnerships critical for progress in the future.

For more information please visit the conference webpage:

www.wcrp-climate.org/conference2011

or contact the Conference Secretariat

info.conf2011@wcrp-climate.org

An Abbreviated History of VOCALS

Mechoso, C.M[1]., R. Wood[2], Department of Atmospheric Sciences, [1]University of California, Los Angeles, Los Angeles, CA, US, [2]Department of Atmospheric Sciences, University of Washington, Seattle, WA, US
Corresponding author: mechoso@atmos.ucla.edu

1. Introduction

One of the major elements of CLIVAR's scientific organization is the panel on the Variability of the American Monsoon Systems (VAMOS). The scientific goals of VAMOS and preliminary plans for approaching those objectives had been developed and incorporated into the CLIVAR Implementation Plan by early 1998. Around that same time, the pilot phase of the U.S. Pan-American Climate Study (PACS) was in the field at 125°W near the equator, and planning had started for the more comprehensive Eastern Pacific Investigation of Climate Processes in the Coupled Ocean-Atmosphere System (EPIC). The need to further develop these efforts in the eastern Pacific to include the cloud systems, interactions with the aerosol, and a modelling component led to a process that culminated in the VAMOS Ocean-Cloud-Atmosphere-Land Study (VOCALS) programme, one of the largest in CLIVAR so far.

VOCALS focuses on the southeastern Pacific (SEP) climate on diurnal to interannual timescales. The subject is fascinating since the climate targeted is characterized by strong coastal upwelling, the coldest SSTs at comparable latitudes, and the most extended and poorly observed subtropical stratocumulus deck on Earth. VOCALS strategy is based on developing and promoting scientific activities leading to achievement of two major objectives in the SEP 1) elimination of coupled atmosphere-ocean general circulation model (CGCM) systematic errors in the region and improved model simulations of the coupled system in the region, and global impacts of its variability, and 2) improved understanding and regional/global model representation of aerosol indirect effects over the region.

This article presents a brief story of how VOCALS came to be and has been since its establishment. Our goals are two fold: 1) to review the long process required to make reality a large research programme, and 2) to set up the stage for the other papers in this special issue of Exchanges.

2. VEPIC 1999-2003

The origins of VAMOS can be traced back to the Fifth Session of the CLIVAR Scientific Steering Group (SSG) held in Sapporo, Japan, June 1996. The success of the U.S.-led PACS prompted consideration of the great potential advantages of establishing a truly international climate programme across the Americas with an emphasis on the warm season. As a first step, the SSG encouraged the realization of an international conference to gauge the community response to the idea. The Conference on American Monsoons (CONAM) was held in Mexico City in March 1997, and showed that key experts in the climate of the Americas welcomed the opportunity of working together on an impressive array of first-class problems in climate change and their impacts on human activities. A Science Plan was put together and reviewed by the SSG at its following meeting in Washington DC, June 1997. The formal approval of the Science Plan launched a new CLIVAR panel and VAMOS started with C. Roberto Mechoso as chair.

The new panel immediately decided to encourage the development of an enhanced monitoring system in order to provide the observational basis for improvement of operational coupled ocean-atmosphere analysis and prediction systems in the SEP, and endorsed EPIC's plans. It also created a VAMOS Stratus Working Group with Bruce Albrecht as chair. The group was asked to 1) develop cooperative, international research on the links between stratocumulus in the eastern Pacific Ocean and the American monsoon systems, and 2) explore the options for VAMOS field work on SEP stratocumulus. The group responded to 1) by formulating hypotheses on the connections between heating and rising motion over the Amazon basin and the Altiplano and subsidence in the SEP; subsidence being essential to the existence of low-level clouds in region. In response to 2) the group outlined a plan for a coastal experiment with an oceanographic focus in January-February 2001, and for another coastal experiment based on combined aircraft/ship observations. The second experiment would include estimations of the atmospheric divergent motions with an upper air array and would occur in the timeframe of the second phase of EPIC in January/February 2003. It should be highlighted that the group was working in the framework of several ongoing process studies along the Chilean coast by scientists from Chile, Perú and the U.S. These activities were carried out under a very friendly and strong collaboration, which would become one of VOCALS trademarks and would set the background for special observing periods in future field campaigns.

In 2000 the Stratus Working group changed its name to VEPIC. Work continued towards the planning of a field campaign, which now contemplated the installation of observing stations on islands and buoy deployments. Chris Bretherton chaired the Working Group during this crucial growing period. The annual meeting of the VAMOS panel in 2002 included a VEPIC Workshop, in which other relevant field experiments such as the Dynamics and Chemistry of Marine Stratocumulus - Phase II: Entrainment Studies (DYCOMS-II), were thoroughly reviewed and evaluated. At the meeting of the VAMOS Panel in 2003 it became clear that plans had gone far beyond just a continuation of EPIC and the group renamed itself as VOCALS.

3. Planning 2003-2007

The period 2003-2007 was dedicated to exhaustive analysis of plans for enhanced monitoring and to pilot studies designed to capitalize on the unique physical and infrastructural features of SEP. In 2004, Rob Wood, Chris Fairall, and Barry Huebert, joined the programme, and their leadership broadened the plans in the areas of cloud microphysics and aerosols/biogeochemical processes. VOCALS-related scientific issues were more sharply defined to encompass the time and space scales of cloud-topped boundary layer/continent interaction; regional seasonal/interannual feedbacks between stratocumulus clouds, surface winds, upwelling, coastal currents and SSTs in the eastern Pacific; and feedbacks of eastern Pacific cloud topped boundary layer properties on overall tropical circulation and El Niño/Southern Oscillation (ENSO). In addition, based on findings from the EPIC Stratocumulus Cruise, subsequent Stratus cruises under VEPIC, and the data from the IMET buoy (of the Woods Hole Institute of Oceanography) it became evident that the field program should also extend to the climatic importance of cloud/aerosol interactions, diurnal cycle of the marine boundary layer, and mesoscale ocean structure. Plans for the field work started to incorporate cruises by the U.S. NOAA RV Ronald H Brown with different patterns along a transect between the WHOI buoy and the Chilean coast, with aircraft such as the NCAR C-130 flying overhead along the transect.

Bob Weller became chair of VOCALS in 2005, bringing with him a long experience with field work in the SEP in collaboration with regional scientists. The organized work was already producing new results. A daytime subsidence wave initiated by Andean slope heating that propagates about 1500 km offshore over the southeastern Pacific stratocumulus region was discovered. The wave lowered the inversion and enhanced daytime cloud thinning. Work at operational centers had started to improve the modeling and prediction of the SEP climate. C. Roberto Mechoso replaced Weller as VOCALS chair in 2006. In December of the same year VOCALS briefed the major funding agencies of the U.S., and was encouraged to submit a proposal in order to support the project's activities including the realization of a regional experiment (VOCALS-Rex).

4. Proposal and Implementation

The VOCALS proposal was submitted to the U.S. National Science Foundation (NSF) and National Oceanic and Atmospheric Administration (NOAA) on September 2006 by Rob Wood (PI) and Chris Bretherton, Barry Huebert, C. Roberto Mechoso, and Bob Weller (co-PIs). NSF/NOAA decided that "VOCALS was GO" the following December. A flurry of activity followed this announcement. As usual, there was a VOCALS Workshop at the VAMOS panel meeting in 2007. Shortly thereafter, the First VOCALS Modeling Workshop was held at NCAR. Altogether, about 24 university groups, 20 research institutions, and 6 major operational centers would contribute to VOCALS.

Similar efforts to secure funding for VOCALS were pursued with success in Chile (José Rutllant), Perú (Carmen Grados) and the UK (Julia Slingo, Hugh Coe). The Chilean component was supported by the Consejo Nacional de Investigaciones Científicas y Técnicas (CONICYT). The Peruvian component was sponsored by the Instituto del Mar de Perú (IMARPE). A VOCALS Consortium was established in the UK and submitted a successful proposal to the National Environmental Research Counsel (NERC).

Rob Wood became Principal Investigator of VOCALS-Rex and the First Rex Preparatory Workshop was convened at NCAR. The field campaign itself occurred during October and November 2008, when some 150 scientists from 40 institutions in 8 nations gathered in northern Chile to conduct the experiment. A total of five aircraft including the NSF C-130, the DoE G-1, the CIRPAS Twin Otter, and two aircraft from the UK and two research vessels (the NOAA RV Ron Brown and the Peruvian IMARPE RV José Olaya), sampled the lower atmosphere and upper-ocean during REx (Wood and Mechoso 2008). Two land-based sampling sites on the Chilean coast complemented the aircraft and ship platforms.

Science meetings have continued after VOCALS-Rex in the U. S., Chile, Perú, and the U.K. Special sessions were organized at national and international scientific meetings. A Special Issue on VOCALS is in progress in Atmospheric Chemistry and Physics - a journal of the European Geophysical Union (EGU). VOCALS endorsed the Chilean Upwelling Experiment (CUpEx), which took place in Nov-Dec 2009 (see paper by Rene Garreaud in this issue.)

5. The contemporary VOCALS

To better and more efficiently reach its objectives VOCALS has been organized in three components: 1) a modeling component with a model hierarchy ranging from the local to global scales, 2) a suite of extended observations from regular research cruises, instrumented moorings, and satellites, and 3) an international VOCALS Regional Experiment (Rex). VOCALS has been designed for maximum international collaboration and strongest synergy among of intensive field measurements, long-term observations, and modeling in maximum compliance with the Best Practices for Process Studies predicated by US CLIVAR. The current work has been organized around the evaluation of "VOCALS hypotheses", the latest versions of which are given in the Table. The papers by VOCALS researchers in this issue of Exchanges are a selection of the work in progress.

6. Looking back to the very beginning and thinking about the future

The impetus that drove VOCALS started even before VAMOS, at a development meeting convened by the PACS programme in Miami, Florida, 7-10 February 1995. The meeting was organized in the usual way, with break out sessions for empirical, modeling, and observational studies. Those at the modeling break out soon focused on the difficulties of CGCMs in the SEP that are referred to as the "double ITCZ syndrome." A consensus was then reached on the tremendous potential for scientific advancement of research focused on the marked hemispheric asymmetry and strong seasonality that characterize the cold tongue/ITCZ complexes in the eastern equatorial Pacific and Atlantic. In these regions, southeasterly trade winds drive equatorial and coastal upwelling leading to cooler surface waters along and to the south of the equator. In contrast, north of the equator in the eastern Pacific and Atlantic, surface temperatures are warmer in the vicinity of the ITCZ. At comparable latitudes in the southern hemisphere, large-scale subsidence over cool surface waters leads to the formation of low-level stratocumulus decks and minimal surface precipitation. The modelers, led by George Philander, wondered about whether data on the structure of the atmosphere and ocean, surface fluxes, and cloud systems would be available to evaluate model performance, test hypothesis, and improve parameterizations. Unable to provide an answer they called for a joint session with the

VOCALS HYPOTHESES

1) AEROSOL-CLOUD-DRIZZLE HYPOTHESES

a) Variability in the physicochemical properties of aerosols has a measurable impact upon the formation of drizzle in stratocumulus clouds over the SEP.

b) Precipitation is a necessary condition for the formation and maintenance of pockets of open cells (POCs) within stratocumulus clouds.

c) The small effective radii measured from space in the coastal region of the SEP are primarily controlled by anthropogenic, rather than natural, aerosol production, and entrainment of polluted air from the lower free-troposphere is an important source of cloud condensation nuclei (CCN).

d) Depletion of aerosols by coalescence scavenging is necessary for the maintenance of POCs.

2) COUPLED OCEAN-ATMOSPHERE-LAND HYPOTHESES

a) Improvement of CGCMs performance in the SEP is key to the successful simulation of the ITCZ/SPCZ, complex, which will also benefit simulation of other regions. A significant improvement can be achieved through better representing the effects of stratocumulus clouds on the underlying surface fluxes and those of oceanic mesoscale eddies in the transport of heat.

b) Oceanic mesoscale eddies play a major role in the transport of fresh water from the coastal upwelling region and in the production of sea-water and atmospheric DMS in the coastal and offshore regions. Upwelling, by changing the physical and chemical properties of the upper ocean, has a systematic and noticeable effect on aerosol precursor gases and the aerosol size distribution in the MBL over the SEP.

c) The diurnal subsidence wave ("upsidence wave") originating in northern Chile/southern Peru has an impact upon the diurnal cycle of clouds that is well-represented in numerical models.

d) The entrainment of cool fresh intermediate water from below the surface layer during mixing associated with energetic near-inertial oscillations generated by transients in the magnitude of the trade winds is an important process to maintain heat and salt balance of the surface layer of the ocean in the SEP.

observationalists led by Mike Wallace (atmosphere) and Michael McPhaden (ocean). And the answer was that the data was not there. First EPIC and later VOCALS were born to fill that void in the SEP and have created unprecedented datasets on the coupled ocean-clouds-atmosphere-land system. The eastern tropical Atlantic is waiting its turn. VOCALS has started to leave a legacy in the many datasets available at the programme's web site, and is beginning to think about a long-term future.

Acknowledgements.
It is practically impossible to acknowledge all the people who have contributed to VOCALS, but we can attempt to recognize the various groups that have dedicated their resources, efforts, sweat and tears to the planning and execution of the programme. First, we need to thank the teams led by Bob Weller at WHOI that deployed and maintained with annual cruises the IMET buoy, which has provided almost a decade of high quality meteorological, radiation and oceanographic measurements. Thanks to Chris Fairall and coworkers at ESRL, and the scientists involved in the EPIC Stratocumulus cruise, these ship-borne programmes have led to a wealth of scientific data. We are extremely grateful to the support staff, crew and scientists who helped make the VOCALS-REx a success. These include the PIs of the six aircraft platforms (the NSF/NCAR C-130, the UK FAAM BAe-146, the DoE G-1, the CIRPAS Twin Otter, the UK NERC Dornier 228, and, in the 2010 CupEx phase, the Chilean King Air), the two ships (the NOAA Ronald H Brown, and the Peruvian IMARPE José Olaya), and the land stations at Iquique and Paposo. The NCAR Earth Observing Laboratory, and José Meitin in particular, are thanked for their dedication to coordinating and executing field logistics and data archive support for VOCALS Rex. Finally, the cooperation of our hosts in Chile and Peru who provided various critical facilities and support during REx is gratefully acknowledged. It is also a great pleasure to recognize our two science monitors in the U.S.: NSF's Walter Robinson and NOAA's Jin Huang. And there were constant friends at CLIVAR's International and US CLIVAR's Project Offices: Howard Cattle, and David Legler.

Reference

Wood, R. and C. R. Mechoso, 2008: Southeastern Pacific Coupled Climate Field Experiment. EOS Trans. AGU, 89(33), 303.

The project web site is at www.eol.ucar.edu/projects/vocals.

VOCALS-CUpEx: The Chilean Upwelling Experiment

Garreaud, R.D[1]., J. Rutllant[1,2], R. Muñoz[1], D. Rahn[1] , M. Ramos[2] and D. Figueroa[3]
[1]Department of Geophysics, Universidad de Chile, [2]Center for Advanced Studies in Arid Zones (CEAZA), Chile, [3]Department of Geophysics, Universidad de Concepción
Corresponding author: rgarreau@dgf.uchile.cl

1. Presentation

The VAMOS Ocean-Cloud-Atmosphere-Land Study (VOCALS) is an international program that targets the subtropical Southeast Pacific region (Wood et al., 2006; see also paper by Mechoso and Wood in this issue). To address the many VOCALS' science questions, a major regional experiment, VOCALS-REx (see online description at http://www.eol.ucar.edu/projects/vocals/rex.html), was carried out during October and November 2008 off northern Chile and southern Peru, including an unprecedented number of atmospheric and oceanographic measurements taken concurrently from five aircrafts, two research vessels and two land sites.

It was originally planned that VOCALS-REx would include a coastal component encompassing the near-shore region at about 30°S. In practice, most of the action during VOCALS-REx took place in a zonal band between 25°S and 16°S because of logistic constrains. About a year later, however, several Chilean institutions (Table 1) have teamed to conduct an additional field experiment to fill our observational gap. The so-called Chilean Upwelling Experiment (CUpEx) is therefore a regional component of VOCALS aimed at understanding the atmosphere-ocean dynamics that characterize the nearshore (0-200 km) region off north-central Chile (30-35°S). VOCALS-CUpEx not only has relevance for regional climate studies but is also important in a broader context, as many of the transient features that populate the SE Pacific are originated along the semiarid coast of Chile and are subsequently advected offshore (e.g., Rahn and Garreaud, 2009).

2. The study region

The semiarid coast of Chile (25-35°S) is under the year-round influence of the southeast (SE) Pacific anticyclone, resulting in predominantly southerly (coastal parallel) low-level winds, and a strong temperature inversion that caps a cool atmospheric marine boundary layer (AMBL). The surface stress exerted by the southerly winds foster the upwelling of cold, nutrient-rich waters supporting a wealth of fishery resources. The synoptic-scale variability in this region is associated with the occurrence of coastal lows (Garreaud and Rutllant, 2003) that are in turn forced by the passage of surface anticyclones farther south. During the coastal low development, the near-surface wind forms an intense coastal jet –in turn fostering upwelling episodes- and the AMBL depresses, often resulting in coastal clearing (Garreaud and Muñoz, 2005). The coastal low demise typically features a relaxation of the southerlies and the recovery of the cloud-topped AMBL.

The Chilean coast is oriented almost straight north-south between 33°S and 30°S (Point Lengua de Vaca; LdV), bounded to the east by a mountain range with average elevation between 500 and 1000 m above sea level (ASL, Figure 1). The coastal mountains in this area are interrupted by several river valleys in contrast with a much more continuous coastal cliff of (that stand at) about 1000 m ASL farther north (between Paposo and Arica; 25-18°S). To the north of LdV the coastline sharply retracts eastward about 40 km, forming a wide embayment, including the bays of Tongoy and Coquimbo, and returns to the west at about 29°S (Point Choros).

The southerly flow along the semiarid coast of Chile often exhibits a low-level jet structure, with its core about 100 km off the coast (Garreaud and Muñoz, 2005). Accordingly, the coastal strip features marked cross-shore gradients of wind, sea surface temperature (SST), and MBL depth. The amplitude of the diurnal cycle of wind and cloudiness also increases strongly over this strip forced by the continental heating/cooling cycle. Another conspicuous feature of the semiarid coast is the along-shore structure in cloudiness (and presumably in MBL depth). Of particular relevance are the semi-permanent low-clouds intercepting the coastal mountains just south of 30°S which maintain fog-dependent green forests, in an otherwise arid landscape, and the coastal clearing tendency just north of LdV.

3. Experimental setup

Despite its proximity to land, processes embedded in the near-coastal strip around 30°S have been poorly documented because of the lack of observational platforms. To fill this gap, VOCALS-CUpEx includes long-term monitoring, an intensive two-week field campaign and ongoing off-shore research flights (Figure 1). Surface meteorology (air temperature, humidity, barometric pressure, wind and solar radiation) is recorded every 15 min in five automatic weather stations (AWS) along the coast. From south to north, the first AWS is located at Talcaruca, about 15 km to the south (upstream) of LdV where the coastline is straight. The next station is at point LdV, followed by one station in the sheltered bay of Tongoy.

Platform & Instruments	PI	Funding
AIMMS-20 on BE90	R. Garreaud (DGF)	FONDECYT-Grant 1090492, DGF-UCH, DGAC
AWS, Radiosondes at Tongoy and Talcaruca	J. Rutllant (DGF) R. Muñoz (DGF)	FONDECYT-Grant 1090492, DMC, CNE, DGF-UCH
Tongoy bay buoy and AWS Islote Pajaros	M. Ramos (CEAZA)	CEAZA, INOVA-Corfo 07CN13IXM-150, FONDECYT 1080606
Surface Current Radars	Dante Figueroa (DGEO)	FONDEF-Grant D03I-1104
Ocean moorings	Oscar Pizarro (DGEO)	FONDECYT-Grant 1090791

DGF : Department of Geophysics, Universidad de Chile
DGEO: Department of Geophysics, Universidad de Concepción
CEAZA: Centro de Estudios Avanzados de Zonas Áridas
DGAC: Dirección General de Aeronáutica Civil
DMC: Dirección Meteorológica de Chile
CNE: Comisión Nacional de Energía

The AWS at Tongoy was complemented with a laser ceilometer providing cloud frequency and cloud base height every 1 minute. The northernmost coastal AWS is at 29°S where the coastline curves back to the west. Surface meteorology is also recorded at a coastal buoy in the bay of Tongoy and at Islote Pájaros (Figure 1). All these AWSs were installed during (or prior to) November 2009 and will be maintained for a year, providing a long-term context of the low-level circulation in the CUpEx area.

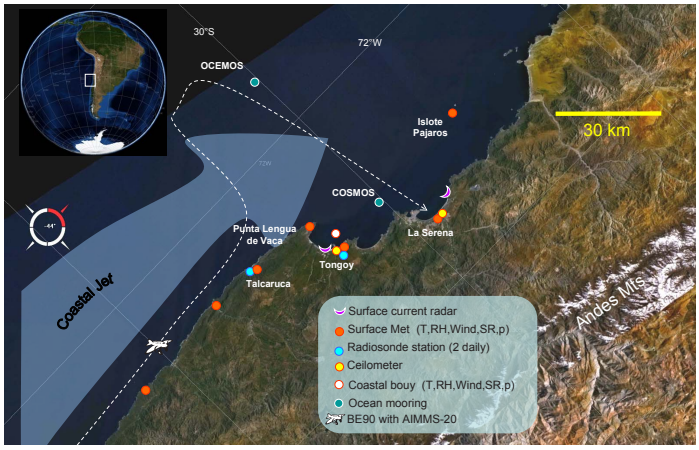

Figure 1. The VOCALS-CUpEx region. The different platforms are indicated in the topographic map.

The intensive observation period (IOP) extended from 21 November to 5 December, 2009. The IOP exhibits typical spring-time conditions, with a well developed coastal jet, except for two brief periods at the beginning and at the middle of the campaing when the southerlies relaxed in connection with the demise of a coastal low. During this period, we launched radiosondes at 08:00 and 17:00 LT (1200 and 2100 UTC) at Talcaruca (upstream of LdV) and Tongoy (downstream of LdV) in order to capture the differences in the MBL and low-level circulation between the straight-coastline sector and the bay of Tongoy. These radiosondes provide the first systematic tropospheric observation at 30°S. The nearest routine radiosondes are launched by the National Weather Service at Santo Domingo (33.5°S) and Antofagasta (23°S). During the IOP and several weeks prior to it, two high-frequency radars (Figure 1) provided near-continuous measurements of the surface waves and ocean currents from the coast up to about 50 km offshore over the Tongoy-La Serena bay area. These data will be key in assessing the ocean response to the strong surface winds in the near-shore strip.

To complement the coastal observations and explore the offshore MBL structure VOCALS-CUpEx airborne meteorological observations were conducted off the central Chile coast. We installed an Aircraft Integrated Meteorological Measurement System (AIMMS-20) under the wing of a Beechcraft King Air BE-90. The aircraft belongs to the Chilean Civil Aviation Directorate (DGAC) and its two turboprops provide more than 2500 km of endurance. The AIMMS-20 measures air temperature, relative humidity, wind speed and direction (three components), pressure and aircraft position (latitude-longitude-elevation) at 1 Hz. The AIMMS-20 was developed by Aventech Inc. in Canada and its has been used by meteorology research groups at the University of Manchester, UK, (Beswick et al. 2008) and Duke University, USA, (Avissar et al., 2009). At the time of writing this paper we have performed three scientific missions off central Chile described on line at http://www.dgf.uchile.cl/rene/AIMMS20/

4. Preliminary results

Since most of the measurements associated with VOCALS-CUpEx took place at the end of 2009 (and some of them are occurring now) this section only provides a glimpse of the scientific results expected from this project. Figure 2 shows the morning (07-09 LT) and afternoon (16-18 LT) near-surface winds averaged during November-December 2009 around 30°S. The inland stations and those along the bay of Tongoy/Coquimbo show a marked diurnal cycle in speed and direction associated with the development of a sea breeze during afternoon, as a response to the surface heating and topography. A dramatic case occurs at Tongoy where the afternoon wind blows from the north in an area otherwise dominated by southerly flow. The northerly flow at Tongoy is, however, restricted to the first 200 m capped by southerlies aloft (Figure 3a). The surface stations south of

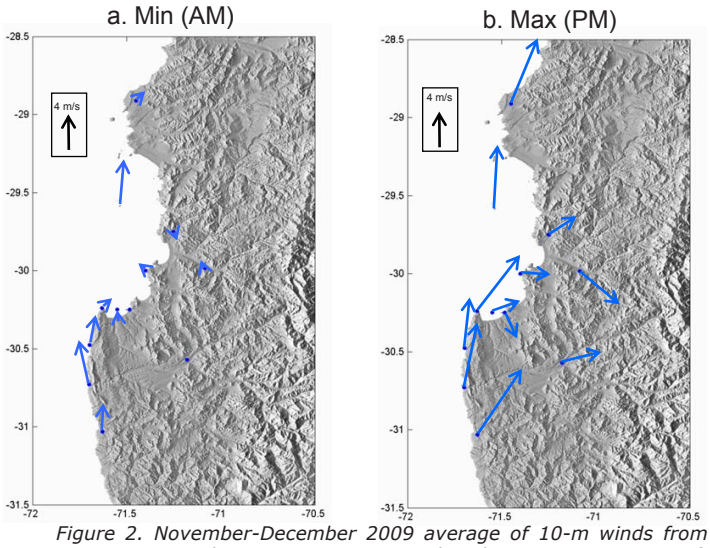

Figure 2. November-December 2009 average of 10-m winds from automatic weather stations associated with VOCALS-CUpEx. Left panel: early morning conditions (07-09 LT). Right panel: afternoon conditions (16-18 LT).

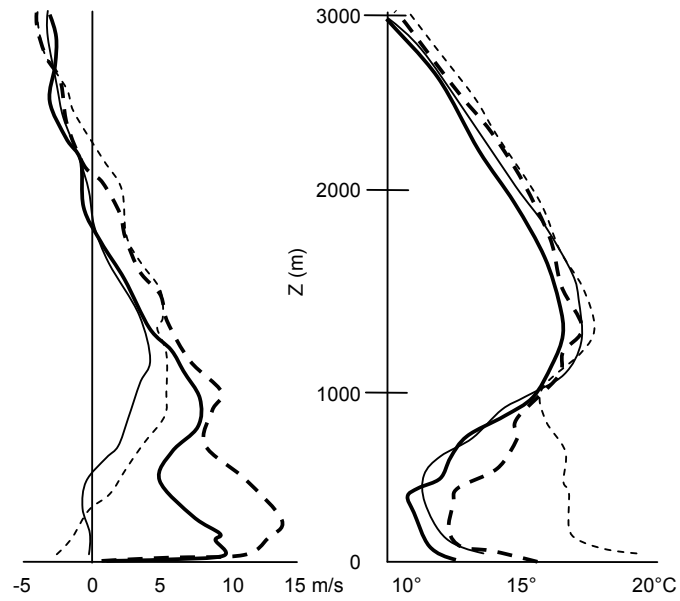

Figure 3. Average vertical profiles during VOCALS-CUpEx from radiosonde observations at Talcaruca (thick lines) and Tongoy (thin lines) at 08:00 LT (solid line) and 17:00 LT (dashed). Left panel: meridional wind; right panel: air temperature.

LdV and Islote Pájaros show a weaker diurnal cycle in wind speed, and the direction remains nearly fixed from the S-SW during the whole day.

Figure 3 shows the AM and PM vertical profiles of meridional wind and air temperature at Tongoy and Talcaruca averaged during VOCALS-CUpEx. In both stations the MBL is about 400 m deep capped by a temperature inversion that extends up to about 1500 m. In the morning there is little difference between the temperature profiles at the two locations. During the day both profiles show a warming of the MBL and the inversion layer, but relatively modest in Talcarruca (2°C) and very strong in Tongoy. The Tongoy profiles also exhibit a significant afternoon drying of the MBL (not shown). We hypothesize that the afternoon warming/drying at Tongoy signals the arrival of continental air parcels. The advection of continental air over the Tongoy bay could explain the clear sky conditions that often characterize this area in an otherwise cloudy region.

Research flights with the AIMMS-20 mounted in the wing of the BE90 occurred in late December and January, when the core of the coastal jet has moved to the south of the Tongoy region. For this reason, our flight missions were flown offshore

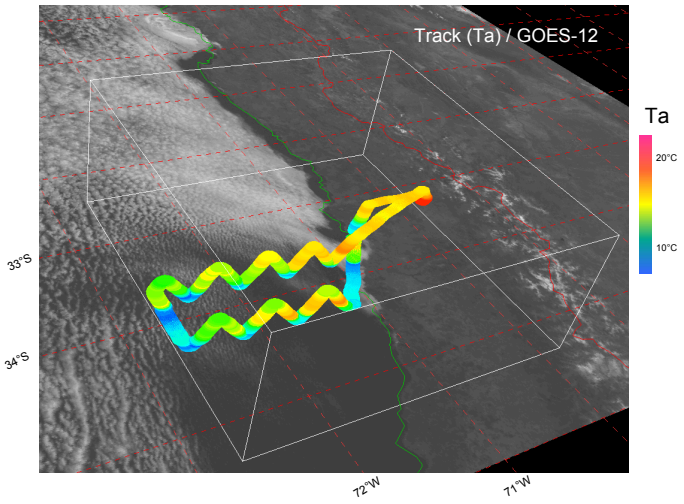

Figure 4. Track of the BE90 during research flight No. 2 (January 7, 2009, from 11:00 to 13:00 LT) colored according to air temperature measured by the AIMMS-20. The track was superimposed on the GOES-12 visible image corresponding at the time of aircraft landing.

of 33.5°S (instead of 30°S) attempting to sample the MBL near the exit of the coastal jet as well as the wind and MBL gradients in the coastal strip. The missions have occurred under weak, moderate and strong southerly flow. Figure 4 shows an example of the air temperature during the 2nd research mission (January 7) superimposed over a satellite image. Considering the intra-flight and inter-flight datasets we have found significant correlations between wind speed, MBL depth and cloudiness, such that the strongest winds develop atop of shallow MBL with little or no clouds. This unprecedented aircraft data is being used to assess operational numerical simulations and better characterize the MBL, including a prominent near-shore jet north of LdV (Figure 5).

Acknowledgements

VOCALS-CUpEx is supported by several research grants from CONICYT (Chile). In particular, we acknowledge FONDECYT grants 1090492, 1080606 and 1090791, as well as FONDEF grant D03I-1104 and INNOVA-Chile 07CN13IXM-150. We also thank the National Weather Service (DMC) and the National Civil Aviation Directorate (DGAC) for their support during the intensive observation period and the research flights.

References

Avissar, R., H. Holder, N. Abehserra, M. Bolch, K. Novick, P. Canning, K. Prince, J. Magalhaes, N. Matayoshi, and G. Katul, 2009: The Duke University Helicopter Observation Platform. *Bulletin of the American Meteorological Society*, **90**, 939-954.

Beswick, K., M. Gallagher, A. Webb, E. Norton, and F. Perry, 2008: Application of the Aventech AIMMS20AQ airborne probe for turbulence measurements during the Convective Storm Initiation Project. *Atmos. Chem. Phys*, 8, 5449-5463.

Garreaud, R. and J. Rutllant, 2003: Coastal lows in north-central Chile: Numerical simulation of a typical case. Mon. Wea. Rev., 131, 891-908

Garreaud, R. and R. Muñoz, 2005: The low-level jet off the west coast of subtropical South America: Structure and variability. *Monthly Weather Review*, **133**, 2246-2261.

Rahn, D., and R. Garreaud, 2009: Marine boundary layer over the subtropical southeast Pacific during VOCALS-REx. Part II: Synoptic variability.Open Discussion Atmospheric Chemistry and Physics. *VOCALS-REx Special Issue*. November 2009

Wood, R., and others, 2006: VOCALS REx: Scientific program overview. http://www.atmos.washington.edu/~robwood/VOCALS/VOCALS_SPO_Complete.pdf

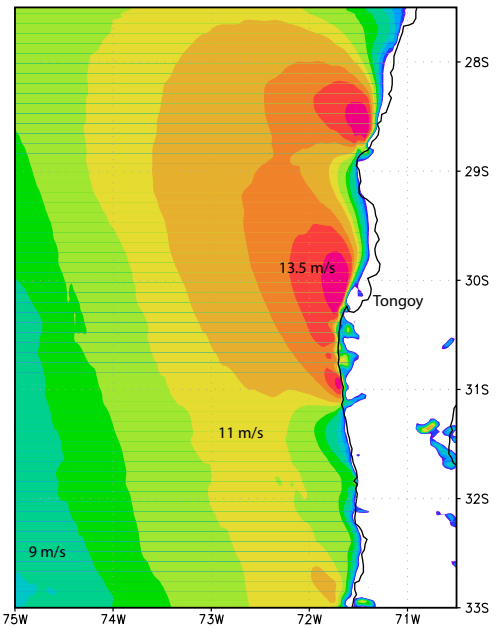

Figure 5. Evening (5-7 PM) average of surface wind speed simulated by WRF during CUpEx.

Gravity waves as a causal mechanism for transition from closed to open cellular convection in the remote South East Pacific

Allen[1], G.,G. Vaughan[1], P. Connolly[1], P. Cook[1], H. Coe[1], P. Minnis[2], and T. Toniazzo[3]
[1]Centre for Atmospheric Science, University of Manchester, UK, [2]NASA Langley NASA Langley Research Center, USA, [3]University of Reading, UK.
Corresponding author: grant.allen@manchester.ac.uk

1 Introduction

This work discusses observations of satellite-retrieved cloud bulk properties during early October 2008, which clearly illustrate the propagation of several gravity waves in the Marine Boundary Layer (MBL), emanating from a trough at 30°S, off the coast of Chile. The waves were manifest by their modulation of cloud top height by up to 500 metres peak-to-trough, with wave propagation perpendicular to the mean flow. The waves were seen to propagate through the South East Pacific (SEP – 15-30°S, 70-90°W) between 7 Oct to 11 Oct 2008 and were seen to affect changes in cloud structure such that areas of clear sky were essentially opened up in the troughs of passing gravity wave fronts. The formative mechanisms of cloud-free regions, or so-called Pockets of Open Cells (POCs), observed as cell-like (openly-convecting) cloud-free areas embedded in remote marine stratocumulus sheets, are currently the subject of intense speculation and scientific interest (e.g. Bretherton et al., 2004; Stevens et al., 2005; Comstock et al., 2005, 2007 and references therein). Such interest exists not only because of the nature of coupling between cloud microphysics, aerosol and boundary layer dynamics, but also because these structures can act to modulate the thermodynamic and radiative properties of large areas of the MBL, as well as modifying the composition of the remote MBL through the washout of already scarce particulate matter (Cloud Condensation Nuclei - CCN). Moreover, the important potential climate impact of these structures, through their radiative properties, is not represented in climate or regional-scale models.

The necessary conditions, or "tipping points" for the transition between the metastable closed and open cell dynamic states is also the subject of much speculation and has been observed by aircraft to be linked to the scavenging of available CCN by drizzle (Van Zanten and Stevens, 2005; Sharon et al., 2006, Wood et al., 2008), with consequent feedback on the underlying convective dynamic of the cloud. This work investigates the possible role gravity waves can play in initiating such a condition. We do not propose that gravity waves are the sole mechanism for POC formation, rather that they are one way to induce drizzle formation and changes in vertical dynamics; with drizzle formation and increased vertical mixing being the likely necessary action for POC formation.

Preliminary model simulations with the aid of a Large Eddy Model (LEM) indicate that perturbations in the boundary layer depth, consistent with those observed from the satellite observations of the gravity waves in the cases studied suggest that such changes are able to effectively induce drizzle and increase vertical mixing through their effect on MBL and cloud dynamics, thus promoting open-cellular convection and scavenging of available CCN.

2 The VOCALS campaign and data sources

The POCs and gravity waves discussed here were observed immediately prior to the intensive phase of the VAMOS Ocean Atmosphere Land Study Regional Experiment (VOCALS-REx) campaign and make use of data recorded as part of this international multi-platform campaign. A key objective of the VOCALS project is to reduce uncertainties in current and future climate projections, especially those associated with marine stratocumulus and coupled ocean-atmosphere processes. The field campaign consisted of the following measurement platforms: five aircraft, two cruise ships, two surface measurement sites and data from two IMET Buoys (positioned at 20ºS, 85ºW and 20ºS, 75ºW) as well as a host of supporting satellite data and specialist model output to inform mission planning in the field. Further details of the context, platforms and instrumentation operated during VOCALS-REx will be presented in forthcoming papers which will be submitted to *Atmospheric Chemistry and Physics* in 2010.

We make use of infrared brightness temperature data recorded by the GOES 10 geostationary weather satellite, operated by NOAA/NASA, which routinely provided infrared

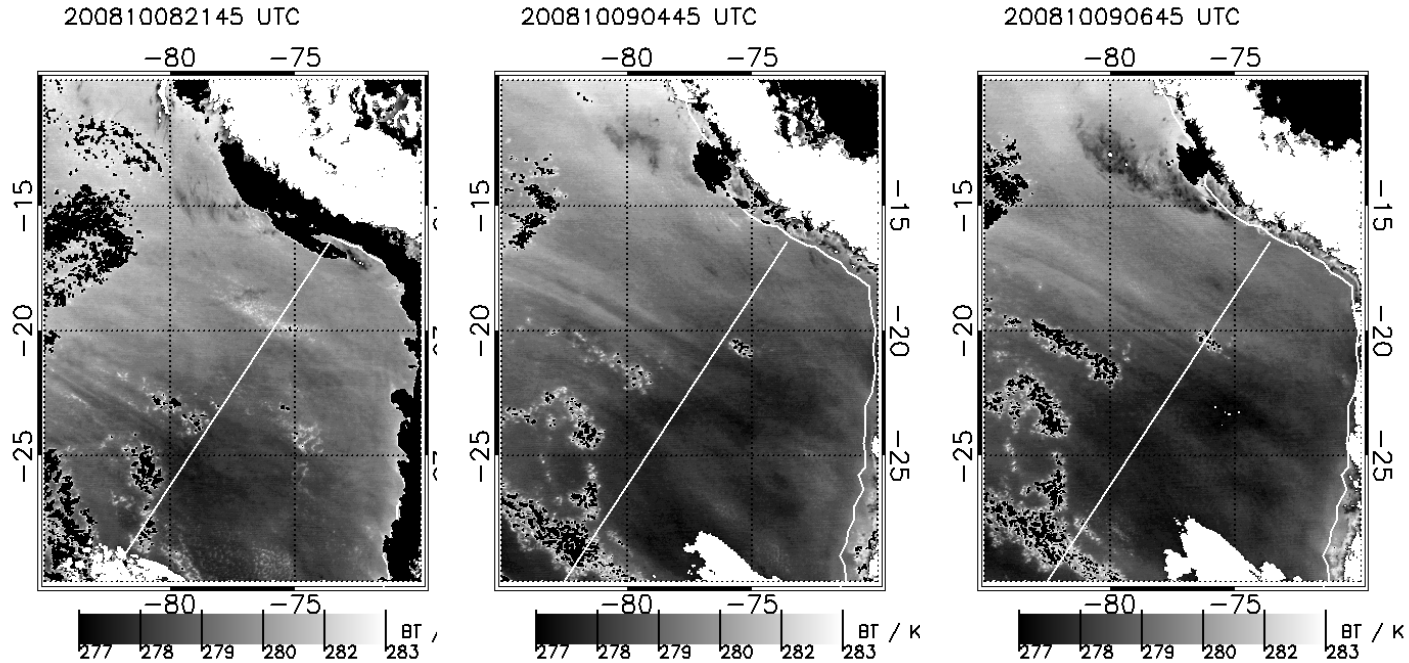

Figure 1. Time sequence of GOES-10 Channel 4 grayscale brightness temperature fields recorded at 21:45 UTC (17:45 local time), 04:45 UTC (01:45 local time) on 8 Oct 2008 and 06:45 UTC (03:45 local time) on 9 Oct 2008, showing gravity wave fronts between 15-25ºS and 75-85ºW. The solid line in each plot guides the direction of propagation of the wave fronts.

and visible images of the South American region from 1997 until its decommission in 2009. GOES-10 recorded images in 5 spectral bands covering the far and near infrared as well as a further visible channel and was the third satellite in a series of geostationary platforms (see Menzel and Putdom, 1994 for further technical details). In this work we use brightness temperatures recorded in GOES-10 Channel 4 (10.2-11.2Mm) to qualitatively illustrate the propagation of gravity waves using this as a proxy for cloud top temperature and hence cloud top height. Cloud data products used in this study and provided for the VOCALS campaign were retrieved from GOES-10 imagery, using the Visible Infrared Solar-Infrared Split Window Technique (VISST) and the Solar-Infrared Infrared Split Window Technique (SIST) method of Minnis et al., (1995). This method uses GOES-10 brightness temperatures in all channels during daytime (VISST) and night-time (SIST) in conjunction with other available satellite and meteorological observations to derive information on cloud top height, cloud phase, cloud thickness, liquid water path and other parameters.

Clouds simulated here were modelled using the UK Met Office Large Eddy Model (LEM), described further by Derbyshire et al., 1994, and Gray et al., 2001. The LEM has a horizontal grid spacing of 30 m, increasing to 10 m in the vertical and was initialised here in Boussinesq mode, with active precipitation, for a 3-hour run between 0800 and 1100 local time for thermodynamic and cloud conditions simulated to be typical of the period 8 Oct to 10 Oct 2008 using measurements recorded by dropsondes and cloud instrumentation over the same region (76°W, 20°S) onboard the aircraft later in the VOCALS campaign. An initial cloud droplet concentration of 108 droplets kg-1 up to cloud top, with saturation in the marine surface layer was used.

For the purposes of theoretical modelling of gravity wave propagation, thermodynamic and wind fields were taken from data hosted by the British Atmospheric Data Centre (BADC) and produced by the European Centre for Medium Range Weather Forecasting (ECMWF) operational analysis Integrated Forecasting System (IFS Cycle 29r2). The above fields were provided on a 1.125° x 1.125° grid on 91 hybrid model levels and interpolated onto an LEM grid.

3 Satellite observations

Figure 1 shows a time sequence of GOES-10 Channel 4 brightness temperature fields between 21:45 UTC (18:45 local time) on 8 Oct 2008 and 06:45 UTC (03:45 local time) on 9 Oct 2008. This sequence shows several parallel fronts in brightness temperature evident in the cloud-field aligned roughly in a North West/South East direction. Such fronts (or light and dark banding) in brightness temperature can be thought of qualitatively as peaks and troughs in cloud top temperature and hence cloud top height. The first 2 panels of Figure 1 show that in the intervening 7 hours between those images, the wave fronts have propagated to the North East, toward the coast of Peru. A more detailed tracing of each wave front from a full sequence of GOES-10 imagery (recorded at half-hourly intervals) reveals that each wave front propagates through approximately 4.5 degrees of latitude and 5 degrees of longitude during this time, equating to a phase speed of approximately 55 km hr-1. Furthermore, analysis of the inter-arrival time between these fronts at a fixed location yields a wave period of approximately 60 minutes and hence a wavelength of 55 km. Analysis of retrieved cloud top temperature reveal that the peak-to-trough differences in cloud top height peak at 500 m around a mean of ~1300 m at 20°S, 76°W.

These highly periodic undulations in cloud top height also appear to propagate at a near perpendicular direction to the mean boundary layer flow. This observation is confirmed by path tracing of the broader cloud field and other embedded features which take a near northwestward path as opposed to the near northeastward propagation of the wave fronts. This is further confirmed by analysis of the MBL wind field in ECMWF reanalysis data, which is also northwestward. Together,

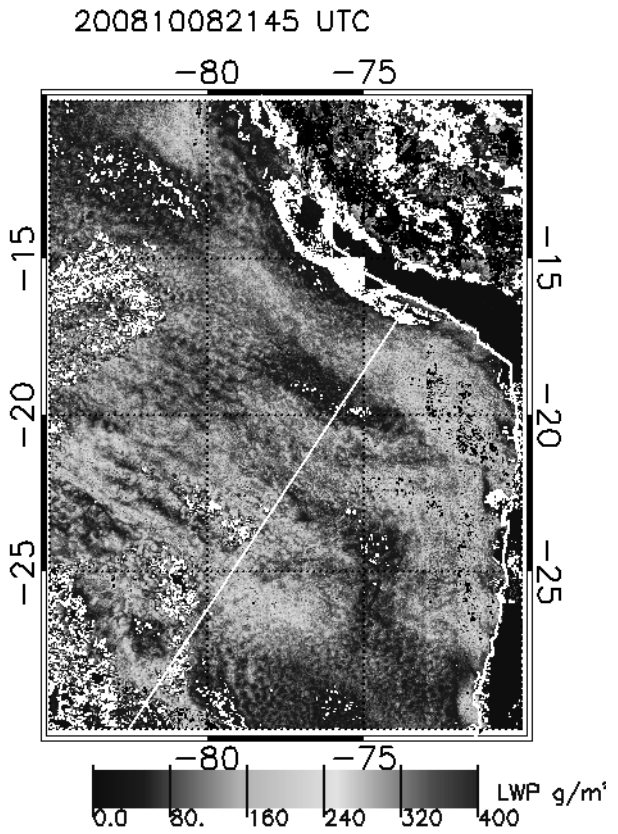

Figure 2 – Colour-scaled Liquid Water Path (LWP) retrieved from GOES-10 radiances over the SEP at 21:45 UTC (17:45 local time) on 8 Oct 2008, showing gravity wave fronts near 20-25ºS and 80-85ºW. The solid line in each plot guides the direction of propagation of the wave fronts.

these observations of a rapidly propagating, highly periodic, cross-flow wave in the cloud field point only to a gravity wave mechanism.

The wave fronts are noted to originate near 30ºS, 85ºW in an area of cyclonic disturbance and cirrus generation indicating strong convective activity. The baroclinic instability associated with this trough is thought to provide the generating mechanism for the observed gravity waves.

The second panel of Figure 1 shows the state of the cloud field at 04:45 UTC (01:45 local time) on 9 Oct 2008. Of note in this figure is the appearance of a POC area at 22.5ºS, 80ºW, which formed in the trough of a passing wave front between two consecutive satellite images (within half an hour). Once formed, this POC remains open and propagates to the North West with the mean flow, although there is evidence to suggest (from the full satellite sequence) that a thin cloud layer does reform within the POC as each successive wave front passes through. This reformation of thin cloud within the POCs occurs in each wave front and is not noted to be associated with the observed filling in of POCs seen as a result of the normal diurnal cycle in MBL thermodynamics.

Figure 2 shows a snapshot of retrieved Liquid Water Path (LWP) at 21:45 UTC (17:45 local time) on 8 Oct 2008 corresponding to the first panel of Figure 1. This shows cloud LWP is indeed enhanced as the MBL increases in depth at wave peaks (up to 170 g/m^2) and is depleted in the troughs (<30 g/m^2) relative to the background cloud field (~50 g/m^2). This indicates that clouds in the peaks of the propagating waves may be more susceptible to the initiation of precipitation. Conversely, clouds in the troughs of the passing waves appear thinner. Strikingly, these large changes or oscillations in cloud bulk properties occurred over the time period of each passing wave, just one hour.

Furthermore, the wave fronts seen here propagate for over 18

hours and over a distance calculated to be in excess of 1000 km, much larger than those associated with mountain waves for example, suggesting a large wave energy and potential trapping of wave energy between layers associated with large gradients in density or wind sheer. An ongoing theoretical examination of the potential for such trapping, initiated with ECMWF thermodynamic data, does suggest that gravity wave energy may be efficiently trapped between the boundary layer and upper troposphere. Further theoretical tests of gravity wave propagation will help to clarify the nature of this long-range propagation.

4 Modelling studies

A gravity wave was simulated in the model for the cases presented here by applying a constant forcing in vertical velocity field of 0.1 ms^{-1} and a period of 1-hour (consistent with satellite observations). Such forcing is intrinsically isentropic (as gravity wave perturbations are) in the model and acts to "lift" the cloud layer in such a manner. The inversion height was set initially to be 1300m in-line with observed retrieved cloud top heights seen in a region of POCs at 20ºS, 76ºW.

Figure 3 shows snapshots of the LEM model fields of LWP taken at the same time (1100 local time), with the left hand panel showing a cloud field modelled without any gravity wave passing through the model domain; and the right hand panel showing the same field with immediately after a simulated gravity wave has passed through. The clear difference between these two panels is that in the right hand panel, regions of significant LWP (cloud) are more localized and carry much higher LWP compared to the non-wave case. This represents the existence of open-cellular dynamics in the gravity wave case with the patchy and more linear structures of high LWP areas representing wall clouds around cloud-free areas, analogous to POCs.

Figure 4 shows vertical cross-sections of the simulated vertical velocity field for the null case (left panel) and simulated gravity wave case (right panel). The gravity wave case shows the vertical velocity field immediately after the passage of the wave, which is seen to induce significant increases in boundary layer mixing and can be seen by the higher up and downdraft speeds below cloud between 500 and 800 m. This increased vertical mixing is seen to modify the temperature profile through he boundary layer which acts to redistribute water vapour and liquid water through the profile. The increased boundary layer mixing in the gravity wave case leads to regions of thicker cloud and evaporated cloud across the domain relative to the null case.

In summary, simple preliminary simulated gravity waves can induce changes in boundary layer dynamics which may act to promote the transition to open cellular dynamics. Ongoing modelling studies will probe the influence of simulated gravity waves on the cloud field further by more closely representing the theoretically modelled vertical velocity field induced by passing waves,

5 Conclusions and further work

We have shown that changes in the structure of the boundary layer, in our example case caused by gravity waves, can lead to significant changes in the depth of boundary layer cloud, and hence, potentially, on cloud cover by inducing drizzle formation and promoting boundary layer mixing. This illustrates one mechanism by which open cellular features can be induced in the cloud field. Once formed, such features do not readily dissipate with time. Propagating gravity waves, initiated in a cyclonic disturbance in the Subtropical South Pacific have been observed to propagate across the South East Pacific over distances in excess of 1000 km between 8 Oct and 10 Oct 2008. These waves were observed to modulate the marine boundary layer stratiform cloud field as they passed, causing an increase and decrease of the cloud top height in the peaks and troughs of successive waves with a period of around one hour and a wavelength of 55 km. Preliminary modelling of these variations using a LEM suggests that changes induced in the boundary layer by the observed gravity waves may be capable of inducing vertical mixing and the generation of drizzle over the period of such waves. The model simulations indicate that enhanced vertical mixing at cloud top and increased boundary layer turnover, as well as CCN scavenging by washout of scarce CCN, all appear to lead to the breakup of closed-cellular dynamics and a more patch and POC-like cloud field. Further LEM simulations are being conducted to investigate the sensitivities of these responses to the period and amplitude of the waves. Further modelling and theoretical work will aim to exact the mechanisms for such waves to be generated and to propagate over such large distances, respectively.

Acknowledgements

The UK element of the VOCALS-Rex campaign was funded by a Natural Environment Research Council consortium grant. European Centre for Medium-Range Weather Forecasts (ECMWF) Operational Analysis data, were provided by the British Atmospheric Data Centre. Available from: http://badc.nerc.ac.uk/data/ecmwf-op/. Support for the GOES10 analyses was provided by the Department of Energy ARM Program.

References

Bretherton, C. S., Uttal, T., Fairall, C.W., Yuter, S. E.,Weller, R. A., Baumgardner, D., Comstock, K., and Wood, R.: The EPIC 2001 stratocumulus study, *Bull. Am. Meteor. Soc.*, **85**, 967–977, 2004.

Comstock, K., Bretherton, C. S., and Yuter, S.: Mesoscale variability and drizzle in Southeast Pacific stratocumulus, J. Atmos. Sci., 62, 3792–3807, 2005.

Comstock, K., Yuter, S. E., Wood, R., and Bretherton, C. S.:

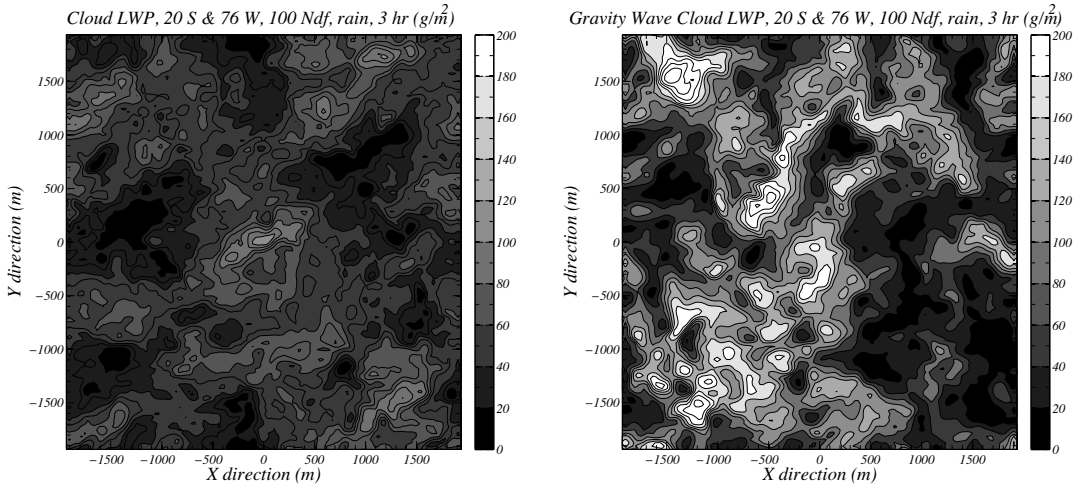

Figure 3 Colour-scaled horizontal liquid water path LEM field at 1100 (local time) UTC centred at 76 W, 20 S for left) no gravity wave; and right) immediately after simulated gravity wave

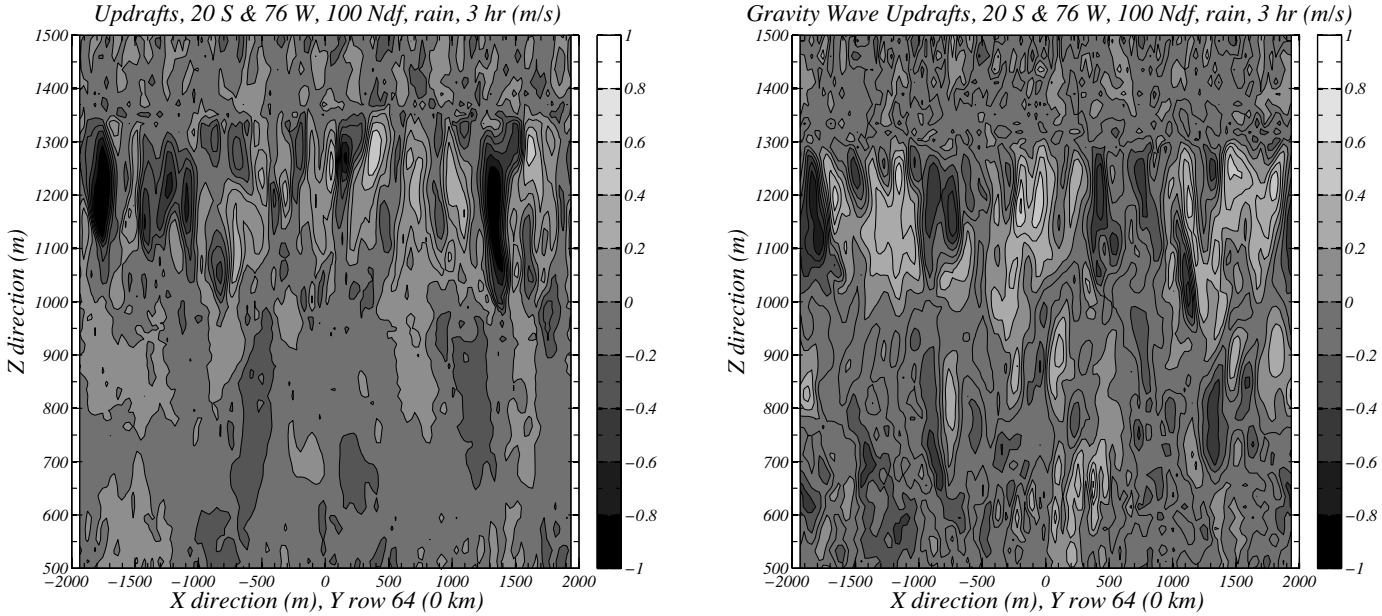

Figure 4 Vertical cross-section of LEM updraft velocity LEM field at 1100 local time on centred at 76 W, 20 S for left: no gravity wave; and right: immediately after simulated gravity wave.

The three dimensional structure and kinematics of drizzling stratocumulus, *Mon. Wea. Rev*., **135**, 3767–3784, 2007.

Derbyshire, S. H., A. R. Brown and A. P. Lock, The Meteorological Office Large-Eddy Simulation model, *Met O (APR) Turbulence and Diffusion Note* No. **213** (1994).

M. E. B. Gray, J. Petch, S. H. Derbyshire, A. R. Brown, A. P. Lock, H. A. Swann and P. R. A. Brown., Version 2.3 of the Met. Office Large Eddy Model: Part II. Scientific Documentation, *Met O (APR) Turbulence and Diffusion Note* No. **276** (2001).

Menzel, W. P., and J. F. YV. Purdom, Introducing GOES I: The first of a new generation of Geostationary Operational Environmental Satellites, *Bull. Am. Meteorol. Soc*., **75**, 757-781, 1994.

Minnis, P., et al., 1995: Cloud Optical Property Retrieval (Subsystem 4.3). "Clouds and the Earth's Radiant Energy System (CERES) Algorithm Theoretical Basis Document, Volume III: Cloud Analyses and Radiance Inversions (Subsystem 4)", *NASA RP 1376* Vol. 3, edited by CERES Science Team, pp. 135-176.

Sharon, T. M., Albrecht, B. A., Jonsson, H., Minnis, P., Khaiyer, M. M., VanReken, T. M., Seinfeld, J., and Flagan, R.: Aerosol and cloud microphysical characteristics of rifts and gradients in maritime stratocumulus clouds, *J. Atmos. Sci*., **63**, 983–997. 2006.

Stevens, B., Vali, G., Comstock, K., Wood, R., VanZanten, M., Austin, P. H., Bretherton, C. S., and Lenschow, D. H.: Pockets of Open Cells (POCs) and Drizzle in Marine Stratocumulus, *Bull. Am. Meteor. Soc*., **86**, 51–57, 2005.

Wood, R., Comstock, K. K., Bretherton, C. S., Cornish, C., Tomlinson, J., Collins, D. R., and Fairall, C.: Open cellular structure in marine stratocumulus sheets, *J. Geophys. Res*., **113**, doi:10.1029/2007JD009 596, 2008.

van Zanten, M. C., and B. Stevens, 2005: On the observed structure of heavily precipitating marine stratocumulus. *J. Atmos. Sci.*, **62**, 4327–4342.

Ship-based observation of drizzling stratocumulus clouds from EPIC to VOCALS

de Szoeke, S.P[1]., S.E. Yuter[2], P. Zuidema[3], C.W. Fairall[4], W.A. Brewer[5],
[1]Oregon State University, Corvallis, OR., [2]North Carolina State University, Raleigh, NC., [3]University of Miami, FL., [4]NOAA ESRL Physical Sciences Division, Boulder, CO., [5]NOAA ESRL Chemical Sciences Division, Boulder, CO. USA.
Corresponding author: sdeszoek@coas.oregonstate.edu

Extensive high-albedo marine stratocumulus clouds are found in the subtropical and tropical eastern oceans, where they have a strong cooling influence on the top-of-atmosphere and surface radiation budgets. Feedbacks among upwelling, sea surface temperature (SST), surface fluxes, and stratocumulus clouds are difficult for coupled general circulation models to simulate, resulting in SST errors greater than 1°C in parts of the southeastern tropical Pacific Ocean (de Szoeke et al., 2010). Although errors in coupled models for the region have been recognized for some time, the southeastern tropical Pacific was only sparsely observed before 2001.

Stratocumulus clouds were observed on seven NOAA research cruises to the southeastern tropical Pacific Ocean in 2001 and 2003-2008. The NOAA ship *Ronald H. Brown* was deployed on two research cruises in 2008 as part of the VAMOS Ocean Cloud Atmosphere Land Study (VOCALS) Regional Experiment. Each cruise traversed 20°S, 75-85°W, offshore of the Arica Bight between Peru and Chile. Several sensors were used in combination to observe marine atmospheric boundary layer clouds and precipitation during each cruis. Microwave radiometers measured the column water vapor and liquid water path (LWP, Zuidema, 2005). Laser ceilometers measured cloud base height and temporal cloud fraction. Radar wind profilers retrieved inversion height. Surface air temperature, humidity, and winds, as well as vertical fluxes of heat and humidity, were measured by instruments on a mast at the bow of the ship (de Szoeke et al., 2010). Radiometers measured downwelling solar and longwave thermal radiation. A scanning C-band radar measured reflectivity from precipitation-sized drops (Comstock et al., 2004). In 2001 and 2008, millimeter-wavelength radar profiled clouds above the ship.

On the VOCALS regional experiment in 2008, a new motion-stabilized sensitive W-band 3.2 mm cloud radar instrument provided for the first time a unique view of clouds, in-cloud turbulence, and drizzle for over 500 hours. Additionally, observations from the NOAA scanning high-resolution Doppler

lidar provided aerosol backscatter, mean horizontal wind, vertical wind, and surface mixing layer height estimates below the cloud (Tucker et al., 2009).

Seven years measuring marine stratocumulus in the southeastern tropical Pacific

A new synthesis data set contains SST, surface meteorology and radiation, upper-air profiles from rawinsondes, and air-sea flux measurements for eight research cruises along 20°S, 75-85°W in boreal fall in 7 years (2001, 2003-2008; de Szoeke et al., 2010). Macroscopic cloud properties are also summarized in the synthesis data set. Figure 1a shows cloud top and cloud base height, surface lifting condensation level (LCL), and liquid water path (LWP) averaged in 2.5° longitude bins for the eight cruises. Cloud top height is detected from vertically pointing cloud radar or inferred from either the boundary layer inversion height in radiosonde temperature profiles or 915 MHz wind profiler data. Stratocumulus cloud base height is measured optically by the ceilometer. Stratocumulus cloud base height data is filtered to minimize the effect of occasional cumulus clouds below the stratocumulus. Stratocumulus cloud base height and cloud top height increase toward the west by ~300m over 10° longitude, while cloud thickness is nearly unchanged. Surface LCL is nearly flat with longitude, yet the stratocumulus cloud base is higher to the west.

Mean LWP is about 75 g m^{-2} east of 80°W, and more than 100 g m-2 west of 80°W. Whiskers on the mean LWP are the standard error of the 10-minute data, assuming a decorrelation time scale of one hour. Cloud LWP is expected to be nearly quadratic with cloud thickness, with condensation of water vapor following the moist-adiabatic temperature profile in the cloud. Whether clouds are raining or not, columns were found to have LWP slightly below this adiabatic amount (Zuidema et al., 2005). Since mean stratocumulus cloud thickness does not increase westward, the LWP increase could be related to increasing liquid water content per unit volume within the cloud. Intermittent shallow cumulus clouds between the LCL and the stratocumulus cloud base could also explain higher LWP to the west.

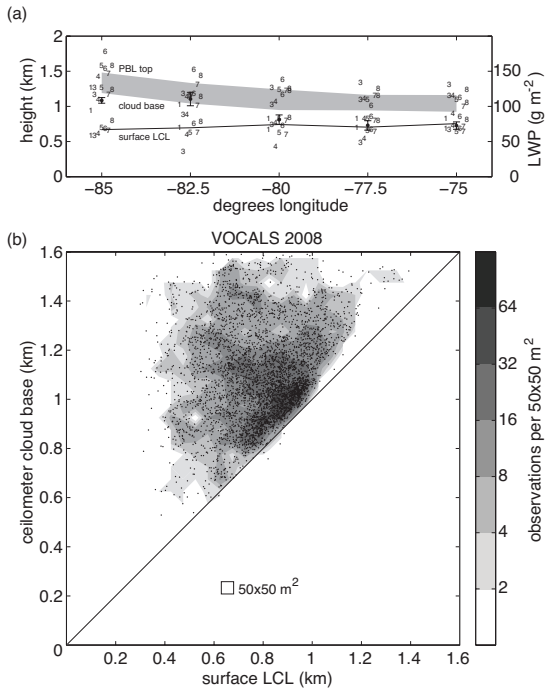

Figure 1. (a) Mean cloud base and top height (gray), and surface parcel lifting condensation level (LCL) in 2.5° longitude bins along 20°S, 75-85°W for all stratocumulus research cruises. The mean for each cruise year (2001, 2003-2008) is indicated by the last digit of the year (1, 2-8). Filled circles and whiskers show liquid water path (LWP). (b) Cloud base height measured by the ceilometer compared against surface LCL for VOCALS 2008. Clouds that condense above the surface LCL indicate the clouds are decoupled from the surface, or surface moisture is diluted by dry air in the boundary layer.

Figure 1b shows the surface LCL and ceilometer cloud base for each 10-minute average during VOCALS 2008. Cloud base is almost always observed above the LCL. The mode of the distribution corresponds to cloud base nearly 100 m above LCL. Cloud bases several hundred meters higher than LCL also occur, with 20% of cloud bases more than 500 m above the LCL. Since SST is warmer than the air, we expect a buoyancy-driven surface mixed layer, yet Figure 1b shows undiluted parcels from the surface often do not reach cloud base. Some soundings show conditionally unstable layers between the adiabatic surface layer and the moist-adiabatic cloud layer. Doppler lidar data collected in VOCALS can be employed to show the time-varying depth of turbulent mixing connected to the surface.

Enhanced radar observations of cloud and drizzle for VOCALS

In addition to the yearly observations of cloud boundaries, surface meteorology, and fluxes, two Doppler radars, a millimeter-wavelength W-band cloud radar and a centimeter-wavelength C-band precipitation radar, were deployed on the Brown.

The W-band radar pointed vertically and sampled the overlying column 3 times per second at 25-m vertical resolution. Sensitivity of the W-band radar was enhanced for the second VOCALS cruise leg so that it could detect cloud particles with reflectivity down to -30 dBZ.

Figure 2a shows W-band radar reflectivity, cloud top height, and cloud base height for November 12-15, when the ship was stationed at 75°W. Radar reflectivity is weak for clouds and stronger for drizzle. The ceilometer cloud fraction is 0.94 during the entire VOCALS cloud radar record. Of the clouds detected by the ceilometer, 14% are too weak to be detected by the cloud radar. Drizzle can be seen as high reflectivity that emerges below the cloud base. Drizzle detected near the surface is only a fraction of the times that there is drizzle at cloud base.

Examination of data from multiple years indicates that clouds have a strong diurnal cycle in cloud top height at 85°W, and a weak diurnal cycle at 75°W. This is explained by the diurnal vertical velocity perturbations of the "upsidence-wave", a gravity wave propagating offshore from its heat source in the Andes (Rahn and Garreaud, 2010). At 85°W the upsidence wave reinforces the typical diurnal cycle of nighttime deepening and daytime dissipation driven by solar radiation-modulated cloud-top entrainment. At 75°W the upsidence wave destructively interferes with the local diurnal cycle. As a result, at 85°W vertical velocity in the inversion varies with a strong diurnal component, while at 75°W, the diurnal component of vertical velocity is weaker and a semidiurnal component is present. VOCALS provides an unprecedented look at what actually happens to clouds and the boundary layer over the diurnal cycle.

The period from 12 UTC November 12 to 0 UTC November 15 shows variations at 75°W consistent with the diurnal cycle in cloud top height, cloud thickness, and radar reflectivity (Figure 2a). The LWP observed on November 12-15 (Figure 2b) was consistent with the long-term climatology from satellites (O'Dell et al., 2008). In Figure 2a clouds are higher and thicker at approximately 0 and 12 hours UTC (19 and 7 hours local, approximately 1 hour after sunset and sunrise). Radar reflectivity is higher within and below the cloud, indicating more intense clouds and drizzle when cloud tops extended to higher altitudes. Liquid water path variations from the microwave radiometer over November 12-15 also follow the cycles of cloud thickness and drizzle (Figure 2b). Adiabatic LWP (gray) depends only on the cloud thickness squared, and predicts the microwave-retrieved LWP (black) well.

Figure 2c shows a histogram of W-band radar column

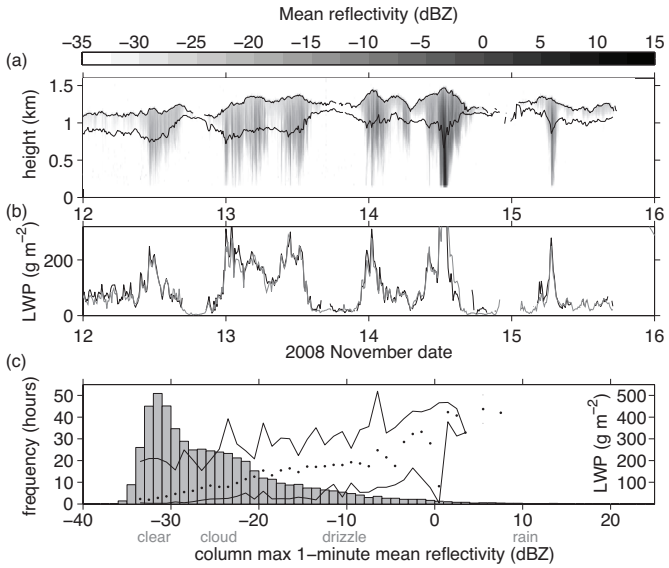

Figure 2. (a) Mean reflectivity from the W-band cloud radar for November 12-15, when the ship was near 20°S, 75°W. Thin lines are cloud top height estimated from the radar and cloud base height from the ceilometer. (b) Liquid water path (LWP) from the microwave instrument (black) and adiabatic LWP from cloud thickness (gray). There are two distinct peaks in cloud top, liquid water, and precipitation for each day, especially November 13-14. Bars in (c) show the frequency of occurrence in hours of column maximum reflectivity (dBZ) of 1-minute samples for all 538 hours of the VOCALS cloud radar record. The median and range of 10-minute LWP (g m-2, dots and lines) are binned by column maximum reflectivity.

maximum reflectivity (CMR) over all 538 hours the radar operated in VOCALS 2008. The 4-day period in Figs. 2a and b are a subset of these 538 hours. CMR is averaged over 1-minute intervals and counted in 1-dBZ wide reflectivity bins. Frequency of observing 1-minute mean CMR in each bin is given in hours. The mode of the distribution (-35 to -30 dBZ) represents clear-air noise and reflectivity too weak to exceed the level of instrumental noise. The distribution is positively skewed: 2% of minutes have CMR > -10 dBZ, 0.6% have CMR > 0 dBZ, 0.1% have CMR > 10 dBZ.

Liquid water path is composited within the 1-dBZ reflectivity bins. Dots in Figure 2c show the median LWP, and lines show the range of LWP found for each reflectivity bin. A linear fit of about 9 g m^{-2} per dBZ is reliable for clouds with weak (-35 to -20 dBZ) maximum reflectivity. The LWP-reflectivity relationship has weaker LWP dependence on CMR in the light drizzle regime of -20 to -10 dBZ. Columns with precipitation (0-10 dBZ) appear to contribute more strongly to LWP.

Columns with maximum reflectivity between -30 and -20 dBZ likely correspond to nonprecipitating clouds. A long tail of decreasing probability from -20 dBZ extends to about +10 dBZ. Column maximum reflectivity above -20 dBZ is associated with a distribution of Doppler velocities that is biased slightly downward, indicating that a subset of particles are large enough to fall and to be classified as precipitation. By about 0 dBZ columns almost certainly contain drizzle. Maximal reflectivity in a nonprecipitating cloud is probably found at cloud top, where the temperature is lowest and there is most condensate. Maximal reflectivity for a precipitating cloud is probably found at cloud base. Drizzle forms and falls out of the stratocumulus cloud and often re-evaporates before reaching the ground (cf. Figure 2a), thereby approximately conserving the combination of water vapor, liquid cloud, and rain water in the atmospheric column (Comstock et al., 2004).

The C-band radar scanned 60-km radius volumes and made four range-height scans along and across the prevailing wind direction every three minutes. Satellite images coincident with the volume scans show the pattern of clouds and their mesoscale organization. C-band radar volumes show the evolution of mesoscale precipitation structures within the clouds. Following the trend in the distribution of reflectivity from the W-band cloud radar, the distribution of C-band reflectivity is strongly skewed toward low values. The C-band radar fills in the higher ranges of reflectivity that the W-band cloud radar cannot observe. On a few occasions, small areas of precipitation greater than 40 dBZ were observed by the C-band radar. Scanning an 11 000 km^2 area continuously for more than 1000 hours, the C-band radar sampled mesoscale precipitation structure more than any other combination of instruments in the VOCALS regional experiment.

One hypothesis tested in VOCALS was whether drizzle is a necessary condition for the formation and maintenance of pockets of open-cell convection (POCs, Stevens et al., 2005). Precipitation observations from the C-band radar tell a subtler story. Cloud and precipitation images from satellite were classified into closed-cell conditions (unbroken clouds) or open-cell conditions (broken clouds). The C-band radar detects precipitation over the volume, so images can be categorized as drizzling or non-drizzling. Some open-cell scenes had drizzle, while other open-cell scenes had no C-band radar-detectable drizzle. Closed-cells were also observed both with and without C-band radar detectable drizzle. It is possible drizzle was present in open-cell clouds that was so light it could not be detected by the C-band radar. Unless cells pass directly over the ship, they cannot be observed by the vertically pointing W-band radar. Work is in progress to compare the statistics of the more sensitive W-band radar reflectivity over the ship with the C-band radar's less sensitive but wider-area measurements to assess the probability of missed drizzling echo under different cloudiness conditions.

Ship-based observations of clouds already provide valuable data for validating satellite products and numerical models over the southeastern tropical Pacific Ocean (e.g. Brunke et al., 2010). Further analysis of the observations will test the VOCALS hypotheses and refine our knowledge of cloud and precipitation processes in drizzling and non-drizzling stratocumulus clouds.

References

Brunke, M. A., S. P. de Szoeke, P. Zuidema, and X. Zeng, 2010: A comparison of ship and satellite measurements of cloud properties in the southeast Pacific stratus deck. *Atmos. Chem. and Phys. Disc*. in press.

Caldwell, P., C. S. Bretherton, and R. Wood, 2005: Mixed-lay budget analysis of the diurnal cycle of entrainment in southeast Pacific stratocumulus. *J. Atmos. Sci*. **62**, 3775-3791.

Comstock, K. K., R. Wood, S. E. Yuter, and C. S. Bretherton, 2004: Reflectivity and rain rate in and below drizzling stratocumulus. *Quart. J. Roy. Meteor. Soc*. **103**, 2891-2918.

de Szoeke, S. P., C. W. Fairall, D. E. Wolfe, L. Bariteau, P. Zuidema, 2010: Surface flux observations on the southeastern tropical Pacific Ocean and attribution of SST errors in coupled ocean-atmosphere models. *J. Climate*, submitted.

O'Dell, C. W., F. J. Wentz, and R. Bennartz, 2008: Cloud Liquid Water Path from Satellite-Based Passive Microwave Observations: A New Climatology over the Global Oceans. *J. Climate*, **21**, 1721-1739.

Rahn, D. and R. Garreaud, 2009: Marine boundary layer over the subtropical southeast Pacific during VOCALS-REx – Part 1: Mean structure and diurnal cycle. *Atmos. Chem. and Phys. Disc*. **9**, 26029-26062.

Stevens, B., G. Vali, K. Comstock, R. Wood, M. C. van Zanten, P. H. Austin, C. S. Bretherton, D. H. Lenschow, 2005: Pockets of open cells in and drizzle in marine stratocumulus. *Bull. Amer. Met. Soc*. **86**, 51-57. doi:10.1175/BAMS-86-1-51.

Tucker, S. C., and Coauthors, 2009: Doppler Lidar Estimation of Mixing Height Using Turbulence, Shear, and Aerosol Profiles. *J. Atmos. and Oceanic Tech*., **26**, 673-688.

Zuidema, P., E. R. Westwater, C. Fairall, and D. Hazen, 2005: Ship-based liquid water path estimates in marine stratocumulus. *J. Geophys. Res*. **110**, D20206. doi:10.1029/2005JD005833.

Climate Heat Balance off Western South America: Regional Oceanic Circulation and Eddies

McWilliams, J.C, and F. Colas
University of California, Los Angeles, USA
Corresponding author: jcm@atmos.ucla.edu

The coastal margin and adjacent ocean of western South America is climatically very interesting. It is home to El Niño near the equator. Further south off Peru and Chile it has distinctive elements of a stratus cloud deck; alongshore-parallel winds; upwelling boundary currents and mesoscale eddies; sharp changes at the coastline in the surface heat-moisture-drag fluxes; high marine biological productivity; biogenic and anthropogenic aerosol emissions; and subsurface hypoxia/anoxia. Some of these features have rather small lateral scales. Interannual variability can be large, e.g., due to nearby El Niños. In global coupled climate models, the simulation errors are relatively high in this region. There is also significant upscaling potential for regional influences on global features: by intervention in the near-boundary ocean fields in a coupled model, Large and Danabasoglu (2006) show significant, favorable impacts on tropical precipitation around the globe. The purpose of the VOCALS experiment is to understand the regional climate dynamics and its global importance.

We focus on the particular issue of near-surface heat balance. The stratus deck requires a cold oceanic surface for its existence, yet there is a strong atmospheric heating of the ocean of 40-100 W/m^2 (Colbo and Weller, 2007; deSzoeke et al., 2010) over a coastal transition zone several hundred km wide. The equilibrium oceanic circulation must provide a balancing lateral flux to keep the surface from warming. Yet the cooling by offshore Ekman transport (due to equatorward wind stress) of cold water (due to coastal upwelling) is too small to provide this balance by about a factor of two. The remaining oceanic advective heat flux divergence occurs through a combination of mean circulation and mesoscale eddy transport.

We report on how regional heat balance occurs in simulation of the general circulation off Peru and Chile. Our premise is that only with less compromised grid resolution, compared to what is globally feasible, can the upwelling currents and eddy processes be well represented. The domain extends in latitude between 40°S and 10ºN, and its zonal extent is more than 1000 km west from the South American coast; the horizontal grid scale is 7 km. This posing of the calculation uses mean-monthly climatological data for the open-ocean lateral boundary conditions and surface buoyancy and momentum fluxes, and the integration is performed over more than a decade to approximate equilibrium. The methodology and results are extensions of previous simulations by Penven et al. (2005) and Colas et al. (2008). The present simulation is more fully reported in Colas et al. (2010).

Peru and Chile provide an eastern boundary to the Pacific equatorial currents and subtropical gyre. The wind stress is mainly equatorward and is largest in two extrema around 15S and 30ºS. This contributes to somewhat different circulations off Peru and Chile, with the VOCALS measurements mostly located in the transition zone between them. Equatorward wind stress and its associated anti-cyclonic curl induce strong upwelling of cold water brought to the surface within about 50 km of the coast. With alongshore and time averaging, the circulation $\underline{\mathbf{u}}$ is equatorward near the surface and poleward in the Undercurrent against the continental slope, and it is offshore in the Ekman layer and onshore in the underlying thermocline (Strub et al., 1998). The coastal upwelling and horizontal circulation are zonally wider and vertically more superficial off Peru than Chile due to poleward decreases in the air-sea heat flux, density stratification, and deformation radius (inverse Coriolis frequency).

The regional circulation is baroclinically unstable and generates mesoscale eddies, with broad maxima in surface eddy kinetic energy associated with the separate Peru and Chile wind stress maxima. The offshore width of the eddy-active zone is about 500 km. There is generally good correspondence between the magnitude and geographical distribution of simulated eddy energy and the geostrophic estimate from altimetry, with sampling uncertainties at the level of tens of percent in both estimates.

The tendency equation for the temperature T at any point in the ocean involves thermal advection A and mixing D,

$$dT/dt = A + D.$$

For the time-average in climate equilibrium, the tendency vanishes and $\overline{A} + \overline{D} = 0$.

In our simulations the mixing is almost entirely due to the parameterized surface planetary boundary layer turbulence that transports the surface air-sea heat flux Q and mixes it

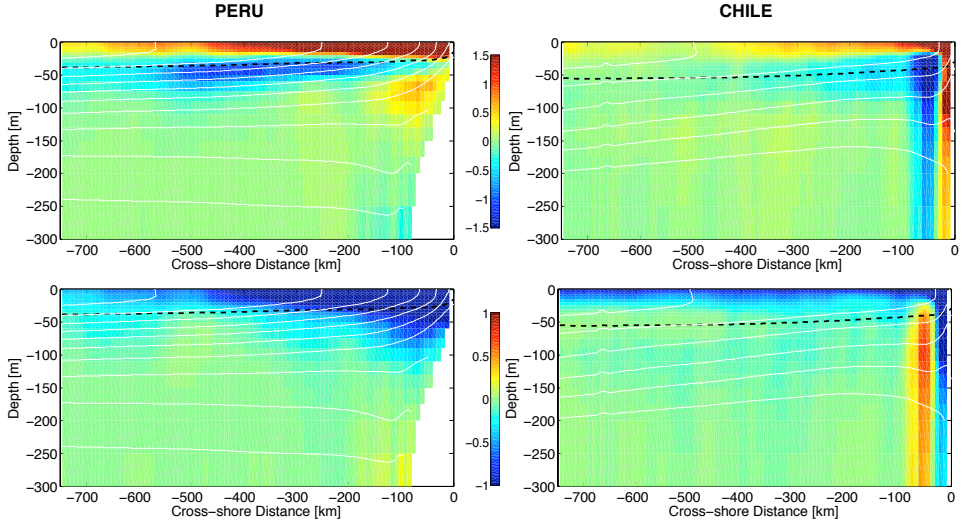

Figure 1 Vertical sections of annual-mean eddy $\overline{A}_e$ *(top) and mean* $\overline{A}_m$ *(bottom) advective heat flux divergence [W/m³], alongshore averaged between 7°S and 13°S (i.e., Peru; left) and between 25°S and 35°S (Chile; right). White contours indicate the mean temperature* $\overline{T}$ *(1°C intervals), and the black dashed line is the mean boundary-layer depth* $\overline{h}$ *.*

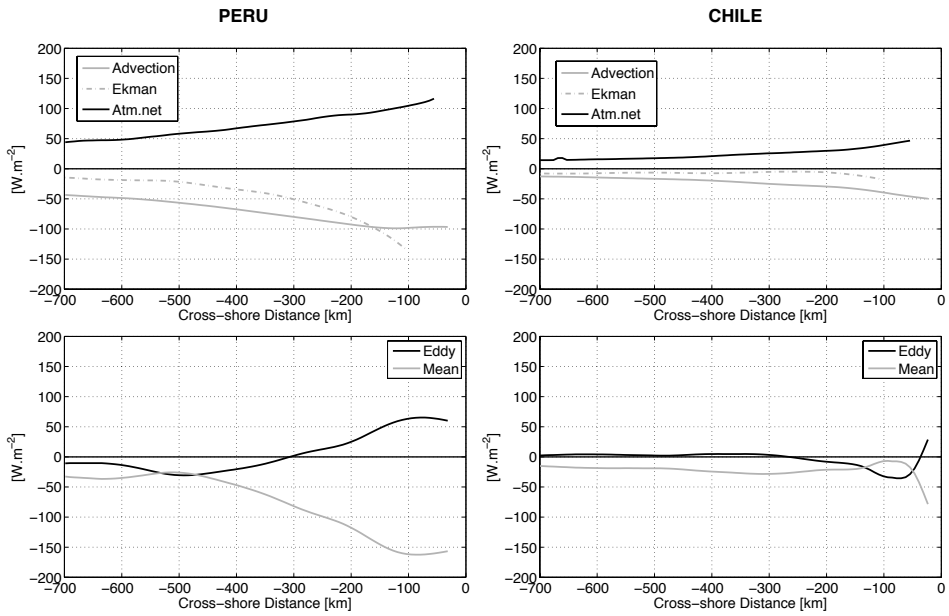

Figure 2 (Top) Annual-mean of vertically integrated (0 to 200 m depth) total advective heat flux divergence $\int \overline{A}\, dz$, Ekman-advection contribution, and net air-sea flux Q [W/m^2], averaged alongshore for the Peruvian (left) and Chilean (right) sectors. (Bottom) Decomposition of integrated advective heat flux divergence into contributions from mean circulation $\int \overline{A}_m\, dz$ and mesoscale eddies $\int \overline{A}_e\, dz$.

over the boundary layer thickness h; hence

$$\int D\, dz = Q.$$

This mixing contributes nothing to the climate equilibrium, hence the vertically integrated lateral oceanic heat flux divergence $\int \overline{A}\, dz$ must balance $\overline{Q}$, and the way this occurs in this region is our primary focus in this note. Since $\overline{Q} > 0$ (oceanic heating), $\int \overline{A}\, dz$ must be cooling (< 0).
If we decompose *T* and ***u*** into time-mean and fluctuating (eddy) components, then the mean advective tendency is the sum of mean and eddy quadratic products:

$$\overline{A} = \overline{A}_m + \overline{A}_e$$

$$\equiv - \nabla \cdot (\overline{\mathbf{u}}\, \overline{T} + [\overline{\mathbf{u}'T'}]).$$

$\overline{A}$ does have a lateral flux divergence, and its equilibrium vertical integral balance is

$$0 = \overline{Q} + \int \overline{A}_m\, dz + \int \overline{A}_e\, dz$$

Cross-sections of $\overline{A}_m$ and $\overline{A}_e$ for Peru and Chile are shown in Figure 1. Mean advection $\overline{A}_m$ is always cooling against the coast because of the upwelling. It also is always cooling in the surface layer, largely because of offshore Ekman transport of upwelled coastal water. Eddy advection $\overline{A}_e$ is a combination of cooling and warming. Adjacent to the coast and in the surface layer it is warming partly in cancellation with $\overline{A}_m$, but it also exhibits subsurface cooling in the offshore region. The mean and eddy flux divergence magnitudes are larger for Peru than Chile. The cross-shore width of the eddy-cooling zone is very much larger for Peru than Chile. For Peru it reaches more than 700 km offshore, while it is no wider than about 300 km off Chile and strongly negative only within 100 km of the coast. The offshore structure of eddy heating-above and cooling-below is a manifestation of restratification by eddy vertical buoyancy flux (i.e. $[\overline{w'T'}] > 0$), as is typical for eddy energy generation by baroclinic instability. The lateral heat exchange between the coast and offshore occurs mainly in the thermocline, with vertical eddy flux completing the connection to the surface.

The vertically integrated heat balance (Figure 2, top), as anticipated, shows $\overline{Q} > 0$ balanced by $\int \overline{A}\, dz < 0$ with both quantities increasing shoreward. Both are also larger in magnitude for Peru than Chile. $\int \overline{A}\, dz$ is larger than the Ekman transport contribution $(-\nabla \cdot \int \mathbf{u}_{EK}\, SST\, dz)$ except near the Peruvian coast, and the difference is provided by the rest of the mean and eddy advection. The vertical integrals of $\overline{A}_m$ and $\overline{A}_e$ are separated in Figure 2 (bottom). The mean circulation effect is always cooling, while the eddies are warming near the coast and cooling offshore, consistent with down-gradient flux across the cross-shore gradient in $\overline{T}$. Off Peru the eddy-cooling zone extends very far offshore, while it is limited to within 200 km of the Chilean coast.

In different simulations with nested grids and much finer horizontal resolution (dx = 0.5 km), there is a strong outbreak of submesoscale currents in the upper 100 m of the ocean. It takes the form of horizontal fronts and filaments in T and coherent spiral-arm vortices. In this case the vertical eddy heat increases substantially over the mesoscale simulation, again in the sense of density restratification but now additionally due to submesoscale fluctuations (as in the idealized eastern boundary current circulation simulation by Capet *et al*., 2008). This greatly enhances the eddy heating-above and cooling-below offshore structure seen in Figure 2 (top). However, it does not appreciably alter the vertically integrated heat balance in Figure 2 (bottom); i.e., $\overline{Q}$ is balanced by lateral heat flux divergence, and the eddy contribution to lateral flux is primarily by the mesoscale. Nevertheless, both mesoscale and submesoscale eddies influence the upper oceanic thermal profile through their restratification flux. There is a partly compensating increase in the destratifying flux of the boundary layer turbulent mixing D in response to increased eddy flux, even for a fixed level of turbulent kinetic energy, because of the modest increase in mean stratification.

In summary, oceanic cooling by lateral heat transport from the upwelling coastal zone is essential to maintain the surface SST conditions necessary for the stratus cloud regime off South America. Both mean currents and eddies participate in this lateral flux in various combinations with season and locale (n.b., the alongshore structure of the heat balance is not discussed here). Direct empirical verification of the circulation effects is still elusive in part because sampling uncertainty is large for eddy fluxes, especially at specific geographical locations (rather than with alongshore, as here, or other spatial averaging).

We have made this demonstration in a regional equilibrium oceanic simulation that adequately resolves the upwelling

circulation and eddies. They are more difficult to represent in coarser-grid global models, but nevertheless these regional oceanic effects are essential for maintaining the regional climate.

Two recent papers also examine the Peru-Chile regional heat balance: Toniazzo et al. (2009) with an eddy permitting, global coupled climate model and Zheng et al. (2010) with an eddy-resolving global oceanic general circulation model. Both see clear eddy heating adjacent to South America and at least some instances of offshore eddy cooling, although the point-wise sampling estimation errors are large in their maps for $\int \overline{A}\, dz$ (especially in the latter study). The latter paper concludes that the eddy role is very small averaged over the very large region of the Southeastern Pacific stratus deck, but this includes the far-offshore region where $\overline{Q}$ drops to a very small value (~10 W/m^2), and the balancing oceanic cooling is correspondingly small.

References

Capet, X., J. C. McWilliams, M. J. Molemaker, and A. Shchepetkin, 2008: Mesoscale to submesoscale transition in the California Current System. I: Flow structure, eddy flux, and observational tests. J. *Phys. Ocean*., **38**, 29-43.

Colas, F., J. C. McWilliams, X. Capet, and J. Kurian, 2010: Dynamics of the Peru-Chile Current System. *J. Geophys. Res*., submitted.

Colas, F., X. Capet, J. C. McWilliams, and A. F. Shchepetkin, 2008: 1997-98 El Niño off Peru: A numerical study. *Prog. Ocean*., **79**, 138-155.

Colbo, K. and R. A. Weller, 2007: The variability and heat budget of the upper ocean under the Chile-Peru stratus. *J. Marine Res*., **65**, 607-637.

de Szoeke, S. P., C. W. Fairall, D. E. Wolfe, L. Bariteau, and P. Zuidema, 2010: Surface flux observations on the southeastern tropical Pacific Ocean and attribution of SST errors in coupled ocean-atmosphere models. *J. Climate*, submitted.

Large, W. G. and G. Danabasoglu, 2006: Attributions and impacts of upper-ocean biases in CCSM3. *J. Climate*, **19**, 2325-2346.

Penven, P., V. Echevin, J. Pasapera, F. Colas, and J. Tam, 2005: Average circulation, seasonal cycle, and mesoscale dynamics of the Peru Current System: A modeling approach. *J. Geophys. Res*., **110**, doi:10.1029/2005JC002945110.

Strub, P. T., J. M. Mesias, V. Montecino, J. Ruttlant, and S. Salinas, 1998: Coastal ocean circulation off western South America. In: *The Sea*. John Wiley & Sons, Boston, **11**, 29-67.

Toniazzo, T., C. R. Mechoso, L. C. Shaffrey, and J. M. Slingo, 2009: Upper-ocean heat budget and ocean eddy transport in the southeast Pacific in a high-resolution coupled model. *Climate Dyn.*, doi 10.101007/s00382-009-0703-8.

Zheng, J., T. Shinoda, G. N. Kiladis, J. Lin, E. J. Metzger, H. E. Hurlburt, and B. S. Giese, 2010: Upper-ocean processes under the stratus cloud deck in the Southeast Pacific Ocean. *J. Phys. Ocean*., **40**, 103-120.

Connection between the South Pacific anti-cyclone, Peruvian Stratocumulus and the South American Monsoon System

Ma, H. -Y.[1], C. R. Mechoso[1], H. Xiao[1], C. -M. Wu[1], Y. Xue[1,2], and F. De Sales[2]
[1]Department of Atmospheric and Oceanic Sciences, University of California Los Angeles, Los Angeles, CA
[2]Department of Geography, University of California Los Angeles, Los Angeles, CA
Corresponding author: hyma@ucla.edu

1. Introduction

The South American Monsoon System (SAMS) affects and is affected by several other climate features, such as the Intertropical Convergence Zone (ITCZ) and sea surface temperature (SST) distributions over both the Pacific and Atlantic Oceans, and the stratocumulus clouds decks in the southeastern tropical Pacific (Nogués-Paegle et al., 2002; Vera et al., 2006). Monsoon convection associated with SAMS originates both Kelvin waves that propagate eastward and Rossby waves that propagate westward and poleward with associated subsidence that can be enhanced by diabatic and other effects (Rodwell and Hoskins, 2001; Miyasaka and Nakamura, personal communication).

The existence of these interactions suggests that simulation of the oceanic features by a coupled ocean-atmosphere general circulation model (CGCM) would be sensitive to the representation of convection over the continents in the atmospheric component (AGCM). In this case, different treatments of land surface processes (LSPs) would impact the results over both continents and oceans. An intriguing possibility, therefore, is that upgrading the LSP parameterization might help reduce the systematic errors in the tropics that plague CGCMs (e.g., Mechoso et al., 1995).

The present paper explores such possibility of error reduction. The topic is well aligned with one of the main goals of VOCALS, which is the elimination of tropical errors of CGCMs. Our approach is based on comparing northern winter simulations by a CGCM with different land surface schemes. We have already determined in an AGCM study (Ma et al., 2010) that the simulation of diabatic heating over the South American continent is sensitive to the representation of LSPs. For example, upgrading the LSP parameterization as described later in Section 2 improved the simulation of precipitation over the tropical region - including Amazonia - and provided a stronger and more realistic surface heat flux in the Chaco Low over the central region. Differences in the simulations over the tropical oceans are not affected by oceanic feedbacks, however, as the same SST distribution is prescribed in the AGCM runs with the different LSP parameterizations. In the present paper we examine whether the results in Ma et al. (2005) are affected by allowing for atmosphere-ocean interactions, i.e. by using a CGCM. The remainder of the text is organized into three more sections. Section 2 provides a brief reference of models and experiments. Section 3 examines the response of the south Pacific anti-cyclone and Peruvian stratocumulus to different convection intensity and distribution from two LSP schemes. Section 4 presents a summary of the results.

2. Models and Experiments

We examine two century-long simulations with the University of California Los Angeles (UCLA) AGCM version 7.1 (Mechoso et al., 2000) coupled to the global Massachusetts Institute of Technology oceanic GCM (MIT OGCM, http://www.mitgcm.org). The horizontal resolution of the AGCM is 2.5° longitude and 2° latitude; there are 29 layers in the vertical. The horizontal resolution of the OGCM is 1° longitude and 0.3° latitude within 10° of the Equator increasing to 1° latitude poleward of 22°N and of 22°S; there are 46 levels in the vertical.

One CGCM experiment is control, and is performed with a simple LSP scheme that specifies soil moisture availability (Ma et al., 2010). The other experiment is with the same model, except for use in the AGCM component of the first generation of Simplified Simple Biosphere Model (SSiB; Xue et al., 1991). Both simulations produce reasonable amounts of annual mean precipitation and SST distributions, and a good seasonal cycle of equatorial Pacific SST. In general, the simulation is more successful when SSiB is used. The experiments with the simple land scheme and with SSiB will be referred to as CGCM/SLS and CGCM/SSiB, respectively. In the following we concentrate

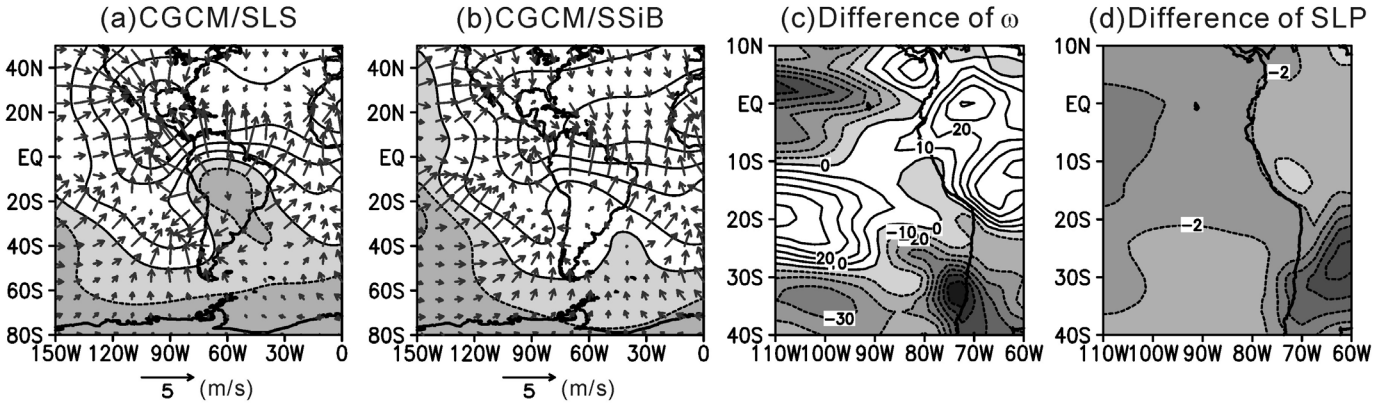

Figure 1: Dec-Feb mean velocity potential ($m^2 \cdot s_{-1}$, shaded) and divergent winds ($m \cdot s^{-1}$) at 200 hPa from the CGCM with (a) the simple land scheme and (b) SSiB. Also plotted is the difference between the CGCM with SSiB and with the simple land scheme of (c) vertical velocity ($mb \cdot day^{-1}$), at 700 hPa and (d) sea level pressure (hPa).

on South America and the southeastern Pacific (SEP) during the December - February (DJF) period.

3. Response of South Pacific anticyclone and Peruvian stratocumulus

According to Ma et al. (2010), incorporation of SSiB in the UCLA AGCM has a significant impact on the intensity and vertical profile of diabatic heating over the continents. In particular for South America, the comparison between CGCM/SLS and CGCM/SSiB reveals that the latter simulation produces significant less precipitation in the core region of SAMS, and higher sensible heat flux at the surface over central sector with a strengthened Chaco low. Furthermore, the simulation with the more detailed LSP scheme is closer to the observation.

Figures 1a and 1b present the DJF mean velocity potential and divergent wind fields at 200 hPa from CGCM/SLS and CGCM/SSiB, respectively. At that level there are strong divergent outflows from the core region of SAMS in CGCM/SLS. These outflows are weaker in CGCM/SSiB, as expected from the weaker (and more realistic) convection obtained with this model configuration. Figures 1c and 1d present the differences between the DJF mean vertical velocity (subsidence) and sea level pressure from CGCM/SLS and CGCM/SSiB, respectively. The values of these two fields in the SEP are weaker in CGCM/SSiB. This simulation, therefore, produces a weaker South Pacific high in the SEP.

We next focus on the total cloud cover along the Peruvian coast where the contribution from the stratocumulus is dominant. According to Figure 2 for DJF, both model versions produce too high and extensive cloud cover compared to observational estimates by the International Satellite Cloud Climatology Project (ISCCP). Nevertheless, CGCM/SSiB shows decreased and better total cloud cover and closer agreement with the observation.

Let us attempt an interpretation of these results in the light of connections among monsoon, anticyclone, and stratocumulus found in previous specialized studies with GCMs in both idealized and realistic scenarios. From Rodwell-Hoskins we expect a weaker South Pacific anticyclone in CGCM/SSiB, in which SAMS is weaker. The impact expected from Miyasaka-Nakamura is in the opposite direction: we expect a stronger South Pacific anticyclone in CGCM/SSiB, in which low-level diabatic heating over the Chaco Low is stronger. The longwave cooling over the less extensive stratocumulus decks is weaker, however. In principle, therefore, the two mechanisms mentioned would compensate each other, at least partially. Our results indicate that the Rodwell-Hoskins dominates farther away from the South America coast, where sea level pressure decreases in CGCM/SSiB; while Miyasaka-Nakamura prevails near the coast, along which low-level southerlies strengthen.

Additional effects arise in the coupled system since SST changes can also impact stratocumulus coverage. We indicated earlier in this section that stratocumulus incidence and extent is better captured in CGCM/SSiB. The stratocumulus amount in the observation is positively correlated with the inversion strength or static stability of the lower troposphere (Klein and Hartmann 1993), which is defined as the potential temperature difference between 700 hPa and the surface. The change of cloud incidence between the two simulations we are analyzing is consistent with the change in static stability of the lower troposphere. A close look at the reasons for changes in this parameter reveals that they are both due to weaker subsidence and warmer SSTs along the Peruvian coast. With less stratocumulus and more solar radiation incident at the ocean surface, the SST becomes warmer, which leads to lesser clouds and even warmer SST in a positive feedback. In contrast, in the uncoupled AGCM experiments (not show) cloudiness over the SEP is hardly affected since the same SST distribution is prescribed.

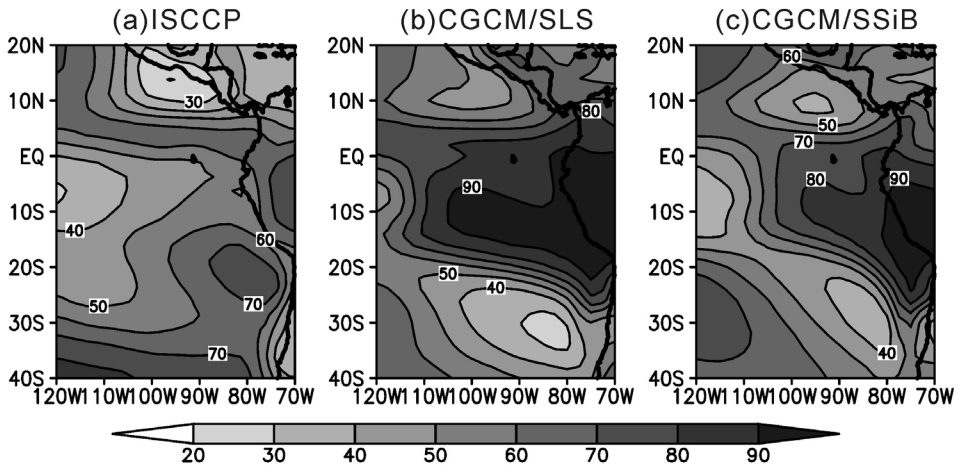

Figure2 Dec-Feb mean total cloud cover (%) from (a) ISCCP, (b) CGCM with the simple land scheme, and (c) CGCM with SSiB.

4. Summary

We examined the connection between the strength of the South Pacific anti-cyclone, Peruvian stratocumulus, and the South American Monsoon System. The approach is based on experiments with a coupled ocean-atmosphere GCM in which different parameterizations of LSPs in the atmospheric model provide different representations of convection over the continents in general and South America in particular. Using the more detailed parameterization (SSiB, an advanced land surface model that allows for consideration of soil and vegetation biophysical processes) the simulation of the coupled atmosphere-ocean system is more successful than with the simpler scheme.

The CGCM/SSiB simulation shows weaker convection over tropical South America, and an enhanced Chaco Low. The impact on the southeastern Pacific involves subsidence weakening and SST increasing, both of which contribute to the lower but more realistic Peruvian stratocumulus amount. The lower sea level pressures away from the South American coast are consistent with decreased convection over Amazonia (Rodwell-Hoskins mechanism). However, this outcome was not evident a priori since erroneous convection decrease over central South America is replaced by stronger low level heating over the Chaco Low, which would enhance the sea level pressures to the west (Miyasaka and Nakamura mechanism). In addition, the enhanced low-level heating is partially compensated by reduced stratocumulus incidence in the SEP. The results suggest that the stronger Chaco Low leads to stronger low-level southerlies along the coast.

An important result is that including atmosphere-ocean interactions strongly influences the simulations by allowing for establishment of positive feedbacks between stratocumulus and underlying SST. Stratocumulus incidence decreases in the SEP despite weaker subsidence in the region as static stability of the lower atmosphere weakens primarily due to SST increase.

Our current research aims to clarify further the connections between other monsoons and contemporary oceanic features. We have not shown here, for example, that the other systematic errors of the CGCM in the tropics also appear to decrease with a better simulation of the monsoons. A confirmation of this result would help achieve one of the primary goals of VOCALS.

Acknowledgements: This research was supported by NOAA under grant NA07OAR4310236. Computing resources were provided from the NCAR Computational and Information Systems Laboratory.

References

Klein, S. A. and D. L. Hartmann, 1993: The seasonal cycle of low stratiform clouds. *J. Climate*, **6**, 1587-1606.

Ma, H. -Y., C. R. Mechoso, Y. Xue, H. Xiao, C. -M. Wu, J. -L. Li, and F. De Sales, 2010: Impact of land surface processes on the South American warm season climate. *Clim. Dyn*. Sub Judice.

Mechoso, C. R., J. –Y. Yu and A. Arakawa, 2000: A coupled GCM pilgrimage: From climate catastrophe to ENSO simulations. General Circulation Model Development: Past, present and future. Proceedings of a Symposium in Honor of Professor Akio Arakawa. D. A. Randall. Ed., Academic Press, 539–575.

Mechoso C. R., and Co-Authors, 1995: The seasonal cycle over the Tropical Pacific in General Circulation Models. *Mon. Wea. Rev*., **123**, 2825-2838.

Nogués-Paegle, J. and Co-Authors, 2002: Progress in Pan American CLIVAR Research: Understanding the South American Monsoon. *Meteorológica*, **27**, 3-33.

Rodwell, M. J., and B. J. Hoskins, 2001: Subtropical anticyclones and summer monsoons. *J. Climate*, **14**, 3192-3211.

Vera C., et al. 2006: Toward a unified view of the American Monsoon Systems. *J. Climate*, **19**, 4977–5000.

Xue, Y., P. J. Sellers, J.L. Kinter III, and J. Shukla, 1991: A simplified biosphere model for global climate studies. *J. Climate*, 4, 345–364.

One VOCALS perspective on precipitation closure

Zuidema, P.[1], D. Leon[2], J. R. Snider[2], and R. Wood[3]
[1]University of Miami, Miami, FL. USA., [2]University of Wyoming, Laramie, WY. USA., [3]University of Washington, Seattle, WA. USA.
Corresponding author: pzuidema@rsmas.miami.edu

Stratocumulus albedo is central to the large-scale planetary radiative energy budget. The albedo is primarily determined by cloud fraction and cloud optical depth, which in turn depend on liquid water path LWP and cloud particle size (or cloud droplet concentration N_d), all influenced by processes occurring at small scales. The vertically-integrated cloud liquid water amount is also a key measurement for quantifying, understanding, and modeling aerosol indirect effects (see, e.g., article by Twohy et al., this issue); for distinguishing aerosol from synoptic influences; and for precipitation production. Yet, LWP has been difficult to measure or retrieve in previous aircraft deployments relying on sparsely-sampled profiles, or on coordination with other aircraft enabled with remote sensors.

A unique aspect of the US contribution to the VOCALS Regional Experiment was the inclusion of three cloud remote sensors on the NCAR C-130: the Wyoming Cloud Lidar, the 94 GHz Wyoming Cloud Radar, and an 183 GHz millimeter radiometer. During the subcloud leg traverses the three upward-pointing sensors provided complementary observations of the cloud macrophysics (i.e. cloud boundaries), microphysics (in particular, precipitation), and cloud liquid water path. The vertical column sampled simultaneously, so that measurements of vertically-integrated quantities such as cloud thickness and liquid water path co-occured with a radar-derived view of the precipitation vertical structure. This was a useful complement to *in situ* aircraft measurements of the microphysical and aerosol environment at the flight altitude. The radar had been previously used to study Californian marine stratocumulus (e.g., Leon, 2006), while this was the first stratocumulus Wyoming cloud lidar deployment, and the first (and last) for this particular multi-channel millimeter radiometer (Pazmany, 2006).

A scientifically interesting and useful application for this combination of instruments is acquiring statistics on precipitation sensitivities to LWP and N_d. Precipitation is known to increase with LWP and decrease with N_d but the exact sensitivity is less well-known. Brenguier and Wood (2009) present a compilation from previous field campaigns of observational and modeling rainrate (RR) sensitivities to $LWP^a N_d^{-b}$. Values for "a" only range between 1.5-2.0, but values for "b" range from 0.6 to 1.75 (see also Wang and Feingold, 2009), reflecting a more uncertain understanding of the role played by aerosol. In their figure, a qualitative agreement between the different field campaigns co-exists with order-of-magnitude differences in the rainrates for a given LWP and N_d. Intuitively, one would expect similar microphysical process rates that are independent of location, so that differences between the results from different campaigns probably reflect differences in methodologies and instrumentation. Different model simulations of cloud behavior, done with the results of the individual field campaigns in mind, also show varying agreement with the observed relationships. These factors highlight the need for additional datasets.

A preliminary $RR\_ LWP^a N_d^{-b}$ analysis is shown for VOCALS in Figure 1, comprising data from approximately two-thirds of the subcloud legs. We selected a value for $"a"$ of 3/2 and for $"b"$ of 2/3 based on a subjective best-fit assessment of several published values. The mostly linear relationship between RR and $LWP^{3/2} N_d^{-2/3}$ already suggests a rainrate parameterization

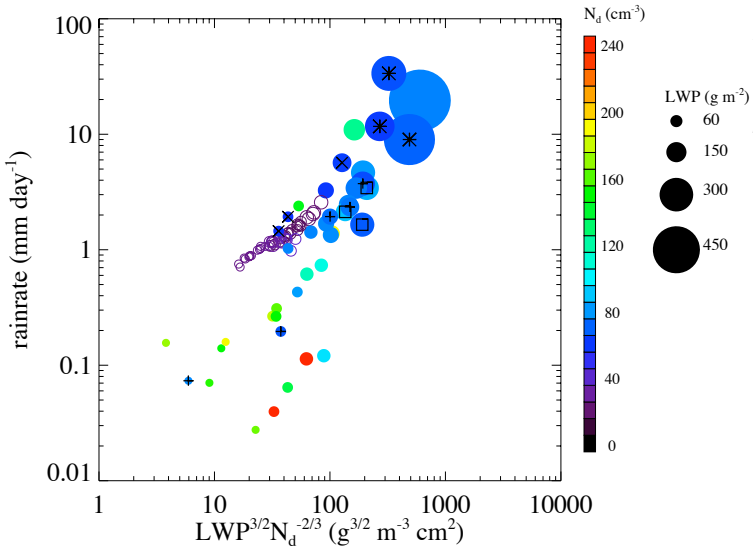

Figure 1: Cloud-base precipitation versus (liquid water path or $LWP)^{3/2}$(cloud droplet number concentration or N_d $)^{-2/3}$, typically averaged over 10-minute intervals. Color denotes N_d concentration, estimated from the accumulation-mode aerosol measured at the sub-cloud flight altitude, and circle size is proportional to LWP. "+" denotes a leg crossing an open/closed cell boundary; squares, X and asterisks indicate closed, open and boundary cells respectively. Open circles denote values reproduced from Wang and Feingold, 2009, Figure 9b; their open- and closed-celled structures are not identified separately.

with less sensitivity to N_d than previously derived for the southeast Pacific (e.g., Comstock et al., 2004). For the typical adiabatically-distributed liquid water contents of the southeast Pacific stratocumulus region, a value of 3/2 for "*a*" is equivalent to the cube of the cloud depth (see article by de Szoeke et al. this issue), though in practice different instrument sensitivities need to be considered. The *LWP* values were retrieved using a modification of Zuidema et al. (2005), with the above-aircraft water vapor path estimated from a combination of aircraft data and above-cloud 183 GHz brightness temperatures. The van Zanten et al. (2005) cloud base precipitation - radar reflectivity relationship, developed from data gathered by the same cloud radar during a Californian stratocumulus experiment, was applied to the maximum radar reflectivity within each vertical column. Column-maximum radar reflectivities tend to occur near cloud base for the more heavily precipitating stratocumulus clouds (> 0.1 mm day-1). N_d is estimated from the sub-cloud accumulation-mode aerosol concentration N_a using an empirical fit developed from all VOCALS leg-mean in-cloud N_d and sub-cloud N_a values (Snider et al., 2009).

The low *LWP*/high N_d points are associated with the more coastal clouds in Figure 1, and high *LWP*/low N_d points with offshore clouds. Several of the aircraft flight legs sampled open/closed cell structures and the boundary cells in between, typically within the same 10-minute leg. Open- and closed-cell mesoscale structures are of particular scientific interest because the structures have similar thermodynamic profiles, but have wildly different albedos. The relevant processes have proved challenging to simulate. In Figure 1, the leg averages not subdivided by cellular structure do not seem to differ markedly in *RR* or *LWP* from other flights simply sampling along 20°S, though they do consistently report low N_a values. For one flight shown, the three legs were further subdivided by cellular structure (open, closed, or boundary). For these, the closed cells have higher *LWP* (and N_d) than the open cells, but similar rainrates. The boundary cells are more remarkable, with high *LWP*s and rainrates up to and exceeding 10 mm/day (equivalent to a latent heat flux of ~ 300 W m^{-2} over a 3-4 minute time span). They are among the highest values shown here.

Comparable results from a mesoscale simulation study of stratocumulus open-cell development (Wang and Feingold, 2009, Figure 9b) are also shown and show basic agreement (differences from the observations may still reflect our preliminary analysis). Rather, the main difference between the simulation and observations suggested by Figure 1 is the larger parameter space of the observations. This in turn suggests highly vigorous stratocumulus dynamics occur in nature that are not easily captured by even a sophisticated simulation. In addition, the similarly high *LWP*s and *RR* observed during a different flight on October 21 are associated with a deep, synoptically-induced boundary layer possessing a high cloud cover (discussed in Painemal and Zuidema, 2009 and others at http://www.atmos-chem-phys-discuss.net/special_issue111.html). This suggests another modeling challenge, in that high stratocumulus precipitation rates need not imply an open/closed cell transition.

Figure 1 provides a taste of the results we can expect to glean more fully from forthcoming, more comprehensive analysis of VOCALS measurements by the many investigators involved. The Figure 1 provides a static snapshot of an inherently dynamical process, but such analysis and comparison of observational and modeling metrics will ultimately improve confidence in the models we use to gain insight into the Earth's future climate.

Acknowledgements:
We thank Hailong Wang and Graham Feingold for providing their model values, included in Figure 1.

References:

Brenguier, J.-L. and R. Wood, 2009: From the micro-scale to the meso-scale. From the *Strungmann Forum Report*, Clouds in the Perturbed Climate System: Their Relationship to Energy Balance, Atmospheric Dynamics, and Predicipitation. Ed. by J. Heintzenberg and R. Charlson, MIT Press. ISBN 978-0-262-01287-4.

Comstock, K., R. Wood, S. Yuter, and C. Bretherton, 2004: Reflectivity and rain rate in and below drizzling stratocumulus. *Q. J. Roy. Meteor. Soc.*, **130**, 2891-2919.

Leon, D., 2006: Observations of drizzle-cells in marine stratocumulus, 165 pp. U. of Wyoming, Laramie, WY.

Painemal, D. and P Zuidema, 2009: Synoptically-induced variability in the microphysical properties of the Southeast Pacific stratocumulus deck. *Atmos. Chem. Phys. Disc.*, 9, 25523-25564.

Pazmany, A, 2006: A compact 183 GHz radiometer for airborne and ground-based water vapor and liquid water sensing. IEEE Trans. *Geosci. Rem. Sens.*, **45**(7), pp. 2202-2206.

Snider, J. R., D. Leon, Z. Wang, L. Shank, and S. Howell, 2009: From aerosol to cloud droplet number concentration in VOCALS-REx. *EOS Trans. AGU*, **90**(52), Fall Meet. Suppl., Abstract A13J-0457

van Zanten, M.C., B. Stevens, G. Vali, and D. H Lenschow, 2005: Observations of drizzle in nocturnal marine stratocumulus. *J. Atmos. Sci.*, **62**, pp. 88-106.

Wang, H. and G. Feingold, 2009: Modeling mesoscale cellular structures and drizzle in marine stratocumulus, Part I: Impact of drizzle on the formation and evolution of open cells. *J. Atmos. Sci.*, **66**, pp. 3237-3256.

Zuidema, P., E. Westwater, C. Fairall and D. Hazen, 2005: Ship-based liquid water path estimates in marine stratocumulus. *J. Geophys. Res.* **110**, D20206, doi: 10.1029/2005JD005833.

Atmospheric transport of anthropogenic oxidized sulfur over the Southeast Pacific during VOCALS REx

Spak, S.N.[1], Mena M.A.[2], Carmichael G.R.[1]
[1]Center for Global and Regional Environmental Research, University of Iowa, [2]Facultad de Ecología y Recursos Naturales, Universidad Andrés Bello
Corresponding author: scott-spak@uiowa.edu

Introduction

One of the primary motivations for the VOCALS project is to improve understanding of processes of climatic importance in the eastern boundary coastal areas of the Southeast Pacific across spatial and temporal scales. Among these processes, the impacts of natural and anthropogenic aerosols on the physical and optical properties of the region's extensive marine stratocumulus (Sc) are of particular importance to understanding the energy balance between clouds, ocean and atmosphere. Sulfate (SO_4^{2-}) is among the primary aerosol species of interest, and the consistent presence of anthropogenic sulfur dioxide (SO_2) and SO_4^{2-} off the coast of Chile and Peru has been firmly established by in-situ VOCALS REx field observations and by satellite retrievals of SO_2 (Carn et al., 2007). Modeling has suggested episodic transport of SO_4^{2-} from large point sources in northern Chile potentially increasing cloud droplet number concentration in the region's Sc decks in winter, when synoptic conditions lead to strong easterly winds (Huneeus et al., 2006). However, the lower climatological rates of SO_4^{2-} transport during austral spring, when ocean-atmosphere coupling is strongest, have not been quantified. Biogenic dimethylsulfide (DMS) also oxides to form SO_2 and SO_4^{2-}, so constraining the budget of marine SO_4^{2-} is important for attribution of SO_4^{2-} and its climatic effects on the region's radiative and cloud properties. Shipboard measurements from the National Oceanographic and Atmospheric Administration Research Vessel *Ronald H. Brown* during VOCALS REx indicated a DMS flux from the surface of the ocean of 3-4 μmoles/m^2/day, with average DMS concentrations of 40-60 ppt in the marine boundary layer (MBL) and <10 ppt in the free troposphere (Yang et al., 2009). Both surface and aircraft measurements suggested a clean offshore MBL, with SO_2 concentrations typically <25 ppt, indicating a limited role for anthropogenic sulfur pollution in the offshore MBL sulfur cycle. Meanwhile, strong diurnal cycles have been identified in surface winds (Muñoz, 2008) and MBL height (Rahn and Garreaud, 2009a), two factors that strongly influence atmospheric transport. Here we apply regional scale atmospheric chemical transport modeling to quantify the contributions of anthropogenic sulfur emissions to SO_2 and SO_4^{2-} within and above the MBL, and to identify temporal features in sulfur transport over the Southeast Pacific during VOCALS REx.

Approach

Using hourly simulations with the Weather Research and Forecasting model 3.1 (Skamarock et al., 2008) and the STEM chemical transport model (Carmichael et al., 2003) at 12 km horizontal resolution, we follow atmospheric transport and fate during the VOCALS REx period of October 15 - November 15, 2008. We include recent reported and estimated SO_2 emissions from more than 1,400 points sources in Chile and southern Peru, including volcanoes (http://www.cgrer.uiowa.edu/VOCA_emis/), recognizing that the largest coastal power plants and smelters are responsible for most of the region's total emissions in contemporary inventories (Huneeus et al., 2006).

Regional sulfate distribution

Modeled average SO_4^{2-} concentrations at the surface (Figure 1a) and cloud level (Figure 1b) show a strong coastal plume from the Ilo smelter in southern Peru. As the largest point sources typically have stacks at least 50 m high and coastal emissions are readily entrained above the MBL inversion, spatial patterns in dispersed anthropogenic SO_4^{2-} concentrations at cloud level are comparable to those at the surface. We find high concentrations along the Chilean coast and a large area of dispersed SO_4^{2-} over the ocean due to emissions from central Chile, which are advected northwest over the ocean by the mean eastern boundary flow.

Synoptic variability in anthropogenic sulfate aerosol

From daily model forecasts, we identified five of fourteen NCAR C-130 research flights with elevated levels of SO_4^{2-} from point sources at the surface near the Atacama coast (RF03-RF06 and RF10), which were typically 0.25 - 0.5 μg/m^3 higher than the average during the campaign. These and similar days during the campaign with higher coastal pollution in the MBL were marked by an eastward shift in the surface pressure maximum of the Southeast Pacific Anticyclone due to synoptic disturbances, leading to a narrowing of the coastal airmass and stronger associated southerly coastal winds (Garreaud and Muñoz, 2005). Modeled cloud level differences in average SO_4^{2-} concentrations between these five flight days and the other nine (Figure 2) show that the conditions which led to an intensification of local MBL coastal plumes also reduced transport to the open ocean, with a more coastal path for the distinct polluted Sc tongues from central Chile. Under these conditions, SO_4^{2-} due to point source emissions in northern Chile and southern Peru is directed into the MBL, leading to a >50% reduction in local coastal cloud level concentrations. These results highlight that both central Chile and the large point source point sources further north contribute substantially to anthropogenic sulfur in both coastal and open ocean Sc during austral spring.

Coastal and offshore variability in anthropogenic sulfur

Hourly time series of simulated surface and cloud level SO_2 at coastal Point Alpha (72ºW, 20ºS) and Woods Hole Oceanographic Institute's Stratus buoy (85º W, 20º S) illustrate coastal and open ocean variability in pollution transport, respectively (Figure 3). Here, SO_2 is an effective proxy for total oxidized sulfur over the open ocean, as time series of SO_2 and SO_4^{2-} are highly correlated ($r^2 > 0.94$ in every model vertical layer in the troposphere). Modeled MBL and free troposphere anthropogenic SO_2 at the buoy are also highly correlated, approaching 1 ppt only during distinct episodes, which correspond to periods with positive modeled and observed MBL anomalies driven by synoptic disturbances (Rahn and Garreaud, 2009b). By comparison, SO_2 at Point Alpha episodically exceeds 100 ppt. This supports observational evidence (e.g Yang et al., 2009) that biogenic DMS, not included in this simulation, dominates the MBL sulfur budget far offshore, and strongly affirms the hypothesis that biogenic rather than anthropogenic SO_{42-} is responsible for the majority of cloud condensation nuclei there. We note that SO_2 and SO_4^{2-}

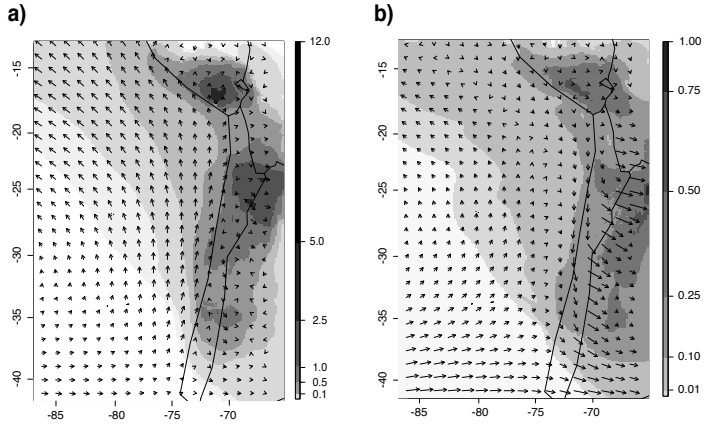

Figure 1. Simulated 10/15/2008 - 11/15/2008 average large point source SO_4^2 concentrations (μg/m^3) and wind vectors at a) surface and b) cloud level.

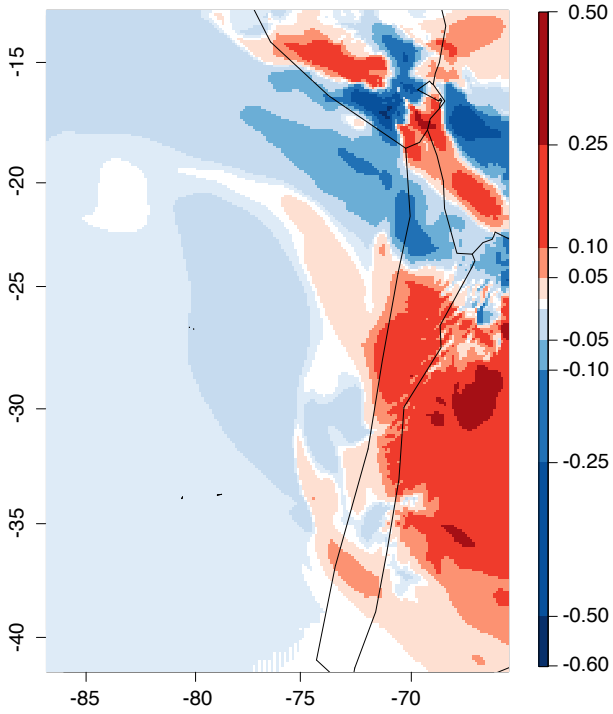

Figure 2. Simulated daily average enhancement in cloud level large point source SO_4^{2-} concentrations (μg/m³) during five NCAR C-130 research flights (RF03-RF06 and RF10) marked by high coastal SO_4^{2-}.

maxima at the buoy occur on days when a SO_4^{2-} plume from central Chile is evident at 20º S latitude (Figure 2). Both SO_4^{2-} and SO_2 concentrations at the buoy are consistently highest directly above the MBL. Diurnal variability due to the diurnal cycle of MBL height is apparent at Point Alpha, especially near the surface, and is reduced during days with strong synoptic influences. Diurnal variability at the Stratus buoy is apparent in and above the MBL throughout the REx period, but is much weaker than the episodic influence, again supporting the dominance of DMS in diurnal cycles of oxidized sulfur.

Summary

We find that the anthropogenic SO_2 emissions impacting coastal stratocumulus were unlikely to contribute to observed concentrations of oxidized sulfur far offshore during the VOCALS REx campaign under typical austral spring conditions, providing evidence that dimethylsulfide is responsible for most observed SO_2 and SO_4^{2-} over the open ocean. Episodic variability in atmospheric transport of anthropogenic oxidized sulfur over the Southeast Pacific is driven by synoptic disturbances correlated with an eastward shift in the Southeast Pacific High, affirming the importance of this climatic driver in modulating the influence of anthropogenic aerosols on both coastal and offshore marine stratocumulus, and their associated feedbacks to local and regional climate. Ongoing efforts in coupled ocean-atmosphere-chemistry modeling will better quantify the impacts of natural and anthropogenic aerosols on marine stratocumulus and further address the complex interactions between aerosols and regional climate.

Acknowledgements

We gratefully acknowledge support from NSF (0748012) and FONDECYT (11090084).

References

Carmichael, G.R., et al., 2003, Regional-scale chemical transport modeling in support of intensive field experiments: overview and analysis of the TRACE-P observations. *Journal of Geophysical Research*, **108**, 8823, doi:10.1029/2002JD003117.

Carn, S. A., A.J. Krueger, N.A. Krotkov, K. Yang, and P.F. Levelt, 2007, Sulfur dioxide emissions from Peruvian copper smelters detected by the Ozone Monitoring Instrument. *Geophysical Research Letters*, **34**, L09801, doi:10.1029/2006GL029020.

Garreaud, R.D., and R.C. Muñoz, 2005, The low-level jet off the west coast of subtropical South America: structure and variability. *Monthly Weather Review*, **133**(8): 2246, doi: 10.1175/MWR2972.1.

Huneeus, N., L. Gallardo, and J. A. Rutllant, 2006, Offshore transport episodes of anthropogenic sulfur in northern Chile: Potential impact on the stratocumulus cloud deck. *Geophysical Research Letters*, **33**, L19819, doi:10.1029/2006GL026921.

Muñoz, R. C., 2008, Diurnal cycle of surface winds over the subtropical southeast Pacific. *Journal of Geophysical Research*, **113**, D13107, doi:10.1029/2008JD009957.

Rahn, D.A., and R. D. Garreaud, 2009a, Marine boundary layer over the subtropical southeast Pacific during VOCALS-REx – Part 1: Mean structure and diurnal cycle. *Atmospheric Chemistry and Physics Discussions*, **9**, 26029–26062.

Rahn, D.A., and R.D. Garreaud, 2009b, Marine boundary layer over the subtropical southeast Pacific during VOCALS-REx – Part 2: Synoptic variability. Atmospheric Chemistry and Physics Discussions, 9, 26063-26094.

Skamarock, W.C., J.B. Klemp, J. Dudhia, D. Gill., D.M. Barker, W. Wang, and J.G. Powers, 2008, A description of the Advanced Research WRF Version 3. *NCAR Technical Note*.

Yang, M., B.W. Blomquist, and B.J. Huebert, 2009, Constraining the concentration of the hydroxyl radical in a stratocumulus-topped marine boundary layer from sea-to-air eddy covariance flux measurements of dimethylsulfide. *Atmospheric Chemistry & Physics*, **9**, 9225-9236.

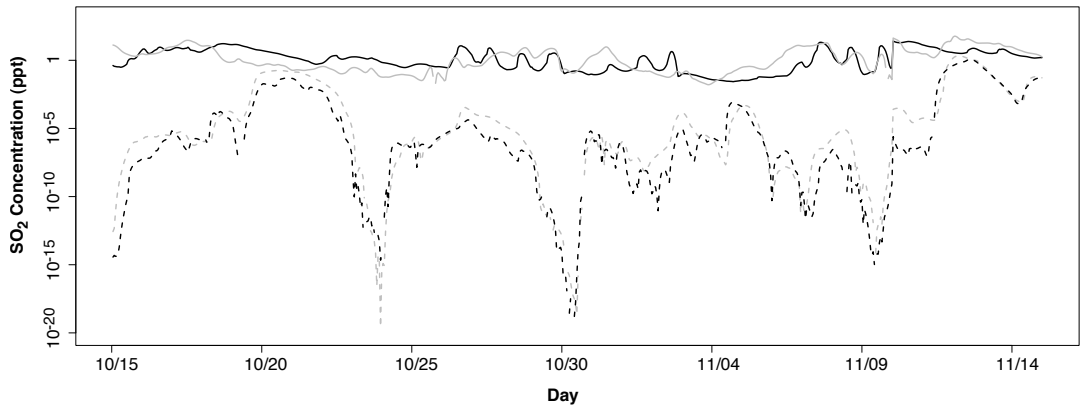

Figure 3. Simulated 10/15/2008 - 11/15/2008 hourly surface (black) and cloud level (grey) large point source SO_2 concentrations (ppt) at coastal Point Alpha (72º W, 20º S, solid lines) and the Woods Hole Oceanographic Institute Stratus buoy (85º W, 20º S, dashed lines).

Factors Controlling the Microphysical and Radiative Properties of Stratocumulus Clouds in the Southeast Pacific

Twohy, C.[1], A. Adams[1], P.Zuidema[2], D. Leon[3], R. George4 and R. Wood[4]
[1]Oregon State University, USA., [2]University of Miami, USA., [3]University of Wyoming, USA., [4]University of Washington, USA.
Corresponding author: twohy@coas.oregonstate.edu

Introduction

Stratocumulus clouds play an important role in the Earth's radiation budget. Their ability to reflect incoming shortwave radiation from the sun helps to cool the surface of the planet and offset warming by greenhouse gases. The albedo of stratocumulus clouds is dependent on the liquid water path (LWP, vertically integrated liquid water content) and the effective droplet radius r_e (Stephens, 1978). Since aerosol particles act as cloud condensation nuclei (CCN), they influence both droplet number concentration and size. The first indirect effect of aerosols on clouds, recognized by Twomey (1974), postulates that an increase in CCN in clouds with constant LWP will result in a decrease in r_e, and thus an increased albedo. While simple in theory, observations of this effect are confounded by variability in LWP over the short time and space scales accessible by aircraft measurements (Twohy et al., 2005; Stevens and Feingold, 2009). Satellite measurements, while able to measure over longer time and larger space scales, may suffer biases near broken clouds due to enhanced scattering of sunlight (Marshak et al., 2008) and hygroscopic growth of aerosols with increasing relative humidity near clouds (Twohy et al., 2009). These effects may produce apparent and erroneous increases in derived aerosol number concentration near clouds. Additionally, aerosol particles themselves may impact cloud LWP through radiative/microphysical interactions (Ackerman et al, 2000, 2003; Lee et al., 2009). Knowledge of the effects of atmospheric aerosols, particularly anthropogenic aerosols, on stratocumulus albedo is a prominent need for accurate climate change assessments (IPCC, 2007).

The southeast Pacific Ocean (SEP) is an ideal environment to study stratocumulus clouds because it has one of the world's most persistent and unexplored cloud decks (Huneeus et al., 2006; Wood et al., 2007). Chile, which borders a large portion of the SEP, has an economy heavily based in mining copper and other metals (Schüller et al., 2008). As a consequence of these and urban sources, Chile is known to emit significant sulfate, organic, and industrial aerosol types (Schüller et al., 2008; Hawkins et al., 2010, Spak et al., this issue). Under the predominately southeasterly flow regime, these particles have the potential to influence the SEP stratocumulus deck through their probable action as CCN. Huneeus et al. (2006) and Wood et al. (2007) found a spatial correlation between sulfur emissions and decreased effective radii off the Chilean coast, especially near Chilean copper smelters, measured by satellite remote sensors.

A U.S. National Science Foundation C-130 aircraft collected data from the SEP stratocumulus deck during October and November of 2008. This was one component of the VAMOS Ocean-Cloud-Atmosphere-Land Systems (VOCALS) project, with the overarching purpose of improving understanding of SEP clouds and their simulation in global climate models. One of the specific VOCALS goals was to determine how the continental pollution from industrial activity affected droplet size (and thereby albedo) in the stratocumulus layer offshore. In particular, the following VOCALS hypothesis (1c) is examined here:

The small effective radii measured from space over the SEP are primarily controlled by anthropogenic, rather than natural, aerosol production, and that entrainment of polluted air from the lower free-troposphere is an important source of cloud condensation nuclei (CCN).

To address this first part of this hypothesis, we analyzed data compiled from seven C-130 flights that transited from the Chilean coastline to offshore along the 20°S latitude line, examining gradients of cloud microphysical and aerosol properties relative to distance from the coast. Flights were based out of Arica, Chile (70°W longitude), and extended as far as 85°W, about 1600 km offshore. Flight legs of ten minutes duration (about 70 km in horizontal extent) were made sequentially below, in, and above the stratocumulus cloud layer. Sub-cloud legs were at approximately 150 m altitude, while in-cloud legs were near the middle of the cloud (between base and top as measured by soundings through the layer.) For the purpose of our analysis, each leg was considered a sampling period, and 1Hz data from the various probes were averaged over the entire leg as long as in-cloud data were available. Data from about 50 aerosol and cloud legs were composited to statistically evaluate changes with distance from shore. George and Wood (2009) showed that variability in cloud fraction is an important factor in the planetary albedo (including cloudy and clear areas) of this region. Because we focus on aerosol effects on cloud properties, however, in-situ data from clear-air regions is not included in flight-leg averages presented here.

A wing-mounted Particle Measuring Systems (PMS) Passive Cavity Aerosol Spectrometer Probe (PCASP-100), and a cabin mounted Ultra High Sensitivity Aerosol Mass Spectrometer (UHSAS) counted and sized particles from 0.10-3.0 μm and 0.055 - 1.0 μm dry diameter, respectively. For smaller particles, a Thermo-Systems Inc. 3760 Condensation Nuclei Counter (CNC) was utilized to quantify total particle concentration larger than 0.01 μm in diameter. Cloud droplets between 2 and 50 μm in diameter were measured optically using a Droplet Measurement Technologies Cloud Droplet Probe (CDP). Drizzle drops larger than about 60 μm were measured using a modified PMS 2D-C optical array probe.

Changes in aerosol and cloud characteristics with distance from coast:

Flights along the 20°S latitude line typically showed a steady and reproducible decrease in droplet number concentration N_d when the C-130 aircraft flew from near the coast to a remote region offshore. A corresponding increase in N_d was observed on return flights within the boundary layer back toward shore. The number concentration of aerosol particles larger than 0.055 μm and larger than 0.10 μm was also higher near shore in the marine boundary layer. Measurements with an Aerodyne aerosol mass spectrometer as well as electron microscopy and X-ray analysis indicated that more sulfate aerosol (number and mass) was present near shore than offshore. Since near-shore sulfate was not correlated with the marine biogenic tracer dimethylsulfide (B. Blomquist, personal communication), this suggests that particles derived from anthropogenic pollution were acting as CCN and thereby increasing droplet number in the near shore clouds. Measurements of cloud droplet residual size distributions using a counterflow virtual impactor and optical particle counter indicate that near-shore clouds had not only more droplets due to the enhanced CCN, but that the CCN within droplets near shore were larger than those offshore.

Figure 1a shows average aerosol number concentration $N_{a,100}$ (larger than 0.10 μm) measured below cloud vs. distance from shore. $N_{a,100}$ decreases from about 300 cm^{-3} near shore to less than 100 cm^{-3} offshore. Number concentrations of particles larger than 0.055 μm ($N_{a,55}$) showed similar trends, suggesting the continent to be the dominant source of accumulation mode particles near shore. However, smaller particles down to 0.01 μm were sometimes present in higher concentrations offshore than nearshore, indicating other sources of these fine particles such as entrainment from above or gas to particle formation.

Figure 1b shows that cloud droplet number concentration also decreases with increasing distance from shore, in accordance with the trend in accumulation-mode aerosol number concentration. These two are not only highly correlated with

distance from shore but also with each other (not shown), with a coefficient of determination (r_2) value of 0.57.

Both mean droplet diameter and the radiatively important effective radius (r_e) increase with distance from shore (Figure 1c) and decrease with increasing $N_{a,100}$ and $N_{a,55}$. This is in accordance with the expected Twomey or albedo effect of increasing cloud condensation nuclei producing smaller droplets. Additionally (Figure 1d), drizzle is generally larger and often more prevalent offshore. This is a result of the larger droplet size; some droplets are large enough to initiate collision/coalescence and eventually grow to drizzle sizes. This process is inhibited near shore in the smaller droplet clouds. However, drizzle is also related to mesoscale features (Comstock et al., 2007) and is quite variable in the offshore region.

T-testing (at the p=0.05 probability level) indicated that the most significant relationship is between droplet concentration and distance from shore (or particle number concentration) while relationships with droplet mean diameter, effective radius, and drizzle size are also significant. Drizzle concentration is much more variable and is not significantly correlated with distance from shore.

Potential radiative impact:

Cloud liquid water path, as well as droplet effective radius, determine cloud optical thickness τ through the following approximation:

$$\tau \approx (1.8^* \text{LWP}) / (\rho_w r_e) \quad (1) \text{ (George and Wood, 2009)}$$

LWP was derived for the 20°S missions from the G-band Vapor Radiometer (GVR— Pazmany, 2006), supplemented by adiabatic LWP derived from the on-board radar (Vali et al., 1998) when GVR data were not available. On-board radar and lidar (Wang et al., 2009) were used to measure cloud thickness. While quite variable, generally both cloud thickness and LWP were smaller near shore for the VOCALS time period (Figure 2a), with both being significantly correlated with distance from shore at p=0.05. This change in cloud physical properties is observed in satellite data also (Painemal and Zuidema, 2009) and is probably related to the large scale meteorology; for example, the increased subsidence and thinner boundary layer near shore (Wyant et al., 2009). This feature of the cloud field is very important. Due to condensational growth, droplet size increases with depth throughout the cloud layer. As a result, clouds with smaller thicknesses and liquid water paths will by nature have smaller droplets. Therefore the smaller drop sizes near shore are due not only to increased pollution, but also to the fact that the clouds tend to be thinner there.

Top-of-cloud albedo, A_{TOC}, was calculated for both the in-situ and MODIS satellite data as a function of τ (Eqn 1) and the solar zenith angle following equation 37 of King and Harshvardhan (1986). Since r_e measured from the Cloud Droplet Probe during different cloud legs is highly dependent on the sampling height for the in-situ legs and does not necessarily reflect the near-cloud-top value measured by satellite, r_e was derived here from the measured droplet number concentration as described in George and Wood (2009). MODIS cloud albedo was derived from LWP and r_e from the 10:30 AM local satellite overpass for points along the 20°S latitude line between 15 October to 15 November 2008, a time period coinciding with the VOCALS C-130 flight periods.

Using figure 2b and relying on the satellite data for a more statistically robust data set, it appears that relative to apparently unperturbed clouds 1000 km or farther offshore, MODIS cloud albedo (open squares) increases slightly at about 700 km from shore. Note in Figure 1b and 1c that droplet concentration is enhanced in this region relative to the unperturbed clouds offshore. However, nearer shore, albedo decreases again substantially. Since droplet size is definitely smaller near shore (Figure 1c), this decrease in albedo must be due not to a droplet size effect, but to the decrease in cloud thickness and LWP near shore, which reduces the cloud optical thickness (Eqn. 1). Returning to the VOCALS hypothesis presented earlier, it seems that the small effective radius near shore is due not only to the presence of anthropogenic pollutants incresing droplet number, but also due to the large-scale forcing that causes clouds to be thinner near shore. The net effect of these factors is that cloud albedo actually tends to be smaller near shore, with a slight enhancement offshore where aerosols impact the droplet concentration, but clouds are still relatively thick.

The fact that an increase in albedo is not observed near shore relative to offshore does not mean, however, that present day pollutants are not changing cloud properties relative to pre-industrial values. For example, we can hypothesize that the pre-industrial droplet concentrations throughout the

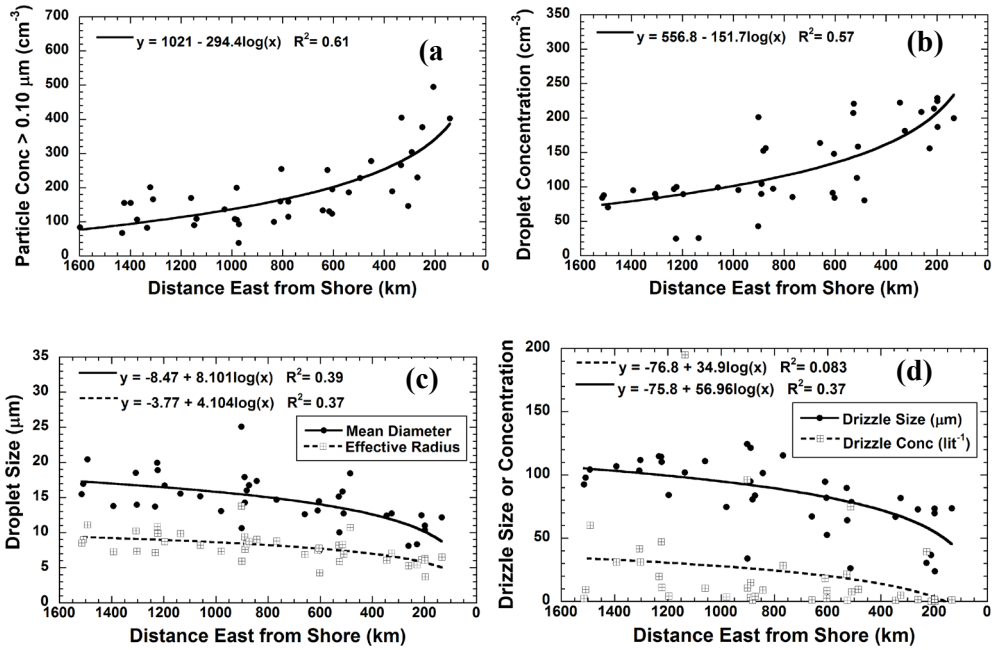

Figure 1a) Below-cloud aerosol number concentration (>0.10 μm) vs. distance from shore along 20°S latitude line for legs on eight different VOCALS C-130 flights. b) Cloud droplet number concentration as a function of distance from shore. c) Cloud droplet mean diameter and effective radius vs. distance from shore. d) Drizzle drop mean size and number concentration as a function of distance from shore.

region were similar to those measured in unperturbed air offshore (approximately 70 cm^{-3}, Figure 1b). Using this droplet concentration and assuming liquid water paths were similar to present day, the pre-industrial albedos were calculated to be about 5% smaller than in 2008. Thus, sulfates, organics, and other pollution being emitted today still may be producing a significant cloud brightening effect. Additionally, the lower droplet concentrations in clean air are more conducive to the formation of pockets of open cells (Stevens et al., 2005) within the marine boundary layer. Present day pollution may inhibit these clear regions which normally reduce the planetary albedo; this is also a potential brightening effect relative to pre-industrial times.

Implications:

To conclude, droplet effective radii are smaller near the Chilean shoreline in the southeast Pacific, but this is a combined effect of anthropogenic aerosol increasing droplet number concentration and meteorological factors decreasing LWP (which also reduces droplet size). Measuring and understanding changes in liquid water path is critical to understanding and predicting aerosol indirect effects in stratocumulus clouds. Assuming, however, that similar liquid water paths were present during pre-industrial times as are present today, cloud albedo in the VOCALS region would be ~5% higher today. This could be significant globally, depending on the spatial extent of this effect.

Acknowledgments

The authors wish to acknowledge information mentioned here that was provided by Lindsey Shank, Steve Howell, Tony Clarke, Alan Bandy and Byron Blomquist, Jim Anderson, and Darin Toohey. Also, we would like to thank the National Center for Atmospheric Research C-130 flight crew for collecting the data used in this research. This material is based upon work supported by the National Science Foundation under ATM-0746685. Any opinions, findings, and conclusions or recommendations expressed in this material are those of the author(s) and do not necessarily reflect the views of the National Science Foundation.

References

Ackerman, A. S., O. B. Toon, D. E. Stevens, A. J. Heymsfield, V. Ramanathan and E. J. Welton, 2000: Reduction of tropical cloudiness by soot. *Science*, **288**, 1042-1047.

Ackerman, A. S., O. B. Toon, D. E. Stevens and J. A. Coakley, Jr. 2003: Enhancement of cloud cover and suppression of nocturnal drizzle in stratocumulus polluted by haze. *Geophys. Res. Lett.*, **30**, 1381, doi:10.1029/2002GL016634.

Comstock, K. K., S. E. Yuter, R. Wood, and C. S. Bretherton, 2007: The three-dimensional structure and kinematics of drizzling stratocumulus. *Mon. Wea. Rev.*,**135**, 3767-3784.

George, R. C. and R. Wood, 2009: Subseasonal variability of low cloud radiative properties over the southeast Pacific Ocean. *Atmos. Chem. Phys. Disc.*, **9**, 25275-25321.

Hawkins, L. N., L. M. Russell, D. S. Covert, P. K. Quinn, and T. S. Bates, 2010: Carboxylic Acids, Sulfates, and Organosulfates in Processed Continental Organic Aerosol over the Southeast Pacific Ocean during Vocals-Rex 2008. *J. Geophys. Res.*, doi:**10.**1029/2009JD013276, in press.

Huneeus, N., L. Gallardo, and J.A. Rutllant, 2006: Offshore transport episodes of anthropogenic sulfur in Northern Chile: Potential impact upon the stratocumulus cloud deck. *Geophys. Res. Lett.*, **33** (19). doi:10.1029/2006GL026921.

Intergovernmental Panel on Climate Change, 2007: Climate change 2007: *Working Group I: The Physical Science Basis*, Cambridge Univ. Press, (Technical Summary, 91 pages.)

King, M. D. and Harshvardhan,1986: Comparative accuracy of selected multiple-scattering approximations. *J. Atmos. Sci.*, **43**, 784–801.

Lee, S.S., J.E. Penner, and S.M. Saleeby, 2009: Aerosol effects on liquid-water path of thin stratocumulus clouds. *J. Geophys. Res.*, **114**, D07204, doi:10.1029/2008JD010513.

Marshak, A., G. Wen, J. A. Coakley Jr., L. A. Remer, N. G. Loeb, and R. F. Cahalan, 2008: A simple model for the cloud adjacency effect and the apparent bluing of aerosols near clouds, *J. Geophys. Res.*, **113**, D14S17, doi:10.1029/2007JD009196.

Painemal, D. and P. Zuidema, 2009: Synoptically-induced variability in the microphysical properties of the South East Pacific stratocumulus deck. *Atmos. Chem. Phys. Discuss.*, **9**, 25523-25564.

Pazmany, A, 2006: A compact 183 GHz radiometer for airborne and ground-based water vapor and liquid water sensing. IEEE Trans. *Geosci. Rem. Sens.*, **45**(7), 2202-2206.

Schüller, M., A. Estrada, and S. Bringezu, 2008: Mapping Environmental Performance of International Raw Material Production Flows: a Comparative Case Study for the Copper Industry of Chile and Germany. *Minerals and Energy,* **1**, 29-45.

Stephens, G.L., 1978: Radiation profiles in extended water clouds, II, Parameterization schemes. *J. Atmos. Sci.*, **25**, 2123-2132.

Stevens, B., G. Vali, K. Comstock, R. Wood, M.C. Van Zanten, P.H. Austin, C.S. Bretherton, and D.H. Lenschow, 2005: Pockets of open cells (POCs) and drizzle in marine stratocumulus. *Bull. Amer. Meteor. Soc.*, **86**, 51–57.

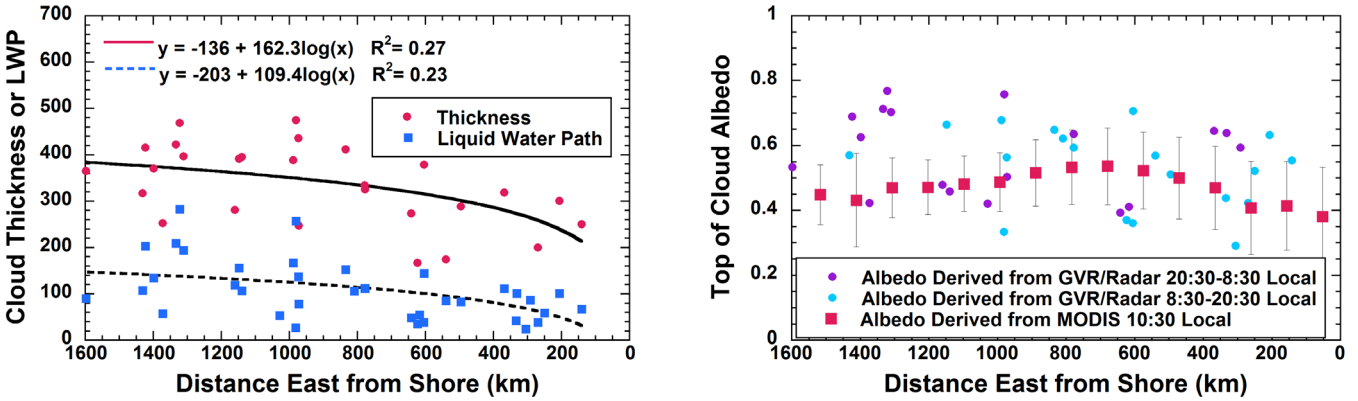

Figure 2a) Cloud thickness and LWP vs. distance from shore. Thickness is from the in-situ radar and lidar, while LWP uses both GVR and radar data. b) Cloud albedo as a function of distance from shore calculated from the in-flight data as described in the text (using 10:30 local values for solar zenith angle) and that derived from MODIS for the 10:30 local time periods during VOCALS. Vertical bars represent one sigma variability in the MODIS data. These values use in-cloud data only, so albedos here are higher than net albedos in partly cloudy regions.

Figure 2b shows cloud albedos derived from the two techniques (in-situ and remote sensing). For the in-situ data, time periods between 8:30 and 20:30 local time, where LWPs tend to be lower in this region (Wood et al. 2002) are plotted separatly from 20:30 to 8:30 local time. Results for satellite and in-situ data are similar in magnitude, particularly for near-shore clouds. MODIS 10:30 local albedos, however, show highest values at about 700-800 km from shore, while those calculated from in-situ data tend to be highest farther offshore, especially for the nighttime and early morning hours. Additionally, the in-situ data points exhibit strong variability, and a t-test shows that any increasing trend offshore is not statistically significant for the in-situ data set.

Stevens, B., and G. Feingold, 2009: Untangling aerosol effects on clouds and precipitation in a buffered system. *Nature*, **461**, 607-613, doi:10.1038/nature08281.

Twohy, C.H., M.D. Petters, J.R. Snider, B. Stevens, W. Tahnk, M. Wetzel, L. Russell and F. Burnet, 2005: Evaluation of aerosol indirect effect in marine stratocumulus clouds: droplet number, size, liquid water path and radiative impact. *J. Geophys. Res*., **110**, doi:10.1029/2004JD005116.

Twohy, C. H., J. A. Coakley, Jr., and W. R. Tahnk, 2009: The effect of changes in relative humidity on aerosol scattering near clouds. *J. Geophys. Res*., **114**, D05205, doi:10.1029/2008JD010991.

Twomey, S., 1974: Pollution and planetary albedo. *Atmos. Environ*., **8**, 1251-1256.

Vali, G., R. D.Kelly, J. French, S. Haimov, D. Leon, R. E.McIntosh and A. Pazmany. 1998: Finescale structure and microphysics of coastal stratus. *J. Atmos. Sci*., **55**, 3540–3564.

Wang, Z., P. Wechsler, W. Kuestner, J. French, A. Rodi, B. Glover, M. Burkhart,and D. Lukens, 2009: Wyoming Cloud Lidar: instrument description and applications. *Optics Express*, **17**, 13576-13587.

Wood, R., C. S. Bretherton and D. L. Hartmann, 2002: Diurnal cycle of liquid water path over the subtropical and tropical oceans. *Geophys. Res. Lett*. doi: 10.1029/2002GL015371.

Wood R., C. R. Mechoso, C.S. Bretherton, B. Huebert, and R. Weller, 2007: The VAMOS Ocean-Cloud-Atmosphere-Land Study (VOCALS). *Clivar Variations*, **5**, No 1.

Wyant, M.C. et al., 2009: The PreVOCA experiment: modeling the lower troposphere in the Southeast Pacific. *Atmos. Chem. Phys. Disc*., **9**, 23909-23953.

Combustion Aerosol, Entrainment and Clouds in the VOCALS Region

Clarke, A.D[1]., S. Freitag[1], V. Brekhovskikh[1], T. Campos[2], J. Snider[3], V. Kapustin[1], S.Howell[1], L. Shank[1], C. McNaughton[1]
[1]Department of Oceanography, University of Hawaii, [2]NCAR, Boulder CO, USA., [3] University of Wyoming, USA.
Corresponding author: tclarke@soest.hawaii.edu

Extensive stratus clouds in the subtropical Southeast Pacific (SEP) respond to dynamic, thermodynamic, diurnal, precipitation, entrainment and microphysical influences that are all coupled to the land-ocean environment. Understanding the role of diverse elements in this coupling is central to VOCALS experiment (Wood and co-authors, 2010). As in all clouds, the nature and variability of aerosol effective as cloud condensation nuclei (CCN) exert a fundamental control over the number of cloud droplets that can form in the updrafts crossing through cloud base. Here we draw attention to the role of natural and combustion aerosol present in the region and their relation to clouds and/or pockets of open cells (POC's).

Most VOCALS flights revealed "patches" and "rivers" of elevated CO and combustion aerosol overlaying the inversion and often immediately above cloud level. Our measurements indicate that a large number fraction of this aerosol has a size and composition making them effective CCN and their concentrations aloft can supply the MBL with CCN through entrainment. We also find that air in the VOCALS marine boundary layer (MBL) with low cloud fractions and in POC's commonly had lower carbon monoxide (CO) concentrations and associated aerosol compared to adjacent cloudy regions. As the lifetime of CO is insensitive to cloud processes and is on the order of two months, CO is conserved over the time scales associated with advection through the VOCALS region and provides a tracer for combustion derived aerosol. Hence, offshore MBL regions of low cloudiness and POC's were least impacted by entrainment of CO (and combustion aerosol) compared to nearby overcast (stratus) regions. We hypothesize that entrainment of this combustion aerosol by MBL stratus clouds can help buffer VOCALS stratus CCN concentrations against their removal by drizzle. Entrainment of these CCN would not only contribute to overall cloud albedo through maintaining higher mean cloud droplet number but also by increasing the lifetime of clouds against dissipation by drizzle. As higher CCN concentrations can suppress drizzle and increase cloudiness (Wood et al., 2010) their entrainment could help maintain greater fractional cloud cover in those regions of the MBL influenced by enhanced combustion aerosol directly above cloud.

The NCAR C-130 flew 14 flights out of Arica, Chile and 140 hours in the VOCALS region between Oct. 15 and Nov. 15. These included eight flights along 20°S between 72°W and 85°W, four POC flights across a POC/cloudy region boundary (Mechoso and Wood et al., this issue) and two N-S flights off the coast between about 20°S and 30°S latitude. All flights typically included legs about 10 min long near the surface, in cloud, above cloud and with occasional legs near cloud base and occasional profiles to about 4 km. POC flight legs were "stacked" above each other and were typically advected with the wind in an attempt to stay in the same airmass. The C-130 was equipped with extensive aerosol, gas, remote sensing and meteorological instruments (Wood and co-authors, 2010) but we will focus here on the relation between CO (Teresa Campos, NCAR) and various aerosol measurements. The latter reported here include cloud condensation nuclei [CCN; Jeff Snider, U. Wyoming], aerosol chemistry via AMS [S. Howell, L. Shank; U. Hawaii] and condensation nuclei (CN), non-volatile CN at 360C, Black Carbon (BC) mass for a Single Particle Soot Photometer (SP2) [all A. Clarke et al, U. of Hawaii]

The larger scale meteorological regime in the SEP is governed by anticyclonic flow linked to large scale subsidence (Rahn and Garreaud, 2009) that results in alongshore equatorward flow along the coast of Chile. The Andes mountains (~4-5km alt.) typically constrained the MBL flow to a N-S direction along the coast with an increasing easterly component to the northwest during transport to lower latitudes. The largest and most persistent stratus clouds in the world are found here and these were occasionally broken by regions of lower cloud fractions and POC's. Surface winds generally entered the VOCALS region from the southerly direction with an increasing southeasterly component typically located just above the inversion. Analysis of these fields using the Weather and Research Forecast model for both the advection and divergence terms result in a residual that is interpreted as an entrainment velocity through the inversion of about 0.4 cm/s along 20S (Rahn and Garreaud, 2010). However, inefficient entrainment over

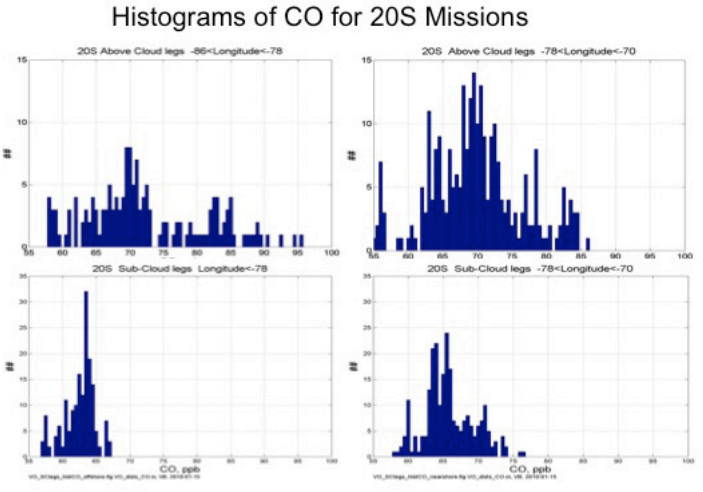

Figure 1: Histograms of CO concentrations for 20ºS legs for above cloud (top) and below cloud (bottom) and west (left) and east (right) of 78ºW.

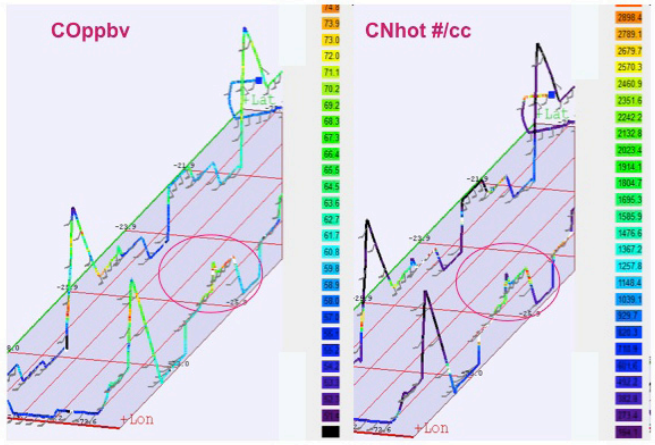

Figure 2: 3-D flight track for C-130 flight 12 to 30S (Nov. 11, 2008) with wind barbs and color coded with CO (ppbv) and CNhot (# cm-3) as a rough proxy for CCN0.3.

POC regions (Wood et al, 2010) and the presence of strong radiative cooling at cloud top implies most entrainment will take place in cloudy regions.

The majority of NCAR C-130 flights were dedicated to survey missions above in and below clouds along 20°S latitude between abut 72°W and 85°W (Wood and co-authors, 2010). Our 20°S data suggested a broad transition in continental influence on CO and aerosol at about 76°-80°W with cleaner MBL air to the west and more polluted to the east. This is evident in histograms of CO for 20°S missions (Figure 1) for east and west of 78°W and above and below cloud level. It is clear the above-cloud legs in both regions have a greater mean and markedly higher values for CO than in the MBL below. West of 78°W, low CO values below about 60ppbv were found in cleanest air above and below the inversion. These were also close to values seen in POC and clear air regions. Values closer to 65 ppbv were more common under cloud while values above cloud are most frequently about 70 ppbv or higher. Direct comparison of specific above and below cloud values are problematic because concurrent sampling above and below cloud was rare. Moreover, concentrations were patchy and both directional and velocity wind shear above cloud continually change the air mass in the free troposphere (FT) present above an air mass moving in the MBL.

Aerosol particles with dry diameters larger than approximately 60 nm were commonly effective as CCN at less than 0.3% supersaturation ($CCN_{0.3}$) in the region. Increases in aerosol number larger than this size tracked with increases in CO. $CCN_{0.3}$ in the clean MBL included natural sulfates and sea-salt aerosol and, although the most common number aloft was typically lower (about 70% of MBL in non-POC regions), similar number concentrations were often seen above and below cloud while sizes aloft were often somewhat smaller. Once entrained into the MBL, growth through heterogeneous chemistry can also be expected to increase their size.

Mean entrainment rates along 20°S of about 0.4 cm^{-1} (Rahn and Garreaud, 2009) are probably higher in cloudy regions (say 0.5 cm s^{-1}) and could mix in about 450m of air from above the inversion in a day. Hence, entrainment influences are comparable to the 1.5 days estimated to remove CCN through coalescence scavenging in a 1km POC (Wood et al, 2010) and overcast regions appear to be less effective at removal than POC regions. Measurements in cloud free regions and POC's west of 78°W consistently showed CO values several ppb or more lower than in adjacent cloudy regions. POC regions also showed depletion of aerosol in $CCN_{0.3}$ to values below 10 cm-3, presumably due to drizzle. These observations raise the question: Can "rivers" or "patches" of advected combustion aerosol entrained into a drizzling stratus deck help stabilize clouds against drizzle removal and increase cloud persistence or cloud fraction?

In the absence of entrained CCN, the time for drizzle to remove MBL aerosol in overcast regions should be longer than the 1.5 days estimated in POC regions. This raises the question of both the origin of elevated CO layers and their relation to cloud properties present in clear air and cloudy regions. The north-south C-130 mission on November 11, 2008 was flown between about 20°S - 30°S and provides some indication of how these features are expressed nearer the coast and their relation to cloudiness. Figure 2 shows the altitude resolved flight tracks with wind barbs and color coded with CO and CNhot. CNhot are measured continuously and tend to be dominated by aerosol sizes larger than 50nm or so. We have found that they can provide a useful and rapid proxy for $CCN_{0.3}$ (not shown) that was measured far less frequently. Dark blue indicates background CO below 55ppb common to air entering the track from the south both in the MBL and above it. CO is clearly elevated in many profiles at altitudes above the MBL up to 3km and higher. However, higher altitude CO is often depleted in aerosol compared to the lower CO layers, presumably due to more effective aerosol precipitation scavenging since leaving the source. This is evident in the right panel where condensation nuclei after heating to 350°C (CHhot) show enhancements above the inversion and at lower altitudes that correlate (not shown) with elevated CO but less so at higher altitudes above about 2.5 km. These higher altitude CO values on flights tended to have various wind directions but the enhanced values above the inversion and cloud typically had a SE direction, as evident here. Because of this directional shear and higher wind speed above the inversion, the elevated CO layers migrate to the west faster than the MBL air below.

Figure 3 includes a GOES cloud image centered on the mission flight time. The color and point size of the track scale with CO concentrations and indicate how CO is often elevated immediately above dense cloud cover. The image also shows how cloud structures appear linked to the coast. The relation to combustion aerosol along the flight is clearly evident in the 3-D track plot of BC mass (soot) measured by the SP2 (lower panel). Air advecting from the south in the cloud free

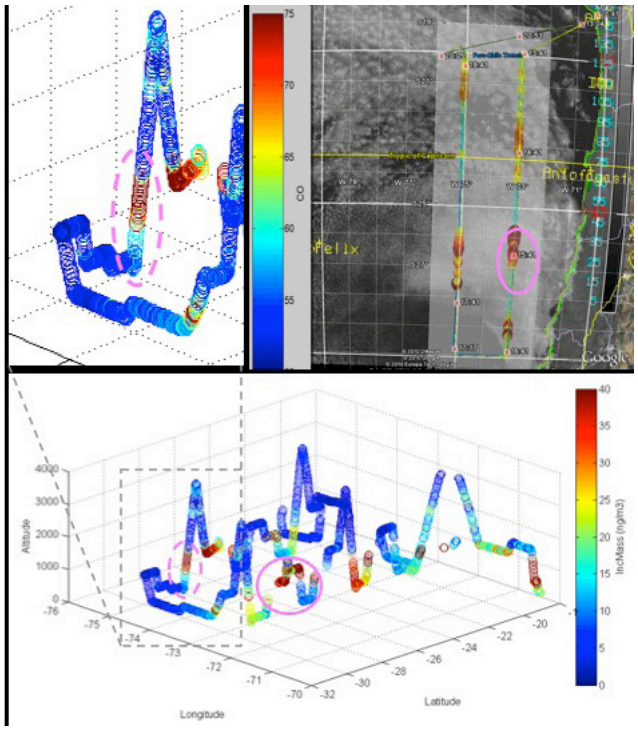

Figure 3: 3-D flight track for RF12 color coded by black carbon mass (ng m-3) with legs discussed in text circled. Highest concentrations are commonly above inversion and gradient to surface evident (eg. See hatched circle in insert). Upper right is GOES image of clouds a midpoint of flight and with CO symbols on track shown larger and more colored (red) at higher concentrations.

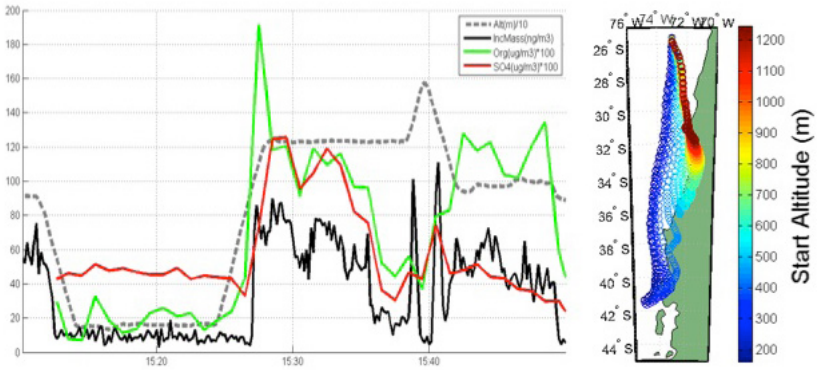

Figure 4: (left) Time series of altitude (m/10), incandescent BC mass (ng m-3) from SP2, total AMS organic aerosol mass and sulfate (µg m-3/100) for legs circled in previous figures. (right) HYSPLIT trajectories every 10s color coded with aircraft altitude for profile starting at 15:25 in time series plot.

SW corner of the track has less than 5 ng g^{-1} BC (dark blue). Values aloft can be an order of magnitude higher (red). CO is high in regions of high BC such as near 26°S (magenta circle) and above the inversion and clouds. This layer is also evident above cloud to the west and the profile (hatched magenta circle) clearly shows a gradient in BC from above cloud to the surface (see enlarged insert). As wind barbs (measured in-situ on the C-130 – Figure 2) are from due south in the MBL the only way this vertical gradient could be established is through entrainment of aerosol from the above cloud layer where winds are transporting combustion aerosol from the SE. Hence, aerosol and CO are being entrained in the region of larger cloud fraction (see GOES image) just north of the patch of clear air evident at the southern end of the flight. The tendency for more polluted air to lie above cloud and be associated with winds having a stronger easterly component than in the MBL was evident on many VOCALS flights.

The chemistry (AMS) of this combustion aerosol for the legs in the magenta circle of Figure 3 is shown in Figure 4. This time series is for N-S legs below cloud at 150m, above cloud at 1200 m and near cloud top at 950 m. BC at 150m is near 10 ng m^{-3} and double values in the clean marine air. OC is low near 10-30 ng m^{-3} while sulfate is about 500 ng m^{-3}. Just above cloud at 950 m, BC and OC increase a factor of about 6 and sulfate nearly triples while all vary together along the leg at 1200 m. Around 15:40hr a short profile reveals a thin layer of enhanced BC near 1300m with clean air above at 1,600 m. These data illustrate patchy pollution layers about 500 m thick above cloud. However, after dropping to 950 m at 15:45hr OC remains elevated while sulfate and BC values trend lower. Higher ratios of OC to sulfate suggest a dominant biomass burning source for this leg. The leg at 1200 m has similar OC concentrations but relatively more sulfate and BC. Trajectories averaged for every 10s over the profile starting at 15:25hr are included to the right of the figure and color coded with aircraft altitude. These reveal the air on lowest leg traveled steadily for 48 hr from the south over the open ocean. The two upper layers are seen to have stagnated for about a day over the coast before moving to the NW. All trajectories are consistent with the C-130 in-situ wind barbs for these altitudes (Figure 2). The highest trajectories also pass near a copper smelting operation in the mountains near 30ºS, possibly accounting for the enhanced sulfate and BC relative to organic carbon (OC) in the 1200m layer.

This N-S flight provides near-coast measurements south of the primary VOCALS regime that point to sources of continental combustion aerosol advected out over clean marine air moving north. These properties are similar to those evident in many 20S flights and POC flights where elevated CO, OC and BC are present above the inversion. Although some CO evident on these flights above cloud (and higher) appear to have other sources, long range transport of South American aerosol above cloud in the VOCALS region (Figure 1) may be common, even though pollution aerosol in the MBL appears confined closer to the coast (George and Wood, 2009).

Our observations suggest that the cloud free regions and POC regions, characterized by the lower CO values in the Figure 1 histograms, have entrained less CO and pollution aerosol from aloft compared to adjacent cloudy regions. POC regions are associated with enhanced drizzle and are characterized by dramatically lower aerosol and $CNN_{0.3}$ number than either clean marine regions or adjacent cloudy regions (Wood et al., 2010). Drizzle was also active in cloudy regions but aerosol and $CCN_{0.3}$ numbers generally remained higher than in POC regions.

We hypothesize that turbulent entrainment of pollution aerosol from above in cloudy regions can buffer depletion of MBL aerosol by drizzle when such aerosol is present. If clean FT air with lower CCN is entrained, this buffering against removal by drizzle may be much reduced and depletion of CCN in the MBL will be more rapid. Left unabated, this depletion could lead to POC conditions. These include an aerosol depleted layer with low turbulence below the inversion that reduces subsequent entrainment (Wood et al., 2010). If pollution is transported over a POC at this stage then entrainment of CCN into the MBL due only to wind shear (speed and direction) will be much less effective compared to cloud top turbulence active over cloudy regions.

While further analysis and modeling is needed to challenge this hypothesis, the process offers a means by which FT aerosol can affect cloud properties in this and similar regions of extended stratus. The effect of entrained pollution can be expected to maintain higher levels of CCN in MBL clouds compared to pollution free regions, thereby increasing cloud albedo relative to the case with clean air aloft. Perhaps more importantly, this resupply of CCN into the MBL could increase cloud persistence and increase mean cloud fractions over the region, consistent with the GOES image in Figure 2. An increase in cloud fraction could be a far greater effective influence on regional cloud albedo (George and Wood, 2010). If this process is effective, and as most combustion sources are recognized as being linked to anthropogenic activity, then one can ask whether combustion aerosol above extended stratus have changed over time (decades) and whether these extended cloud systems have properties that have been changed due to their presence. The entrainment of pollution aerosol into similar regions off the coast of California has also been demonstrated (Clarke et al, 2001) and satellite (CALIPSO) data indicate extensive pollution over cloud is present over the South Atlantic stratus off Namibia. Due to the significance of these large scale cloud systems to global albedo, we hope to use the VOCALS data set to challenge and explore this hypothesis and its significance.

References

Clarke, A., V. Kapustin, W. Collins, P. Rasch, K. Moore, S. Howell and H. Fuelberg, Dust and Pollution Transport on Global Scales: Aerosol Measurements and Model Predictions, *Jour. Geophys. Res.*, **32**,555-32,569, 106, D23, 2001.

George, R and R. Wood, Subseasonal variability of low cloud and radiative properties over the southeast Pacific Ocean,

Atmos. Chem. Phys. Discuss., **9**, 25275-25321, 2009
Rahn, D. and R. Garreaud, Marine boundary layer over the subtropical southeast Pacific during VOCALS-REx. Part II: Synoptic variability, *Atmospheric Chemistry and Physics Discussions*, Volume **9**, Issue 6, 2009, pp.26063-26094
Wood, R. and co-authors: The VAMOS Ocean-Cloud-Atmosphere-Land Study Regional Experiment (VOCALS-REx): Goals, platforms and field operations, *Atmos. Chem. Phys.*, 2010.
Wood, R., C.S. Bretherton, D. Leon, A.D. Clarke, P. Zuidema, G. Allen, and H. Coe; An aircraft study of the spatial transition from closed to open mesoscale cellular convection, *Atmos. Chem. Phys.*; submitted Mar. 2010.

Biogenic DMS Dominates the Sulfur Budget in the VOCALS Region of the Southeast Pacific

Huebert, B[1], B. Blomquist[1], M. Yang[1], C. Fairall[2], J. Johnson[3] and T. Bates[3]
[1]Department of Oceanography, University of Hawaii, USA., [2]NOAA-ESRL, Boulder, CO USA., [3]NOAA-PMEL, Seattle, USA.
Corresponding author: huebert@hawaii.edu

During the VOCALS Rex deployment, our groups measured sulfur gases from the NSF/NCAR C-130, and seawater DMS and DMS fluxes from the R/V Ronald H. Brown. We were surprised by several of our observations.

Dimethylsulfide (DMS) is a gas produced by marine phytoplankton. Most of it is consumed in sea water, but a fraction escapes to the marine atmosphere. There it is oxidized mostly to SO_2, with methanesulfonic acid (MSA), and a variety of minor products accounting for perhaps 10-20% of the original sulfur emitted as DMS. About half the resulting SO_2 is oxidized to sulfate aerosol (NSS), which is a major component of marine cloud condensation nuclei, CCN. Charlson et al. (1987) postulated a feedback cycle in which DMS production modulates cloud reflectivity via CCN, and the clouds then limit DMS production.

Since DMS plays a central role in the marine radiation budget, it is important to know how much DMS the ocean emits per unit time: its sea-to-air flux. Theoretical formulations of this flux still contain factor-of-several uncertainties, so we measured the DMS emission flux from the *Brown* on both legs of VOCALS. These observations fit very logically into a cloud/radiation program like VOCALS, since the supply of sulfur limits the production of sulfate aerosol mass. Long-range transport of (sometimes anthropogenic) SO_2 and NSS can also be significant contributors to forming sulfate aerosol.

Heterogeneity of the DMS source

To model DMS emissions and their climate impact realistically, it is necessary to know what controls its production. We found that it is tightly linked to the control that dynamics exerts on biology. Figure 1 demonstrates the spiky character of DMS fluxes (bottom panel) and the atmospheric DMS concentrations that result from those emissions (top panel). We had expected much more uniform fluxes, based on ~6 km-spaced seawater (SW) DMS measurements from earlier cruises. The heterogeneity of the flux was due largely to a corresponding heterogeneity in the SW DMS concentration, although changing winds also played a role.

We crossed one eddy-interface at 1-2 knots (to improve spatial resolution), and saw SW DMS change from 1.5 to 4 μM in the space of 2 km. Clearly instruments with spatial resolution of 0.5 km or less are needed to map these features: a 1 minute SW DMS measurement, for example, could achieve 0.2 km resolution while cruising at a more economical 10 knots. SST and salinity are routinely measured on those scales.

Atmospheric DMS concentrations followed the fluxes remarkably well, with a superimposed diurnal variation. Atmospheric DMS oxidation is a photochemical process, operating almost entirely in the daytime in the absence of pollution. Night time emissions increase the DMS concentration in air, but the flux is exceeded by photochemical loss of DMS in the daytime, causing concentrations to drop until around sunset (Figure 2).

The principal driver of the spikiness in DMS fluxes was the heterogeneous nature of SW DMS. Whenever we crossed an interface (as between eddies) at which SST or salinity changed, SW DMS would increase dramatically. Sadly, our SW DMS measurement was too slow to determine whether the SW DMS spike was right in the middle of the transition or on the cooler/warmer, saltier/fresher side. This is a clear example of upwelling and surface dynamics creating niches in which various species of phytoplankton thrive. That, in turn creates patterns of DMS production, emission, and ultimately atmospheric concentration. The top panel in figure 1 shows that atmospheric DMS concentrations maintain much of the pattern of DMS emissions. Patchy DMS production makes for patchy atmospheric sulfur concentrations.

Sulfur budget in the VOCALS region

How do natural sulfur sources compare with SO_2 pollution in creating aerosol mass?

VOCALS Hypothesis 1.c. states: "The small effective radii measured from space over the Southeastern Pacific are primarily controlled by anthropogenic, rather than natural, aerosol production, and entrainment of polluted air from the lower free-troposphere is an important source of cloud condensation nuclei (CCN)."

In other words, pollution transport is posited to dominate over natural sources of aerosols. We had the means to test parts of this hypothesis in the VOCALS region itself (72-87ºW, 18-22ºS), although we could not make in situ measurements in the fetch upwind of the region. Flight plans were not well-posed for budget studies, but we were able to construct a project-long summary of sulfur sources.

From our direct measurements we compute a project average sea-to-air flux of ~3 μmol DMS/m^{2}day. Entrainment from above was negligible, because there is virtually no Free Troposphere DMS to entrain. Roughly 90% of atmospheric DMS is oxidized to SO_2, a 2.7 μmol/m^{2}day in situ SO_2 source. Based

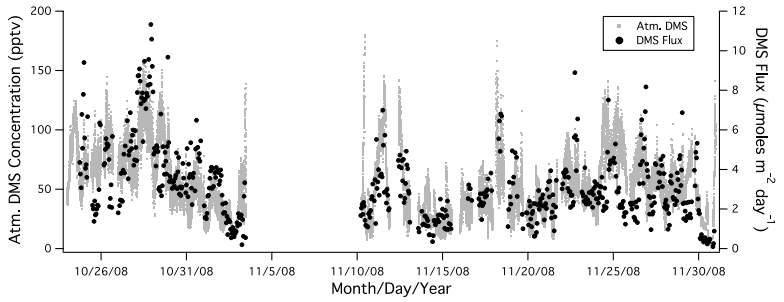

Figure 1. Both atmospheric DMS concentration and the sea-to-air flux of DMS display the spikiness of the DMS source. This is largely due to the impact of ocean dynamics on the biological production of DMS.

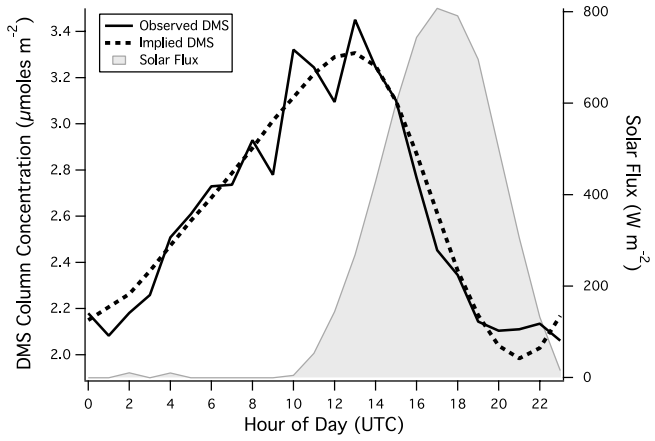

Figure 2. The measured diurnal cycle of atmospheric DMS concentration is reproduced by a simple model in which OH is the only oxidant. Once sunlight starts generating OH, the DMS emitted overnight is depleted by reacting with that OH.

on C-130 SO_2 measurements just above and below the Marine Boundary Layer inversion, the entrainment source of SO_2 is a fraction (<10%) of the in situ source from DMS oxidation. Thus, a huge majority of the SO_2 source west of 75°W in the VOCALS region was from natural DMS emissions. About half that SO_2 will dry deposit to the ocean, while the rest will be oxidized to NSS aerosol.

It would take 7-10 days to regenerate the 200-300 ppt of NSS we encountered with this DMS emission rate. Clearly, then, most of the observed NSS had been generated upwind, where we lack *in situ* measurements. However, Lee et al. (2010) measured SW DMS upwind in 2000 along a westward transit at about 40°S, and computed fluxes based on observed wind speeds. Most fluxes were in the range of 2-4 μmol DMS/m^2d, with spikiness very much like what we observed during VOCALS. It is fair to assume that DMS fluxes were very similar upwind of and within the VOCALS region, and they contributed to the formation of the aerosols we encountered.

There was, of course, a gradient of conditions in the VOCALS region, from high anthropogenic contributions near the coast to very few anthropogenic aerosols at 85W. It is noteworthy that several smelters, normally huge SO_2 sources, were not operating during REx. Close to shore there is no question that anthropogenic sources dominated the sulfur budget. At the western end of the region, DMS-derived aerosol mass predominated.

The extent of the upwind sulfur source is still a subject of debate. Hypothesis 1.c. stated before implies a homogeneity that is not characteristic of the VOCALS region. Perhaps it is more germane to ask how far offshore the anthropogenic signal can be seen.

Sulfur photochemical oxidation

Another piece of the DMS-to-CCN puzzle involves the oxidative mechanisms by which DMS and SO_2 are converted to sulfate aerosols. The hydroxyl radical, OH, is the principal oxidant of DMS and one of three possible oxidants of SO_2. Parallel hydrogen abstraction (from DMS) and OH addition (to DMS) pathways produce different amounts of SO_2 and organic sulfur products. Halogen and nitrate radicals can also initiate DMS oxidation, but we have determined that neither was significant during VOCALS (Yang et al., 2009). Likewise there are three primary SO_2 oxidation mechanisms, which can either make existing CCN larger or create new CCN. In addition to OH, hydrogen peroxide (in cloudwater) and ozone (on sea salt) oxidize SO_2 to NSS, but neither oxidizes DMS.

One difficulty in modeling reactions with OH is its extreme variability. It is produced from ozone, water, and sunlight, and has such a short lifetime that its concentration follows changes in solar intensity. Shadowing by clouds reduces OH, while entrainment of FT ozone makes OH increase. Thus, this critical oxidant depends on many factors that are hard to quantify. In situ measurements of OH represent a point in space and time, but may or may not be representative of the daily or weekly regional-average OH concentrations one needs to compute chemical lifetimes and reaction rates that are determined by OH.

Since OH is the principle oxidant of DMS, we used our DMS flux and concentration measurements to derive an effective, project-average OH concentration. Over a month or so, the source of DMS equals its loss:

$$\frac{F_{DMS}}{z_i} = k_{OH}[OH][DMS] + \omega_e([DMS]_{BL} - [DMS]_{FT})$$

where F_{DMS} is the sea to air flux we measured, z_i is the inversion height (measured in several ways), k_{OH} is the well-known rate constant for the reaction of OH with DMS, [DMS] is the measured atmospheric DMS concentration, ωe is the entrainment velocity, *BL* and *FT* refer to boundary layer and free troposphere, and [OH] is the concentration we seek. Yang et al. (2009) have shown that advection in this context was negligible in the VOCALS study area, and entrainment was a small term.

Both F_{DMS} and [DMS] are measured by the same instrument, so calibration errors would not contribute uncertainty to the project-average effective [OH]: 1.4 (±0.2) x 106 OH/cm^3. Figure 2 shows the diurnal variability of OH and the resulting DMS daily cycle: When sunlight begins to form OH, the DMS concentration drops. It increases through the night; emissions continue but OH is unavailable. Most of the uncertainty in our OH estimate derives from estimates of entrainment velocity and inversion height. Details are given by Yang, et al. (2009).

The stratocumulus regime makes this kind of photochemical computation possible, since exchange through the walls of the study region can be either measured or estimated with confidence. By contrast, the technique would not work in a convective region due to the difficulty of quantifying upward transport.

Physical formulations of gas exchange velocity

The connection between biological production of DMS and its impact on the MBL sulfur budget is, of course, its evasion from the ocean to the atmosphere. This is commonly parameterized as a transfer velocity, k_{DMS}, times a driving force, the concentration difference between water and air.

$$F_{DMS} = k(T,U,?)_{DMS}\{[DMS]_w/\alpha - [DMS]_a\}$$

The dimensionless solubility, α, is used to establish the atmospheric concentration that would be in equilibrium with the measured water concentration. Since DMS is always highly supersaturated in seawater and the atmospheric concentration is small due to the relatively short lifetime with respect to oxidation, the atmospheric term can frequently be ignored. Here the transfer velocity is shown to be a function of temperature and wind speed, U, as well as factors yet unquantified. Empirical formulations of k are frequently expressed as powers of U over the entire wind speed range. However, there are at least three very different physical wind speed regimes. The first is at very low speeds (U < 3-4 m/s), where water-side buoyancy-driven convection (caused by surface cooling) brings water from the bulk to the surface. As gas evasion takes place the water cools and is soon replaced by undepleted bulk water. Wind plays little or no role at the low speeds.

In the mid-range of winds (~3 < U < ~12 m/s), the physics changes dramatically. Now wind stress tangential to the surface causes surface renewal, bringing bulk water to the surface much more rapidly. Capillary waves and microbreaking are among the processes causing gas exchange in these much rougher seas. Here physicists contend that k should be

proportional to friction velocity u^*, a measure of momentum transport from wind to the water surface.

Above 10 or 12 m/s the winds begin to cause the breaking of long waves, covering more of the surface with bubbles and making the interface ambiguous. The fraction of stress that is tangential to the interface is reduced as more and more of the wind stress contributes to "form drag," wind pushing on waves. Flow separation in the lee of waves further reduces the tangential stress that dominated in the mid-range. Bubbles are now the primary exchange agent for most gases, as they scavenge gas from the bulk and deliver it to the surface. Since the tendency of gases to partition into bubbles is a strong function of gas solubility, relatively insoluble gases like CO_2 will experience much greater bubble enhancement than relatively soluble ones like DMS. Thus, the k vs U curves for various gases diverge in this high wind regime.

Although we did not encounter high winds during VOCALS, we were able to confirm that k_{DMS} in the mid-range was proportional to friction velocity. This confirms that the physical formulation is realistic under these conditions. Very little high-wind flux data exists, leaving that physics largely untested.

Summary

The VOCALS DMS data set has educated us about many steps in the relationship between DMS production and aerosol formation. The production of DMS is spatially heterogeneous, with large increases at interfaces between eddies and currents. Dynamics create the chemical and physical environments that favor DMS-producing phytoplankton. The details of this control await further study.

The evasion of SW DMS to the atmosphere is controlled both by the amount of DMS in the water and by stress, the transport of wind momentum to the ocean's surface. We were able to validate a physical description of gas exchange in the mid-range of winds during VOCALS. Much more work is needed to test physical models in high winds.

This natural emission of DMS to the atmosphere dominates the sulfur budget in at least the non-coastal portions of the VOCALS region. While we still have to determine the extent over which upwind anthropogenic sulfur sources may have produced aerosol mass, it is clear that DMS is a major contributor.

Finally, measurements of DMS flux and concentration were used to quantify the project-average effective OH concentration. Since OH is the major oxidant of DMS (in this region, at least), this will be a valuable check on photochemical models leading to NSS and CCN formation.

DMS flux measurements illuminated a range of processes in the VOCALS program. However, many of these insights were qualitative, and therefore of limited utility to climate modelers. The role of dynamics on DMS production, in particular, demonstrates an intriguing connection between physical, biological, and chemical oceanography. No one discipline can understand DMS production in isolation.

Acknowledgements

Support for this work was provided by NSF grants ATM05-26341 and OCE07-43551. We are grateful to NOAA for use of the R/V Ronald H. Brown.

References

Charlson, R. J., J. E. Lovelock, M. O. Andreae, and S. G. Warren (1987), Oceanic phytoplankton, atmospheric sulfur, cloud albedo and climate, *Nature*, **326**, 655-661.

Lee, G., J. Park, Y. Jang, M. Lee, K. R. Kim, J. R. Oh, D. Kim, H. I. Yi, and T. Y. Kim (2010), Vertical variability of seawater DMS in the South Pacific Ocean and its implication for atmospheric and surface seawater DMS, *Chemosphere*, **78**, 1063-1070.

Yang, M. X., B. W. Blomquist, and B. J. Huebert (2009), Constraining the Concentration of the Hydroxyl Radical in a Stratocumulus-topped Marine Boundary layer from Sea-to-air Eddy Covariance Flux Measurements of Dimethylsulfide, *Atmos. Chem. Phys*., **9**, 9225-9236.

The Eastern Pacific Ocean is a source for short lived atmospheric gases: Glyoxal and Iodine Oxide

Volkamer, R.[1,2], S.C. Coburn[1], B.K. Dix[1], R. Sinreich[1]
[1]Department of Chemistry and Biochemistry, University of Colorado, Boulder, CO, USA, [2]CIRES, Boulder, CO, USA
corresponding author: rainer.volkamer@colorado.edu

Ocean's cover 70% of the Earth surface, yet measurements of reactive gases like glyoxal, or iodine oxide have in the past been conducted mostly over land, or in coastal areas (see Figure 1). The open ocean marine atmosphere is among the most poorly probed atmospheric environments of our planet. Glyoxal is a short-lived gas that forms climate cooling secondary organic aerosol (SOA). Iodine oxide forms by destroying tropospheric ozone, and can nucleate new particles. The Atmospheric Trace Molecule Spectroscopy Laboratory (ATMOSpeclab) at the University of Colorado Boulder has designed, and assembled a prototype Ship Multi Axis Differential Absorption Spectroscopy instrument (CU SMAX-DOAS) that is optimized for the use from ships, and capable of measuring glyoxal, and iodine oxide, among other gases sensitively, selectively and directly in the atmosphere. This unique instrument was first deployed as part of the VOCALS-Rex field experiment aboard the NOAA Research Vessel Ron Brown from October through December 2008 over the Eastern tropical Pacific Ocean, and as part of other cruises aboard NOAA Research Vessels as part of the Tropical Atmosphere Ocean Program. The cruise tracks are also shown in Figure 1. We accomplished unambiguous spectral proof for the presence of glyoxal and iodine oxide in elevated concentrations inside the marine boundary layer more than 3000 km from land. This is surprising, because both gases are very short lived (atmospheric lifetime of seconds to hours), and cannot be transported from land sources. Ours are the first direct measurements of glyoxal and iodine oxide over the remote open ocean. Current atmospheric models fail to explain our observations.

The release of climate active gases from biologically active upwelling regions is a subject of ongoing research. Over the open tropical Pacific Ocean some satellite data showed concentrations of glyoxal (CHOCHO) (Kurosu et al., 2005; Wittrock et al., 2006; Vrekoussis et al., 2009) and iodine oxide (IO) (Schoenhardt et al., 2008). However, satellite inferences remain ambiguous. For glyoxal, the amounts differ between two satellite instruments, i.e., OMI and SCIAMACHY. Further, the GEOS-Chem and TM4 global models do not predict any glyoxal over the oceans (Myriokefalitakis et al, 2008; Fu et al., 2008). Finally, at tropical and sub tropical latitudes, the spatial patterns of glyoxal closely resemble those of chlorophyll-a in the surface waters. Chlorophyll-a affects ocean color in the blue spectral range, which is also used by satellites to measure glyoxal and iodine oxide. This spatial correspondence could either indicate ocean sources of glyoxal, or be the result of spectral artifacts caused by light absorption from chlorophyll-a or collocated chromophoric dissolved organic matter (CDOM). For iodine oxide, satellite measurements are inconclusive: two retrievals using the same SCIAMACHY data give different results over the tropical Pacific Ocean. One study finds iodine oxide is enhanced (Schoenhardt et al., 2008), the other study finds a lower upper limit column abundance here, and concludes that iodine oxide is not detectable over the tropical Pacific Ocean (Saiz-Lopez et al., 2007).

Measurements of glyoxal and iodine oxide are generally scarce. Near-surface observations of glyoxal are currently limited to air masses where the glyoxal source is from coastal, and/or

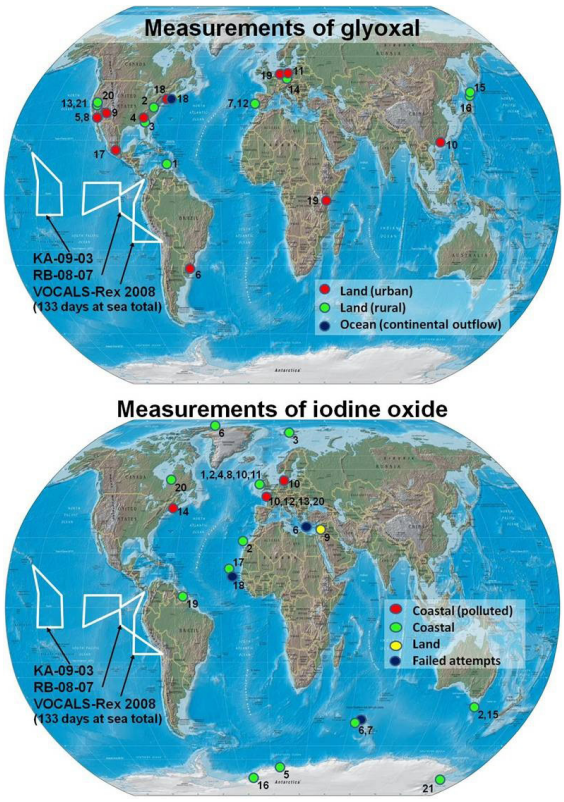

Figure 1: Ship cruise tracks from the VOCALS-REx, and two TAO cruises. Previous glyoxal and iodine oxide measurements exist only over land and in coastal areas. Top: (1) Zhou and Mopper (1990a,b); (2) Munger et al. (1995); (3) Lee et al. (1995); (4) Lee, et al. (1998); (5) Grosjean et al. (1996); (6) Grosjean and Grosjean (1999); (7) Borrego et al. (2000); (8) Kawamura et al. (2000); (9) Jing et al. (2001); (10) Ho and Yu (2002); (11) Moortgat et al. (2002); (12) Cerqueira et al. (2003); (13) Spaulding et al. (2002, 2003); (14) Mueller et al. (2005); (15) Matsunaga et al. (2004); (16) Ieda et al. (2006); (17) Volkamer et al. (2005); (18) Sinreich et al. (2007); (19) Wittrock et al. (2006); (20) Seaman et al. (2006); (21) Huisman et al., (2008). Bottom: 1) Alicke et al. (1999); (2) Allan et al. (2000); (3) Wittrock et al. (2000); (4) Carpenter et al. (2001); (5) Frieß et al. (2001) ; (6) Hönninger (2002); (7) Sebastian (2004); (8) Saiz-Lopez and Plane (2004); (9) Zingler and Platt (2005); (10) Peters et al. (2005); (11) Saiz-Lopez et al. (2006) ; (12) Whalley et al. (2007); (13) Wada et al. (2007); (14) Stutz et al. (2007); (15) Cainey et al. (2007); (16) Saiz-Lopez et al. (2007); (17) Read et al. (2008); (18) Martin et al. (2009); (19) Butz et al. (2009); (20) Mahajan, ULeeds, pers. comm. (2010); (21) Kreher, NIWA, pers. comm. (2010).

terrestrial processes over land (see Figure 1). There is currently no unambiguous direct observation of either glyoxal or iodine oxide over the remote open ocean. This gap in our physical database creates bias in the way we think about the sources of these reactive gases as being mostly from coastal and/or terrestrial sources.

Ship Multi Axis Differential Optical Absorption Spectroscopy (SMAX-DOAS)

In order to assess the validity of satellite retrievals of glyoxal and iodine oxide over the open ocean, the ATMOSpeclab has designed, and assembled an innovative Multi-Axis Differential Optical Absorption Spectroscopy (MAX-DOAS) instrument, the University of Colorado Ship MAX-DOAS (CU SMAX-DOAS), that is optimized for the use from ships. As solar stray light satellites, MAX-DOAS is a passive remote sensing technique (use of solar stray light) based on the well established DOAS technique. DOAS measures atmospheric trace gases by use of their specific narrow band (<5 nm) ultraviolet–visible light absorption structure in the open atmosphere, separating trace gas absorption from broadband molecule and aerosol extinction. MAX-DOAS is well developed for probing the atmosphere from land; however, past ship deployments did either not quantify ship movements, or suffered from a variable field of view due to ship movements which affect the quantitative interpretation of these measurements. The CU SMAX-DOAS actively couples a set of two clinometers that measure pitch and roll of the ship, and compensates the telescope pointing position for ship movements. It has very good signal to noise (~10^{-4} RMS), and features a very low dispersion telescope (0.3 degrees) that is optimized for measurements below clouds. The CU SMAX-DOAS consists of a 19" rack, a laptop PC, two clinometers (all mounted indoors, weight: 30kg, power: 350W, single 110V outlet, size: 93x108 cm^2 bench top space); and a telescope that is mounted outdoors on a railing (weight: 10kg, powered from indoor components; size: 56x13cm2). The telescope is coupled to the indoor components via flexible optical fibers of up to 22m length, allowing an adaptation of the CU SMAX-DOAS onto virtually any ship platform. For a picture of the instrument during VOCALS-REx, and a more detailed description see (Volkamer et al. 2009).

SMAX-DOAS is particularly well suited to test satellite retrievals over the open ocean, see Figure 2A. In contrast to the NADIR view from space, SMAX-DOAS collects scattered sunlight at a series of different elevation angles above the horizon. This makes SMAX-DOAS essentially insensitive to light absorption from chlorophyll, and/or ocean color effects. Over a low surface albedo environment like the ocean (typically <5%), atmospheric absorbers are inherently separated from ocean color effects, because the number of photons that enter the ocean, are scattered back into the atmosphere, and scattering into the SMAX-DOAS telescope is greatly reduced compared to the NADIR view from space (most photons that exit the ocean escape to space); indeed virtually all photons collected by SMAX-DOAS have never "seen" the ocean. Further, the satellite sensitivity varies over the height of the column: satellites need to make assumptions about the vertical distribution of a trace gas, and cannot retrieve information about the vertical distribution of the trace gas directly. In the case for SMAX-DOAS, trace gas column amounts recorded for sets of different elevation angles can be processed into a vertical profile of the atmospheric trace gas. Finally, the sensitivity of satellites is greatly reduced inside the marine boundary layer because of (1) the low surface albedo of water, (2) masking of the marine boundary layer absorbers from clouds, or (3) photons that are scattered back to space at higher altitudes (Rayleigh and Mie scattering). In contrast, SMAX-DOAS is especially sensitive inside the boundary layer. This increased sensitivity stems from the increased path length of the scattered light through the surface layer if the telescope is pointed close to the horizon. Clouds are not necessarily a limitation for SMAX-DOAS. The primary effect of clouds is that they increase the SMAX-DOAS sensitivity inside the cloud volume as the photon path length is greatly increased due to multiple scattering inside a cloud. The photon path length distribution is inherently constrained by observing absorption features of oxygen dimers that have a known distribution in the atmosphere. This enables to constrain the effect of aerosols on radiation fields by means of radiative transfer modeling.

Spectral proof for the presence of glyoxal and iodine oxide during three ship cruises

In order to investigate the presence of glyoxal and iodine oxide over the remote Pacific Ocean, the CU SMAX-DOAS was deployed over the tropical Pacific Ocean in the frameworks of two projects. The first one was the VAMOS Ocean-Cloud-Atmosphere-Land Study – Regional Experiment (VOCALS-Rex, see http://www.eol.ucar.edu/projects/vocals/). Leg 1 of the cruise of the RV Ron Brown for VOCALS started on October 14, 2008, in Panama City heading south into the Pacific Ocean (see Figure 1). At 20° S and 85° W the ship stopped for a buoy replacement and headed Westwards to Arica, Chile, where leg 1 ended (November 3, 2008) and the ship stayed a couple of days in the harbour. Leg 2 (November 9 – December 3, 2008) consisted of going west to this buoy and back to Arica, with some deviations to North and South. The second project, which started after a couple of days, was cruise RB-08-07 as part of

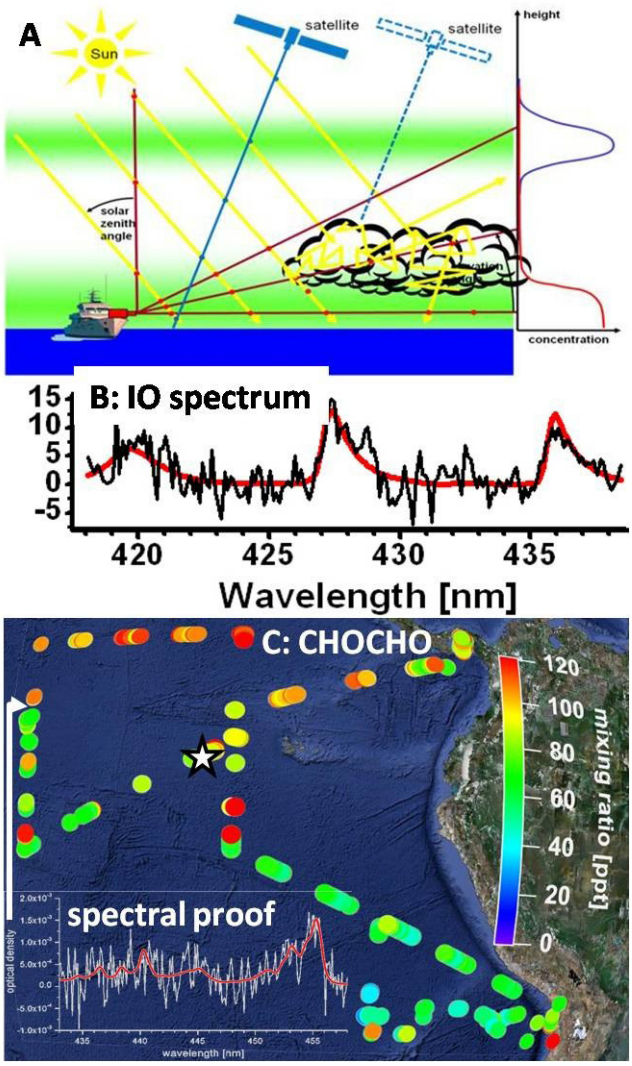

Figure 2: Measurement principle of SMAX-DOAS (panel A, see text), and spectral proof for the presence of glyoxal (B: ~70 ppt) and iodine oxide (C: ~2 ppt) over the tropical Pacific Ocean. The red line shows the scaled reference spectrum; overlaid in grey (black) is the instrument noise. The map shows VOCALS-Rex and TAO-2008 cruise tracks color coded by the mixing ratio of glyoxal (1ppt = 2.46 107 molec cm^{-3}).

the Tropical Atmosphere Ocean (TAO) program (http://www.pmel.noaa.gov/tao/). RB-08-07 started from Arica (December 9, 2008) and headed straight to the buoy line at 95°W servicing a buoy line from 8°S to 0°S. Then, the RV Ron Brown cruised to the 110°W buoy line continuing with buoys located from 8°S through 8°N. Lastly, the buoys between 8°N and 2°N on the 95°W buoy line were serviced before the vessel went straight back to Panama City and arrived there on January 11, 2009. In Figure 2C the whole measurement cruise is plotted with parts of South America on the right.

We succeeded to detect glyoxal and iodine oxide on a regular basis. Our data give unambiguous spectral proof for the presence of up to 120 ppt glyoxal, and up to 3.5 ppt iodine oxide over biologically active upwelling regions of the Pacific Ocean (Figs. 2B and 2C). This is surprising, because global models do not predict any glyoxal over the open ocean. The atmospheric lifetime of glyoxal is very short (few hours), and significant concentrations indicate local sources from the ocean. The source of the glyoxal as well as of IO is currently not understood, and is subject to ongoing activities in the ATMOSpeclab. On global scales, the isoprene oxidation is thought to be the most relevant glyoxal source (Myriokefalitakis et al., 2008; Fu et al., 2008), accounting for about one third of the terrestrial glyoxal source. We find similar or higher glyoxal concentrations over the remote tropical Pacific Ocean than have been observed in remote air masses over land with abundant emissions of biogenic VOC precursor gases (see references in Fig 1). Assuming that 120ppt of glyoxal are produced from isoprene oxidation, an isoprene concentration in excess of one ppb is needed (1ppb = 1000 ppt). Typical isoprene concentrations over phytoplankton bloom areas are a factor of 2-35 lower (Meskhidze and Nenes, 2006); another source of glyoxal appears plausible. Ours is the first direct detection of glyoxal and iodine oxide over the open ocean. Our measurements locate both gases inside the marine boundary layer, and demonstrate for the first time unambiguously that the remote tropical Pacific Ocean is a source for reactive iodine species, and oxygenated hydrocarbons. Our data enable time synchronized comparisons with satellite data, as a prerequisite to assess the quantitative use of satellites to measure these reactive gases reliably, and assess their variability and predictability on global scales. Our data also enables to assess with confidence how these gases cool climate chemically, by (1) destroying the greenhouse gas ozone, (2) forming new particles that reflect a portion of the incoming solar radiation back to space, and (3) growing small particles into larger sizes that activate to form cloud droplets much more efficiently.

Acknowledgements
Financial support from NSF (ATM-0827386, ATM-0841193) and CU Boulder startup funds is gratefully acknowledged. We thank Rob Wood, Roberto Mechoso, Bob Weller, and the TAO program for their help with accommodating the SMAX-DOAS on the cruises, and Hilke Oetjen for comments on the manuscript.

References (titles have been omitted for brevity)

Alicke, B., K.Hebestreit, J.Stutz, and U.Platt, 1999. *Nature*, **397**, 572-573.
Allan, B.J., McFiggans, G., Plane, J.M.C., Coe, H., 2000, J. *Geophys. Res. - Atmos*. **105**, 14363-14369.
Borrego, C., P. Gomes, N. Barros, and A.I. Miranda, 2000, *J. Chromatogr. A*, **889**, 271-279.
Butz, A., Bösch, H., Camy-Peyret, C., Chipperfield, et al., 2009, *Atmos. Chem. Phys*., **9**, 7229-7242.
Cainey, J.M., Keywood, M., Grose, M.R., Krummel, P., et al., 2007, *Environ. Chem*. 4, 143-150.
Carpenter, L.J., Hebestreit, K., Platt, U., Liss, P.S., 2001, *Atmos. Chem. Phys*. 1, 9-18.
Cerqueira, M. A., C. A. Pio, P. A. Gomes, J. S. Matos, and T. V. Nunes, 2003, *Sci. Total Environ*., **313**, 49 – 60, doi:10.1016/S0048-9697(03)00250-X.
Friess, U., Wagner, T., Pundt, I., Pfeilsticker, K., Platt, U., 2001, *Geophys. Res. Lett*. **10**, 1941-1944.
Fu, T.M., D.J.Jacob, D.K.Henze, F.Wittrock, et al., 2008, *J. Geophys. Res.-Atmos*. **113**, D15303.
Grosjean, E., Grosjean, D., Fraser, M. P., and Cass, G. R., 1996, *Environ. Sci. Technol*., **30**, 2687–2703.
Grosjean, E. and D. Grosjean, 1999, *J. Atmos. Chem.*, **32**, 205-232.
Herrmann, 2005. *Atmos. Environ*., **39**, 4219–4231, doi:10.1016/j.atmosenv.2005.02.008.
Ho, S.S.H. and J.Z. Yu, 2002, *Anal. Chem*., **74**, 1232-1240.
Hönninger, G. (2002). Halogen Oxide Studies in the Boundary Layer by Multi Axis Differential Optical Absorption Spectroscopy and Active Longpath-DOAS. *Ph.D. thesis, Institute of Environmental Physics, University of Heidelberg, Germany*.
Huisman, A. J., J. R. Hottle, K. L. Coens, J. P. DiGangi, et al., 2008, *Anal. Chem.*, **80**, 5884–5891.
Ieda, T., Y. Kitamori, M. Mochida, R. Hirata, et al., 2006, *Tellus*, **59B**, 117 – 186, doi:10.1111/j.1600-0889.2006.0179.
Jing, L.H., S.M. Steinberg, and B.J. Johnson, 2001, *J. Air & Waste Man. Assoc*., **51**, 1359-1366.
Kawamura, K., Steinberg, S., and Kaplan, I. R., 2000, *Atmos. Environ*., **34**, 4175–4191.
Lee, Y.-N., X. Zhou, and K. Hallock, 1995, *J. Geophys. Res*., **100**(D12), 25,933–25,944.
Lee, Y.N., X.Zhou, L.I.Kleinman, L.J.Nunnermacker, et al., 1998, *J. Geophys. Res*., **103**(D17), 22,449–22,462.
Matsunaga, S., M. Mochida, and K. Kawamura, 2004, J.

Geophys. Res., **109**, D04302, doi:10.1029/2003JD004100.
Martin, M., D. Pöhler, K. Seitz, R. Sinreich, and U. Platt, 2009, *Atmos. Chem. Phys*., **9**, 9545-9554.
Meskhidze, N., A. Nenes, 2006, *Science*, **314**, 1419-1423.
Moortgat, G. K., Grossmann, D., Boddenberg, A., Dallmann, G., et al., 2002, *J. Atmos. Chem*., **42**, 443–463.
Mueller, K., D. van Pinxteren, A. Plewka, B. Svrcina, et al., 1995, *J. Geophys. Res*., **100**(D5), 9325– 9333.
Munger, et al., 1995, *J. Geophys. Res*., **100**(D5), 9325– 9333.
Myriokefalitakis, S., M.Vrekoussis, K.Tsigaridis, F.Wittrock, et al., 2008, *Atmos. Chem. Phys*. **8**, 4965-4981.
Peters, C., Pechtl, S., Stutz, J., Hebestreit, et al., 2005, *Atmos. Chem. Phys*. **5**: 3357-3375.
Read, K.A., A.S.Mahajan, L.J.Carpenter, M.J.Evans, et al., 2008. *Nature*, **453**, 1232-1235.
Saiz-Lopez, A., A.S.Mahajan, R.A.Salmon, S.J.B.Bauguitte, et al., 2007. *Science*, **317**, 348-351.
Saiz-Lopez, A. and J.M.C.Plane, 2004. *Geophys. Res. Lett*. **31**.
Saiz-Lopez, A., J.A.Shillito, H.Coe, and J.M.C.Plane, 2006. *Atmos. Chem. Phys*. **6**, 1513-1528.
Saiz-Lopez, A., K.Chance, X.Liu, T.P.Kurosu, and S.P.Sander, 2007, *Geophys. Res. Lett*. **34**, L12812.
Schonhardt, A., A.Richter, F.Wittrock, H.Kirk, H.Oetjen, H.K.Roscoe, and J.P.Burrows, 2008, *Atmos. Chem. Phys*. **8**, 637-653.
Sebastián, O. (2004). The relative contribution of free radicals to the oxidation chain of Dimethylsulphide in the marine boundary layer. *Ph.D. thesis, Institute of Environmental Physics, University of Heidelberg, Germany*.
Seaman, V. Y., M. J. Charles, and T. M. Cahill, 2006, *Anal. Chem*., **78**, 2405– 2412.
Sinreich, R., R. Volkamer, F. Filsinger, U. Frieß, et al., 2007, *Atmos. Chem. Phys*., **7**, 1293– 1303.
Spaulding, R. S., R. W. Talbot, and M. J. Charles, 2002, *Environ. Sci. Technol*., **36**, 1798–1808.
Spaulding, R. S., G. W. Schade, A. H. Goldstein, and Charles, 2003, *J. Geophys. Res*., **108**(D8), 4247, doi:10.1029/2002JD002478.
Stutz, J., O.Pikelnaya, S.C.Hurlock, S.Trick, et al., 2007, *Geophys. Res. Lett*., **34**, L22816.
Volkamer, R., L. T. Molina, M. J. Molina, T. Shirley, and W. H. Brune, 2005, *Geophys. Res. Lett*., **32**, L08806, doi:10.1029/2005GL022616.
Volkamer,R., S.Coburn, B.Dix, and R.Sinreich, 2009, SPIE Proceedings „Ultraviolet and Visible Ground- and Space-based Measurements, Trace Gases, Aerosols and Effects", San Diego, Aug 2-9, 2009, paper 7264-4. 2009. doi: 10.1117/12.826792.
Vrekoussis, M., F.Wittrock, A.Richter, and J.P.Burrows, 2009, *Atmos. Chem. Phys*. **9**:4485-4504.
Wada, R., Beames, J.M., Orr-Ewing, A.J., 2007, *J. Atmos. Chem*. **58**: 69-87.
Whalley, L.K., Furneaux, K.L., Gravestock, T., Atkinson, et al., 2007, *J. Atmos. Chem*. **58**, 19-39.
Wittrock, F., Muller, R., Richter, A., Bovensmann, H., Burrows, J.P., 2000, *Geophys. Res. Lett*. **10**, 1471-1474.
Wittrock, F., A.Richter, H.Oetjen, J.P.Burrows, et al., 2006, *Geophys. Res. Lett*. **33**, L16804.
Zingler, J., Platt, U., 2005, *J. Geophys. Res.– Atmos*. **110**, D07307.
Zhou, X., and K. Mopper, 1990a, *Environ. Sci. Technol*., **24**, 1482– 1485.
Zhou, X., and K. Mopper, 1990b, *Environ. Sci. Technol*., **24**, 1864– 1869.

Predicting the Climate of the Coming Decades: A Workshop Summary and Directions for Research

Clement, A., and B. Kirtman
Rosenstiel School of Marine and Atmospheric Science, University of Miami. USA.
Corresponding author: AClement@rsmas.miami.edu

There is general scientific consensus that, because of increasing anthropogenic greenhouse gases, on average, by the middle of this century, the world will be warmer and sea level will be higher. However, because of natural fluctuations of the Earth system unrelated to greenhouse gases, the climate of each successive year may not be warmer than the previous one. Thus there may be clear and robust projections for anthropogenic influence in a particular region, but it is very likely that the climate in any given year or even decade between now and mid-century could be quite different from the projected anthropogenically forced trend. Given these dual 'natural' and anthropogenic influences on climate, how do we best plan on these different timescales?

To begin to tackle this inherently interdisciplinary challenge, we convened a workshop at the Rosenstiel School of Marine and Atmospheric Science of the University of Miami on January 11-14, 2010. The goal of the workshop was to bring together academics and practitioners who have shared interests in predicting the climate of the coming decades. This included researchers who were involved in developing climate prediction systems, studying decision making processes, developing applications of climate information, regional resource managers, and representatives from the insurance industry. This cross disciplinary approach to climate prediction and use is becoming increasingly important as the nations of the world develop new or enhance existing national climate services. Presentations covered three general topics: (1) status of decadal climate prediction efforts, (2) assessing user needs of decadal timescale climate information and (3) constraints on decision making. Here we summarize the main points made during presentations and discussions for each of these topics (all presentations and a list of participants can be found at http://www.clivar.org/organization/decadal/rsmas_decadal/rsmas_talks.php), and suggest ways forward in preparing for the climate of the coming decades.

Status of decadal climate prediction efforts:
The decadal prediction problem represents a new 'frontier' in climate modeling. There is currently relatively high understanding and predictability at the seasonal to interannual timescales. On the longer end, we have a fairly good understanding of how the Earth will respond to greenhouse gas forcing, and have made projections of anthropogenic climate change that are generally consistent with the observed 20th century trends. The decadal timescale is a challenge because it contains both elements of natural fluctuations and anthropogenic change. This is largely uncharted territory in terms of climate prediction and includes a great deal of scientific uncertainty.

A number of presentations addressed the status of efforts to predict climate on a decadal timescale. There is currently a world-wide effort to examine whether including information about the present state of the climate (oceans, land, atmosphere and cryosphere) can introduce some predictability in the 'near-term' (i.e. the coming decades). This is coordinated through the Coupled Model Intercomparison Project (CMIP5), and results will be included in the next scientific assessment of the Intergovernmental Panel on Climate Change (IPCC). Many of the modeling centers involved in this effort were represented at the meeting, including those from the US (IRI, GFDL, NCAR, COLA, U. Miami), Australia (CAWCR-BoM/CSIRO),, UK (Hadley Centre), and Canada. The presentations generally focused separately on predictability in the Atlantic and Pacific basins. In the Atlantic, the source of predictability is thought to come from the Atlantic Meridional Overturning

Circulation (AMOC) of the ocean. In some of the models, this produces patterns of the surface temperature of the North Atlantic basin, which may affect hurricanes, rainfall over North America and temperatures over much of Europe. In fact some presentations showed that experimental decadal prediction being made today indicate modest skill. In the Pacific, much of the discussion focused on the Pacific decadal oscillation, which, for example, has been shown to impact water resources in the western US.

While many of the talks focused on well known "modes of variability" (e.g., AMOC, PDO …), it was also recognized that much of the potential sources of predictability reside in capturing the thermal inertia associated with ocean heat content, and that predicting these modes of variability still requires additional mechanistic understanding. Overall the presentations suggested considerable optimism for decadal predictions that have useful information, yet significant scientific challenges remain and the community as a whole recognized the importance of emphasizing realistic expectations in terms of both what is achievable and that there are difficulties that lie ahead. These challenges include:

- Understanding the sources and mechanisms of decadal variability
- How to measure skill in light of a limited observational record
- How to quantify and identify the numerous sources of uncertainty including the theoretical limits of predictability
- Distinguishing between forced and natural variability
- How to best design observational networks for both forecast initialization and monitoring decadal variability
- How to develop models that provide information that can be used at regional scales and used in application models

Assessing user needs for decadal climate information: Another set of presentations focused on the needs of various user groups for climate information. Several different sectors were discussed, including: insurance, water resources, agriculture, and public lands and marine ecosystems. In each of these sectors, there are existing tools for decision making in which climate information on different timescales can be explicitly included. In some cases these tools are already in use to incorporate climate predictions on seasonal to interannual timescales. However, there are decisions in many sectors that require a longer temporal perspective and therefore information about decadal climate fluctuations and anthropogenic climate change could become useful. Here we briefly summarize the key points of the presentations made in different sectors. A more thorough discussion of user needs that was compiled as part of the World Climate Conference 3 can be found at (http://www.wcc3.org/wcc3docs/pdf/WS9_WP_needs.doc.).

Several presenters noted that the insurance industry can play an important role in encouraging people to engage in adaptation measures that will reduce their vulnerability to climate fluctuations and extreme events, whatever the cause. One mechanism that was discussed was 'long-term' flood insurance in which insurance is tied to property and not individuals, and would hence encourage home improvement to reduce the vulnerability of a property to the impacts of flooding. Government can also play a role in using insurance mechanisms to reduce losses associated with climate change by, for example, incorporating climate information into building codes or investing in natural infrastructure as a buffer to climate change. A common concern that was reiterated was that premiums should reflect risk (not be subsidized). As such, there is a need for climate information in order to aid in quantification of the long-term risks of climate change and climate variability.


WCRP OPEN SCIENCE CONFERENCE
CLIMATE RESEARCH IN SERVICE TO SOCIETY
24–28 October 2011, Denver, Colorado, USA
www.wcrp-climate.org/conference2011

Contents

The CLIVAR Newsletter Exchanges is published by the International CLIVAR Project Office
ISSN No: 1026 - 0471

Editor: Antonio Caltabiano, C. Roberto Mechoso and Howard Cattle
Layout: Sandy Grapes
Printing: Indigo Press, Southampton, UK

CLIVAR Exchanges is distributed free of charge upon request (email: icpo@noc.soton.ac.uk)

The ICPO is supported by the UK Natural Environment Research Council and NASA, NOAA and NSF through US CLIVAR.

If undelivered please return to:
International CLIVAR Project Office
National Oceanography Centre
European Way, Southampton, SO14 3ZH,
United Kingdom
http://www.clivar.org

NATURAL ENVIRONMENT RESEARCH COUNCIL

U.S. CLIVAR Climate Variability & Predictability

National Oceanography Centre
NATURAL ENVIRONMENT RESEARCH COUNCIL

Please recycle this newsletter by passing on to a colleague or library or disposing in a recognised recycle point